CONVECTIVE BOUNDARY LAYER FLOW AND HEAT TRANSFER OF WILLIAMSON HYBRID FERROFLUID WITH VARIOUS EFFECTS

WAN MUHAMMAD HILMI BIN WAN ROSLI

MASTER OF SCIENCE

UNIVERSITI MALAYSIA PAHANG
AL-SULTAN ABDULLAH

UNIVERSITI MALAYSIA PAHANG AL-SULTAN ABDULLAH

DECLARATION OF THESIS AND COPYRIGHT

Author's Full Name	:	WAN MUHAMMAD HILMI BIN WAN ROSLI
Date of Birth	:	12 APRIL 1998
Title	:	CONVECTIVE BOUNDARY LAYER FLOW AND HEAT TRANSFER OF WILLIAMSON HYBRID FERROFLUID WITH VARIOUS EFFECTS
Academic Session	:	SEMESTER II 2023/2024

I declare that this thesis is classified as:

☐	CONFIDENTIAL	(Contains confidential information under the Official Secret Act 1997)*
☐	RESTRICTED	(Contains restricted information as specified by the organization where research was done)*
☒	OPEN ACCESS	I agree that my thesis to be published as online open access (Full Text)

I acknowledge that Universiti Malaysia Pahang Al-Sultan Abdullah reserves the following rights:

1. The Thesis is the Property of Universiti Malaysia Pahang Al-Sultan Abdullah
2. The Library of Universiti Malaysia Pahang Al-Sultan Abdullah has the right to make copies of the thesis for the purpose of research only.
3. The Library has the right to make copies of the thesis for academic exchange.

Certified by:

(Student's Signature)

(Supervisor's Signature)

DR. MUHAMMAD KHAIRUL ANUAR BIN MOHAMED
Name of Supervisor
Date: 5 JULY 2024

Date: 5 JULY 2024

NOTE : * If the thesis is CONFIDENTIAL or RESTRICTED, please attach a thesis declaration letter.

SUPERVISOR'S DECLARATION

We hereby declare that we have checked this thesis and in our opinion, this thesis is adequate in terms of scope and quality for the award of the degree of Master of Science.

____

(Supervisor's Signature)

Full Name : DR MUHAMMAD KHAIRUL ANUAR MOHAMED

Position : Senior Lecturer

Date : 5 JULY 2024

____

(Co-supervisor's Signature)

Full Name : DR NORHAFIZAH MD SARIF

Position : Senior Lecturer

Date : 5 JULY 2024

STUDENT'S DECLARATION

I hereby declare that the work in this thesis is based on my original work except for quotations and citations which have been duly acknowledged. I also declare that it has not been previously or concurrently submitted for any other degree at University Malaysia Pahang Al-Sultan Abdullah or any other institutions.

(Student's Signature)

Full Name : WAN MUHAMMAD HILMI BIN WAN ROSLI I

ID Number : MSE21002

Date : 5 JULY 2024

CONVECTIVE BOUNDARY LAYER FLOW AND HEAT TRANSFER OF WILLIAMSON HYBRID FERROFLUID WITH VARIOUS EFFECTS

WAN MUHAMMAD HILMI BIN WAN ROSLI

Thesis submitted in fulfillment of the requirements
for the award of the degree of
Master of Science

Centre for Mathematical Sciences

UNIVERSITI MALAYSIA PAHANG AL-SULTAN ABDULLAH

JULY 2024

ACKNOWLEDGEMENTS

I want to express my gratitude towards my supervisors Dr. Muhammad Khairul Anuar and Dr Norhafizah for their patience, kindness, dedication, and guidance throughout this research. This research would not have been possible if it were not for their encouragement during my studies. They have shown impressive knowledge and experience in mathematical studies that are helpful in my studies. Their consistent support and beliefs from the first semester until now have provided me with strength in my studies. I also want to thank both of them for their patience in proofreading and correcting many mistakes I made during my study.

This research also would not have been possible without my parents' support. They have provided me with financial and emotional support from the day I started my studies. They have sacrificed a lot for me to further my studies. I am grateful and in debt to them and wish to repay them with my master's graduation.

Lastly, I want to express my gratitude towards all UMPSA staff for providing me with many facilities, information, and guidance from the first semester until now.

ABSTRAK

Aliran dan olakan pemindahan haba ferrobendalir memainkan peranan penting dalam kejuruteraan, elektronik, dan bidang perubatan. Aplikasi aliran seperti ini meluas dalam pembesar suara hi-fi, cakera keras komputer, rawatan kanser, imej resonans magnetik, dan ujian diagnostik lain. Ferrobendalir biasanya mengandungi ferrozarah yang diperbuat daripada oksida, yang mempunyai kekonduksian terma rendah, memberikan prestasi pemindahan haba yang terhad. Gabungan ferrozarah dengan nanozarah lain yang mempunyai kekonduksian terma yang tinggi dalam bendalir asas, dikenali sebagai ferrobendalir hibrid, dijangka dapat meningkatkan pemindahan haba berbanding dengan ferrobendalir biasa. Secara amnya, bendalir asas yang digunakan dalam aplikasi kejuruteraan dan industri, seperti larutan polimer, darah, dan cat, adalah bendalir bukan Newtonan dengan ciri-ciri pseudo-plastik. Disebabkan hanya sedikit data eksperimen dan analisis teori sedia ada bagi mengesahkan penjelasan dalam aliran ferrobendalir hibrid pseudo-plastik, kajian terhadap topik ini perlu dilakukan bagi menambah baik dan meneroka keupayaannya dalam aliran dan olakan pemindahan haba. Dalam kajian ini, aliran bendalir pseudo-plastik ini dimodelkan berdasarkan model Williamson. Tiga masalah dipertimbangkan dalam penyelidikan ini, iaitu aliran titik genangan di atas helaian meregang, aliran di atas helaian telap meregang dengan kehadiran sinaran termal, dan aliran di atas plat bergerak dengan kesan lepasan likat dalam ferrobendalir hibrid Williamson. Persamaan-persamaan menakluk bagi setiap masalah dimodelkan dalam bentuk persamaan-persamaan pembezaan separa tak linear. Persamaan-persamaan ini kemudian dijelmakan menjadi persamaan pembezaan biasa menggunakan penjelmaan keserupaan dan diselesaikan secara berangka menggunakan kaedah kotak Keller. Perisian MATLAB digunakan untuk mengira kod-kod berangka bagi semua masalah. Parameter magnetik, parameter regangan, parameter ferrobendalir Williamson, parameter kadar telapan, parameter sinaran termal, parameter plat bergerak, dan parameter pelesapan likat adalah parameter-parameter yang dipertimbangkan dalam kajian ini. Perbandingan dengan jenis ferrobendalir hibrid lain dan pecahan isipadu ferrozarah yang berbeza juga dipertimbangkan. Hasil kajian menunjukkan bahawa ferrobendalir hibrid Williamson berpotensi memberikan prestasi yang lebih baik dalam keupayaan pemindahan haba berbanding dengan ferrobendalir dengan pecahan isipadu nanozarah yang sama. Nombor Nusselt meningkat apabila parameter magnetik, parameter regangan, parameter kadar kebolehregangan, parameter plat bergerak, dan parameter sinaran termal meningkat, dengan mengurangkan ketebalan aliran lapisan sempadan. Peningkatan parameter magnetik telah meningkatkan nilai pekali geseran kulit bagi semua masalah yang dikaji. Nilai pekali geseran kulit merosot apabila parameter regangan dan plat bergerak meningkat, seterusnya mendorong momentum dalam aliran lapisan sempadan. Apabila parameter Williamson meningkat, pekali geseran kulit meningkat manakala nombor Nusselt tidak terjejas, seperti yang ditunjukkan dalam formula nombor Nusselt.

ABSTRACT

The flow and convective heat transfer of ferrofluid plays an important role in engineering, electronics, and medicine. Such flows are widely applied in hi-fi speakers, computer hard disks, cancer treatment, magnetic resonance imaging, and other diagnostic tests. Ferrofluid usually contains ferroparticles made from oxide, which has low thermal conductivity, thus providing limited heat transfer performance. Combining the ferroparticles with other highly thermally conductive nanoparticles in the based fluid, known as hybrid ferrofluid, is expected to enhance heat transfer over the ferrofluid. Generally, the based fluids employed in engineering and industrial applications such as polymer solutions, blood, and paint are non-Newtonian fluids with pseudo-plastic characteristics. Due to the lack of experimental data and theoretical analysis available to verify such an explanation for a pseudo-plastic hybrid ferrofluid flow, a study on this topic is needed in order to improve and explore its capabilities in flow and convective heat transfer. In this study, the pseudo-plastic fluid flow is modeled based on the Williamson model. Three problems are considered in this research, which are the stagnation point flow over a stretching sheet, the flow over a permeable stretching sheet with the presence of thermal radiation, and the flow over a moving plate with viscous dissipation effects in Williamson hybrid ferrofluid. The governing equations for each problem are modeled in the form of non-linear partial differential equations. These equations are then transformed into ordinary differential equations using the similarity transformation and solved numerically using the Keller-box method (KBM). MATLAB software is used to compute the numerical codes for all the problems. The magnetic parameter, stretching parameter, Williamson fluid parameter, permeability rate parameter, thermal radiation parameter, moving plate parameter, and viscous dissipation parameter are the parameters considered in this research. Comparisons with other types of hybrids ferrofluid and different ferroparticle volume fractions are also considered. The results show that Williamson hybrid ferrofluid potentially provides better performance in heat transfer capability compared to ferrofluid with the same volume of nanoparticle volume fraction. Nusselt number increases as the magnetic parameter, stretching parameter, permeability rate parameter, moving plate parameter, and thermal radiation parameter are induced, thus reducing the thermal boundary layer thickness. The increased magnetic parameter increases the skin friction coefficient for all problem studies. Skin friction coefficient values decrease as stretching and moving parameters increase, which increases momentum in the boundary layer flow. As Williamson parameter increases, the skin friction coefficient increases while Nusselt number does not affected, as shown in Nusselt number formula.

TABLE OF CONTENT

LIST OF TABLES

LIST OF FIGURES

LIST OF SYMBOLS

a,b,c	Constant
B_0	Uniform magnetic field
C_f	Local skin friction coefficient
C_p	Specific heat
$(C_p)_{hnf}$	Heat capacity of hybrid nanofluid
f	Dimensionless stream function
F_x, F_y	Body force in x, y direction, respectively
h	Heat transfer coefficient
h_f	Heat transfer coefficient for convective boundary conditions
k	Thermal conductivity
k_{bf}	Thermal conductivity base fluid
k_{hnf}	Thermal conductivity hybrid nano fluid
k^*	Mean absorption coefficient
L	Length of plate surface
M	Magnetic parameter
N_R	Radiation parameter
Nu	Nusselt number
Nu_x	Local Nusselt number
$\Pr$	Prandtl number
q_r	Radiation heat flux
q_w	Surface heat flux
Re	Reynolds number
Re_x	Local Reynolds number
E_C	Eckert Number
T	Temperature
T_∞	Ambient temperature
u,v	Velocity component in x,y direction, respectively

u_e	External velocity
u_w	Stretching velocity
U, U_∞	Free stream velocity
x, y	Cartesian coordinate

Greek Symbol

α	Thermal diffusivity coefficient
δ	Boundary layer thickness
δ_h	Velocity boundary layer thickness
δ_T	Thermal boundary layer thickness
ε	Stretching parameter
η	Dimensionless similarity variable
λ	Williamson parameter
v	Kinematic viscosity
v_{hnf}	Hybrid ferrofluid kinematic viscosity
ρ	Fluid density
ρ_{hnf}	Hybrid nanofluid density
ρ_∞	Fluid density at ambient temperature
σ	Electric conductivity
σ^*	Stefan-Boltzman constant
μ_{hnf}	Hybrid nanofluid dynamic viscosity
Γ	Time constant
τ	Shear stress
τ_w	Shear stress surface
θ	Dimensionless temperature
ψ	Stream function
w	Surface conditions
∞	Outer boundary layer conditions
ε	Stretching sheet parameter
Ω	Moving plate parameter

Subscript

hnf	Hybrid nanofluid
bf	Base fluid
$s1, s2$	Nanoparticles

Superscript

$'$	Differentiations with respect to η

LIST OF ABBREVIATIONS

KBM	Keller-box method
MHD	Magnetohydrodynamic
AGM	Akbari Ganji method
HPM	Homotopy perturbation method
FEM	Finite element method
RKF	Runge-Kutta-Fehlberg
HAM	Homotopy analysis method
SRM	Spectral relaxation method
API	American Petroleum Institute

LIST OF APPENDICES

CHAPTER 1

PRELIMINARIES

1.1 Introduction

The demand for innovative fluids, such as ferrofluids, is continually increasing. These fluids are specifically engineered to be directed in a particular direction by utilizing magnetic field intensity. This rendered ferrofluid appropriate for use as a manipulable fluid for transportation purposes and as a convective heat transfer agent for maintaining the operational temperature of equipment. Ferrofluid can be found in electronic devices such as electric motors, hi-fi speakers, and computer hard disks. It is also employed in the medical sciences, especially as a drug carrier in cancer treatment. A novel hybrid ferrofluid has been developed with the aim of enhancing the convective heat transfer capabilities of conventional ferrofluids. This type of fluid is upgraded not only within Newtonian fluid-based fluids like water and oil but also involves non-Newtonian substances such as polymer solutions, paint, ketchup, and blood, which have explicitly pseudo-plastic flow characteristics.

1.1.1 Convective Boundary Layer Flow Theory

Ludwig Prandtl (1875–1953) established the idea of the boundary layer in August 1904 through his presentation titled "On the motion of a fluid with very small viscosity," which he delivered at the Third International Congress of Mathematicians. Prandtl found this theory after he built a special water channel to observe the detachment of vortices from curved bodies. He presented his findings with photographic evidence from the channel during his 10-minute presentation at the congress. The idea presented in his research paper is novel and has not been proposed before, thereby providing a pathway to understand fluid dynamics better (Tani, 2003; Anderson, 2005; Eckert, 2017).

Convective heat transfer is the mechanism by which heat is transferred by the movement of gas or fluid over a surface. An example of convective heat transfer is when air flows across the body of an athlete, providing convective cooling for the athlete. There are two types of convection heat transfer: forced convection and free convection. Forced convection exists when there is an external force inducing the fluid motion through mechanical movement such as a fan, motor, blower, condenser, etc. Free or natural convection occurs when a temperature gradient causes a density difference, thus inducing fluid movement. Convection maintains the steep temperature gradient between the body and surrounding fluid, which makes it an effective heat transfer mechanism. The rate of convective heat transfer depends on the fluid and surface temperature, surface area, and velocity of the flow across the surface (Blair, 2007; Mohamed, 2013; Müller, 2019; Sokolova, 2019).

Anderson (2005) and Mohamed (2013) define a boundary layer as a narrow zone that occurs in close proximity to the surface within a fluid flow field. The velocity gradient in this region is large due to the skin friction between the fluid motion and the surface. Hence, it is imperative to consider skin friction and viscosity in investigations of boundary layers unless the drag force is insignificantly small. Figure 1.1 illustrates the fluid flow on a flat plate and boundary layer formation to visualize and understand the boundary layer theory.

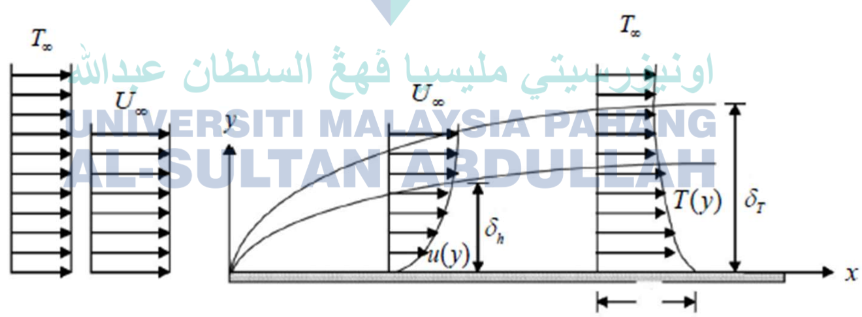

Figure 1.1 Fluid flow on a flat plate boundary layer formation

Figure 1.1 illustrates two boundary layers when fluid flows on the flat plate. The momentum boundary layer, the hydrodynamic boundary layer, and the thermal boundary layer are the two types of boundary layers that can be studied. The momentum boundary layer exists as a result of the no-slip condition, which then causes skin friction drag from the occurrence of a velocity gradient near the wall. In detail, fluid molecules that are attached to the flat surface will assume the velocity is zero, then delay other molecules movement in the layer next to it until $y = \delta_h$ (momentum boundary layer thickness) from the flat surface. The thermal boundary layer, denoted as area δ_T, arises due to a temperature disparity between the free flow and the temperature of the flat plate surface. Similar to the velocity boundary layer, the fluid molecules in contact with the flat plate achieve thermal equilibrium with the surface through conduction. It will transfer the energy to another molecule at another layer until $y = \delta_T$ (Mohamed, 2013). Layers above both regions will not be considered.

1.1.2 Williamson Fluid Model

Non-Newtonian fluids are defined as fluids that do not obey Newton's law of viscosity. Among many types of fluids under non-Newtonian conditions, pseudo-plastic fluid is the most commonly encountered fluid due to its popularity in a wide range of industry applications. Examples of industry applications are plastic sheet forming, asphalts, glues, oils, biological outcomes, etc. (Khan *et al.,* 2022). A pseudo-plastic fluid exhibits shear-thinning characteristics, where its viscosity decreases as the shear rate increases. Typical examples of pseudo-plastic fluids include polymers and solutions containing high-molecular-weight substances (Rapp, 2017). Many fluid models are designed to describe the flow behavior of shear-thinning (pseudo-plastic) fluids. Some notable examples include the Maxwell model, Casson model, Carreau model, Cross model, Ellis model, and others. However, Williamson's model has the upper hand in describing the flow of pseudo-plastic fluid. Williamson (1929) was the pioneer in proposing a model equation to depict the flow behavior of pseudo-plastic fluids. As a result, researchers later named it Williamson fluid.

The advantage of the Williamson fluid model is the inclusion of minimum and maximum viscosities to ensure better results in describing pseudo-plastic fluids. Therefore, this model offers reliable experimental information when compared to other Newtonian and non-Newtonian fluid models for polymer solutions and particle suspensions (Cramer & Marchello, 1968; Jain & Parmar, 2018; Rajendar & Babu, 2018; Subbarayudu *et al.,* 2020; Ullah Awan *et al.,* 2022). Examples of Williamson fluids are human blood, paint, ketchup, whipped cream nail polish, etc. (Khan *et al.,* 2017)).

According to Almeida *et al.*, , blood is a prime example of Williamson fluid, as it reduces blood viscosity when shear strain increases. Previous studies from Almeida *et al.* (2023), Khan *et al.* (2014a), and Hashim *et al.* (2016) also stated that the Williamson fluid model almost fully illustrates the behavior of human blood flow. Additionally, in contrast to other types of Williamson fluid models that require consideration of variables such as fluid type, thermophysical properties, Prandtl number, and so on, human blood can be assumed to have generally fixed physical properties, thermophysical characteristics, and Prandtl number. These assumptions simplify the research by reducing the number of variables to consider. After exploring the pseudo-plastic fluid model, this research considered the Williamson model to describe the fluid model with blood as the base fluid.

1.1.3 Hybrid Ferrofluid

Conventional base fluids typically exhibit low thermal conductivity, hindering effective heat transfer. For instance, water, despite having a high specific heat capacity, requires a substantial amount of energy to raise its temperature, making it insufficient for certain heat transfer applications. One method to enhance the thermal conductivity of a typical base fluid is by introducing non-identical nanoparticles into the fluid, causing them to dissolve. The objective of distributing nanoparticles with different properties into the base fluid is to enhance the individual functionality of each component or to offset any deficiencies, resulting in an optimal heat transfer rate. Therefore, the term "hybrid nanofluid" is employed to describe this particular form of fluid.

The rising popularity of hybrid nanofluid topics among researchers started when Choi (1995) dispersed metallic nanoparticles into a conventional-based fluid to improve the fluid's thermal conductivity. Their research suggests that the smaller size of nanoparticles, with a typical length of 1–50 nm (Zheng *et al.,* 2013), compared to microparticles, is better for fluid incorporation to enhance thermal conductivity. This work established the term "nanofluid" and it has become more popular among academics for investigating and creating novel forms of fluid, namely hybrid nanofluids, to meet the needs of many sectors. In another study conducted by Maxwell (2010), a significant proportion of solid particles was distributed into the base fluid with the aim of potentially enhancing the heat transfer efficiency of the base fluid. However, due to the large volume fraction of solid particles, this results in the occurrence of sedimentation that inhibits heat transfer performance (Yasin *et al.,* 2018b). Compared with these two studies, nanoparticles demonstrate an advantage in enhancing the thermal conductivity of the base fluid. Metal nanoparticles are commonly used Cu, Ag, Au, Fe, Ti, Hg, while non-metallic nanoparticles are Al_2O_3, CuO, SiO_2, TiO_2, etc. (Hashim *et al.,* 2018). The researchers investigated several features, including thermal physical characteristics, viscosity, thermal conductivity, magnetism, plate movement, stretching, stagnation, and other factors. The studies conducted by Mahesh *et al.* (2023) and Yap *et al.* (2023) investigate the influence of heat radiation and viscous dissipation on hybrid nanofluid. Assessment of unique or multiple exact solutions of nonlinear coupled ordinary differential equations to portray the flow and heat field of hybrid $Cu-Al_2O_3$/water flow was done by Usafzai and Aly (2022). Khashi'ie *et al.* (2022a) examine the flow and heat transfer characteristics of a hybrid $Cu-Al_2O_3$/water nanofluid on a stretching/shrinking surface using the bvp4c method. In their study, Gumber *et al.* (2022) examined the effects of surface suction/injection, heat generation/absorption, joule heating, viscosity dissipation, and thermal radiation on the flow of a micropolar $CuO-Ag$/water hybrid nanofluid. Yaseen *et al.* (2021) constructed a model to examine the effects of hybrid nanofluid (SiO_2-MOS_2/water) on the flow across a convectively heated moving surface, both in terms of assistance and opposition. Recent research that studied blood as a base fluid in their hybrid nanofluid studies was done by Waqas *et al.* (2022) and Saeed *et al.* (2021a). They focused on the use of blood as a hybrid nanofluid in their research. Using the optimal homotopy analysis method, Gul *et al.* (2021) investigated the stagnation point inviscid flow of couple stress hybrid nanofluid (TiO_2-Ag/blood) around a rotating sphere. They found that increasing the nanoparticle volume fraction of hybrid nanofluid boosts the thermal conductivity from 5.8 to 11.947%. Basha *et al.* (2022) concluded that fluid with hybrid nanoparticles has better flow and heat transfer compared to fluid with nanoparticles in their studies of fluid transport behavior in an inclined stenosis artery of bio-magnetic blood hybrid nanofluid ($Au-Cu$/blood). Al-Zahrani *et al.* (2023) also produce the same conclusion in their investigation in proposing a new type of biohybrid nanofluid ($Ag-$ graphene/blood), where it is more superior in controlling fluid movement compared to mono-nano biohybrid nanofluid. Sandhya Rani and Venkata

Ramana Reddy (2022) provide a unique study where they consider magnetic fields and electromagnetic fields directed towards the flow direction of blood-based hybrid nanofluid using the Cattaneo-Christov model. They were using the spectral relaxation method (SRM) and found that velocity and temperature profile as electric field factors are enhanced.

Scientists have developed ferrofluid as a fuel for space shuttles to address the challenges of zero-gravity circumstances during the aerospace race. In a zero-gravity environment, fuel exhibits erratic motion without any consistent trajectory. The ferrofluid, a magnetized nanofluid, may be used to guide the fuel-containing ferroparticles into the combustion chamber by means of a magnetic field (Papell, 1965). Nowadays, ferrofluid is employed in plenty of applications. The importance of this kind of magnetic fluid attracted researchers to explore its potential, especially in the convective flow and heat transfer processes.

Research on ferrofluid that includes the study of heat, thermal radiation, and slip flow of ferrofluid towards various geometry like stagnation point, stretching/shrinking surface, as well as a flat surface with heat flux and Newtonian heating boundary conditions was conducted by Ramli *et al.* (2017), Jusoh *et al.* (2018), Mohamed *et al.,* (2019a; 2019b; 2021c; 2021d), Yasin *et al.* (2020), Jamaludin *et al.* (2020) and Anantha Kumar *et al.* (2019). The most recent studies of ferrofluid were done by Yasin *et al.* (2022), who researched the stagnation point flow of ferrofluid over a vertical flat plate with mixed convection of the boundary layer. They concluded that the main contribution of ferrofluid velocity, skin friction, and heat transfer performance behavior is from the ferroparticle volume fraction.

1.1.4 Dimensionless Parameter

A dimensionless parameter is a quantity or value that doesn't have any physical dimensions. These figures frequently arise in computations utilized by process engineers. Dimensionless numbers stay unchanged regardless of whether metric or other units are used in the equations, as long as consistent units are employed (Oyama, 2011). Dimensionless parameters that are used in this research are the Prandtl number, Reynolds number, Nusselt number, and Eckert number. The sub-section below will provide details on this dimensionless parameter.

1.1.4.1 Prandtl Number

The Prandtl number, denoted as $\Pr$, is a dimensionless characteristic of a fluid that is determined by the ratio of its kinematic viscosity, represented by v, to its thermal diffusivity, represented by a (Sundén, 2019):

$$\Pr = \frac{v}{a}.$$

It evaluates the correlation between the ability of a fluid to convey momentum and its ability to transport heat. $\Pr$ is a dimensionless quantity that characterizes the inherent properties of a fluid. Liquids with low Prandtl values are very conductive and hence ideal for heat transfer. The Prandtl number is only a modulus that characterizes the properties of a fluid. The range of the fluid is as follows: 0.001–0.03 for liquid metals, 0.2–1 for gases, 1–10 for water, 5–50 for light organic liquids, and 5–2000 for oils (Shah & London, 1978; Rapp, 2017).

1.1.4.2 Reynolds Number

Reynolds number defined as the ratio of fluid momentum force to viscous shear force. The numerical value was initially developed by Sir George Stokes in 1851 and was subsequently named after Osborne Reynolds by Arnold Sommerfield in 1908. The parameter is used to quantitatively study viscosity (Kumar & Panda, 2022). The Reynolds number, Re, has the following mathematical definition (Guo & Ghalambor, 2005; LaNasa & Upp, 2014; Caket *et al.,* 2022):

$$\mathrm{Re} = \frac{\rho v d}{\mu}$$

Where ρ is density, v is velocity, d is diameter and μ is viscosity of a fluid. To identify whether a fluid is flowing laminarly or turbulently, one uses the Reynolds number. It is thought that a Reynolds number less than or equal to 2100 indicates laminar flow and a Reynolds number more than 2100 indicates turbulent flow based on the American Petroleum Institute, API RP 13D, standards (API, 2010).

1.1.4.3 Nusselt Number

The Nusselt number is a well-recognized dimensionless metric that quantifies the ratio of convective heat transfer to conductive heat transfer at the surface of a material. It can be described as (Herwig, 2016; Caket *et al.,* 2022):

$$Nu_x = \frac{xq_w}{k_f \Delta T} = \frac{xq_w}{k_f (T_w - T_\infty)}.$$

Where q_w is the heat flux, is the characteristic length, k_f is the thermal conductivity of the fluid and ΔT is the temperature difference external flow. The above equation shows that Nusselt number represents the ratio of convective heat transfer, occurring when a fluid layer with a thickness x, wall and ambient temperatures T_w and T_∞ respectively on opposite sides, is in motion, to the conductive heat transfer that occurs when the fluid layer is not moving (Dincer & Siddiqui, 2018). There are two crucial factors to consider when defining the Nusselt number: the characteristic length and the reference temperature difference. The Nusselt number is a significant metric that can enhance the efficiency of heat transfer. It is mostly determined by the Reynolds and Prandtl numbers (Roy & Roy, 2020).

1.1.4.4 Eckert Number

The effect of viscous dissipation was introduced by Gebhart (1962). Using perturbation method, Gebhart studies the viscous dissipation effect in natural convection. Geropp (1969) then extend the research by conducted a theoretical investigation on the Eckert number phenomena. This phenomenon refers to the reversal of heat transfer from a moving wall when the Eckert number, denoted as E_C, is almost equal to 1. The Eckert number quantifies the impact of dissipation effects on a fluid's self-heating. At high flow velocities, the temperature distribution in a fluidic system is influenced not only by the existing temperature gradients, but also by the dissipation effects caused by internal fluid friction. This will lead to self-heating, resulting in a modification of the temperature profile. The Eckert number is used to determine whether the impact of self-heating caused by dissipation may be disregarded ($E_C \ll 1$) or not. This dimensionless number is given by (Gschwendtner, 2004; Rapp, 2017):

$$E_C = \frac{U_\infty^2}{C_p \Delta T} = \frac{U_\infty^2}{\left(C_p\right)_f \left(T_w - T\infty\right)}.$$

1.1.5 Keller-Box Method

The Keller-box method was introduced by Keller (1971; 1978). This method combined both implicit finite difference methods with Newton's method for linearization, which was discovered to be very effective in solving the convective boundary layer problem and the parabolic partial differential equation. In addition, this method can be modified to solve the problem in any order and proves to be unconditionally stable and quickly converges for highly non-linear flows, thus providing a solid reason to use this method for solving boundary layer problems in this study (Vajravelu & Prasad, 2014).

The Keller-box approach has four sequential steps, commencing with the reduction of ordinary differential boundary layer equations into a first-order system. The equations are transformed into difference equations using central differences. These difference equations are then linearized using Newton's method and expressed in matrix-vector form. The linear systems are solved using the block tridiagonal elimination approach (Na, 1979; Cebeci & Bradshaw, 1988; Cebeci & Cousteix, 2005; Mohamed, 2018).

Among the researchers who used this method to solve the boundary layer problems are Ilias *et al.* (2017), Ishak *et al.* (2006), Swalmeh *et al.,* (2018; 2019), Vittal *et al.* (2017a), Yacob *et al.* (2011), Salleh *et al.* (2010), Iqbal *et al.* (2021), Yasin *et al.,* (2018a; 2020; 2021a; 2021b; 2022), Mohamed *et al.,* (2013b; 2014; 2016a; 2016b; 2019c; 2020c; 2021b).

1.2 Problem Statement

Magnetized nanofluids have gained popularity due to their capacity to be manipulated to flow by controlling the position and intensity of the magnetic field. Referred to as a ferrofluid, this liquid has substantial advantages in terms of fluidity and thermal conduction, especially in the medical domain. Applications encompass cancer therapy, hemostasis in critical wounds, magnetic resonance imaging, and other diagnostic examinations.

The ferroparticles found in ferrofluids are often composed of oxide particles, which possess a low thermal conductivity, hence restricting their ability to transport heat effectively. To accomplish the necessary boost in thermal conductivity, one possible solution is to increase the volume percentage of oxide ferroparticles in the ferrofluid. However, the use of a substantial quantity of nanoparticles might result in flow obstruction, as indicated by Sahoo *et al.* (2022) and Yasin *et al.* (2018b). Therefore, oxide ferroparticles alone cannot meet the criteria of optimum thermal conductivity and fluidity, even by increasing the volume of nanoparticles. As mentioned in Section 1.1.3, the addition of metal nanoparticles to a nanofluid enhances the heat transfer performance of the fluid.

Therefore, this research proposes a mathematical modeling study on a new type of ferrofluid named hybrid ferrofluid. The combination of a tiny quantity of metal nanoparticles and oxide ferroparticles mixed in a base fluid is thought to enhance thermal characteristics, preserve friction and fluidity, and also derive advantages from the metal nanoparticles, such as acting as a hygiene control agent. The usual Navier-Stokes equations are insufficient to characterize fluid behavior like ketchup and human blood in medicine; thus, the non-Newtonian Williamson model is considered to describe the fluid. In view of this consideration, three questions are developed in order to guide this theoretical research on the newly upgraded fluid:

i. How to formulate mathematical model of Williamson hybrid ferrofluid:
ii. How to solve the proposed problems using the Keller-box method and develop the numerical algorithm and computations?

iii. What are the effects on the skin friction and Nusselt, as well as the temperature and velocity profile produced when pertinent parameters are applied?

After reviewing previous literature, little experimental data and theoretical analysis are available to answer these questions. This research will cover three (3) related problems:

i. Stagnation point flow over a stretching sheet in a Williamson hybrid ferrofluid with the presence of magnetic parameter.
ii. Boundary layer flow of Williamson hybrid ferrofluid over a stretching sheet in the presence of thermal radiation, suction injection effects
iii. Convective Boundary layer flow of Williamson hybrid ferrofluid over a moving plate with the appearance of viscous dissipation effect.

1.3 Research Objectives

The objectives of this project to:

i. extend the formulation of ferrofluid mathematical model to a Williamson hybrid ferrofluid;
ii. provide mathematical formulations and numerical algorithms for computations;
iii. analyse the numerical results of fluid flow characteristics affected by pertinent fluid parameters

for each of the problems mentioned Section 1.2 that would facilitate the elucidation and validation of the experimental findings in the future regarding the issue of convective boundary layer flow on a stagnation point, a stretching surface, and a moving flat surface immersed in a Williamson hybrid ferrofluid with a constant wall temperature.

1.4 Research Scope

The scope of this research is confined to addressing issues related to the steady, two-dimensional flow of convective boundary layer flows on a stagnation point flow, a stretching sheet, and a moving flat plate in a Williamson hybrid ferrofluid with a constant wall temperature. The governing boundary layer equations for each of the problems are in the form of non-linear partial differential equations, then transformed into ordinary differential equations using similarity transformation. Then, the transformed equations are solved numerically using an implicit finite difference scheme known as the Keller-box method. Figure 1.2 below shows the flow chart solution procedures to solve the problems in this research.

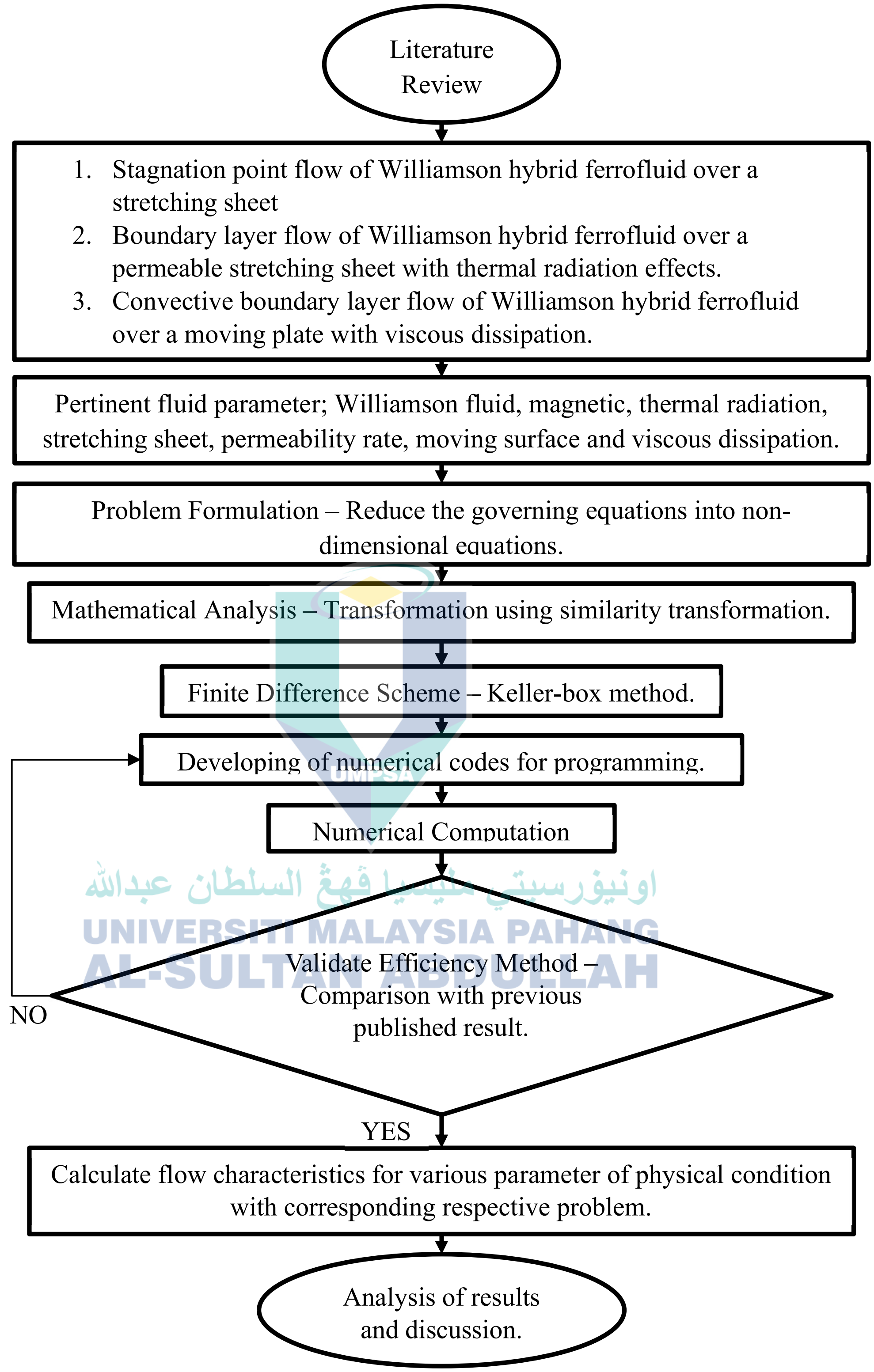

Figure 1.2 Flow chart solution procedures

1.5 Thesis Outline

This thesis contains 7 chapters that will discuss the convective boundary layer flow of Williamson hybrid ferrofluid. The preliminaries, which are Chapter 1, provide introductions to convective boundary layer theory, hybrid ferrofluid, and pseudo-plastic fluid models. This chapter also provides research objectives, research methodology, and problem statements.

The literature review is presented in Chapter 2, covering aspects such as stagnation points, stretching sheets, moving surfaces, and Williamson fluid. This chapter aims to highlight the significance, differences, and gaps in the information pertinent to this study.

The governing equation and numerical method specifically used to solve the first problem are discussed in Chapter 3, using the problem from Chapter 4. The Keller-Box method was chosen as the numerical method for this study because of its well-known reliability in producing numerical results. It is also able to solve ordinary differential equation problems in any order. The Keller-Box method is coded into MATLAB software to solve the equation numerically for each problem. Chapters 5 and 6 will use the same numerical method but with some adjustments to suit the problems, respectively.

Chapters 4, 5, and 6 discuss the results of problems i, ii, and iii that have been stated in Section 1.2, respectively. Using the numerical method from Chapter 3, each problem includes different pertinent parameters except for magnetic parameters and Williamson parameters, which are covered in all the problems studied. The Prandtl number is kept constant throughout the results since the base fluid of this new type of hybrid ferrofluid is human blood.

The conclusion of this research is articulated in Chapter 7, where the summary discusses the findings and conclusions of the study. Additionally, it proposes various conditions and parameters for future research to explore the characteristics of this new type of hybrid ferrofluid.

CHAPTER 2

LITERATURE REVIEW

2.1 Introduction

This chapter discussed previous research that has been done on certain aspects that are related to the scope of this research. Reviewing previous research is important as it will provide knowledge as well as discover significance, differences, and gaps in information and results in doing this research. Moreover, the mathematical models developed in this research resulted from reviewing and comparing previous research. Reviewing previous research will help strengthen the quality of the research, thus providing trusted results.

2.2 Williamson Hybrid Nanofluid

Section 1.1.2 describes the relationships between the Williamson fluid model and pseudo-plastic fluid, highlights the advantages of the Williamson model, and explores the connection between human blood and the Williamson model. This section will review past research on the Williamson fluid model to identify gaps and relationships with the current research on blood hybrid ferrofluid. Human blood, being the closest non-Newtonian fluid resembling a pseudo-plastic, reveals that the conventional Navier-Stokes equations are insufficient in capturing the necessary properties to reflect the model of fluid flow accurately. Hence, some adjustments to the Navier-Stokes equations suggested in the aforementioned literature must be made to accommodate this pseudo-plastic property.

Lyubimov and Perminov (2002), Daprà and Scarpi (2007), and Nadeem and Akbar (2011) expanded upon the Williamson model by examining the solution for a thin oblique layer flow, the fluid pulsatile flow in rock fracture, and the peristaltic flow with radially varying magnetohydrodynamics (MHD), respectively. Nadeem and Akram (2010b) presented their work on two-dimensional peristaltic flow in an asymmetrical channel using the perturbation expansion method to obtain an analytical solution to the non-linear problem. Another study of two-dimensional peristaltic flow was investigated by Nadeem and Akram (2010a), but under the influence of an inclined magnetic field and an inclined symmetric or asymmetrical channel. They were using lubrication to solve the numerical solution. Furthermore, Nadeem and Hussain (2016) concluded that Williamson nanofluid has better thermal conductivity compared to Williamson-based fluids. The homotopy analysis method was also used in this research. They found that the temperature profile increases as magnetic properties are inclined.

Recent studies regarding the heat transfer of Williamson fluid include those by Ahmed *et al.* (2021), where they found in their investigation Williamson nanofluid heat transfer characteristics where skin friction and reduced Nusselt number decrease as Williamson parameter increases. They were using the bvp4c method coded in MATLAB to solve numerically ordinary differential equations. The presence of graphene oxide in Williamson fluid was investigated by Al-Sankoor *et al.* (2021) using the Akbari Ganji method (AGM) and the homotopy perturbation method (HPM) for solving nonlinear equations. Haider *et al.* (2021) studied the thermal performance of hybrid nano-Williamson and found that the thermal conductivity performance of hybrid nanostructures is better than that of nanofluid. The nanoparticles that they were using were molybdenum disulfide and silicon dioxide. The thermal properties of motor oil as a Williamson fluid with a combination of molybdenum disulfide (MoS_2) and zinc oxide (ZnO) were investigated by Yahya *et al.* (2021). They used the Runge-Kutta method with a shooting methodology to solve the ordinary differential equation on a stretched sheet. They provide evidence that the temperature profile rises when Eckert numbers, heat sources, and biot numbers increase. A comparison between Cu -Williamson fluid and $Cu-Al$ -Williamson hybrid fluid was investigated by Almaneea (2022). Using the finite element method (FEM) to solve the model, they found that Lorentz force produces when the magnetic parameter increases for $Cu-Al$ -Williamson are greater than Cu -Williamson fluid. The effects of thermal radiation and the bioconvection of microorganisms in Williamson fluid flow over a stretching sheet under the influence of Brownian motion and thermophoresis diffusion were investigated by Asjad *et al.* (2022). The Runge-Kutta method with shooting technique was used in this research, and they found that temperature rises with parameters of Brownian motion and thermophoresis. Loganathan and Sangeetha (2022) claimed that the Williamson parameter reduces the temperature profile caused by the reduction of intermolecular collisions due to the ability of the Williamson fluid to withstand higher resistance.

Other research that has been reviewed includes studies by Krishnamurthy *et al.* (2016), Kho *et al.,* (2017; 2019), Hashim *et al.,* (2018; 2019a; 2019b), Jain and Parmar (2018), Rashid *et al.* (2020), Srinivasulu and Goud (2021) and Jalili *et al.* (2022). All of this research investigated Williamson fluid or Williamson nanofluid with various conditions, effects, and methods such as stretching sheet, peristaltic flow, thermal radiation and chemical effects, bvp4c function, RKF (45), AGM and HPM, etc.

2.3 Stagnation Point Flow of Williamson Hybrid Fluid

Stagnation point flow refers to the stagnation line generated when vertical flow collides with the horizontal surface. Hence, the term stagnation point flow is defined (Mohamed, 2013). The zone of stagnation located beneath the stagnation line generates the highest levels of pressure, heat transmission, and mass deposition (Wang, 2008; Nandy & Mahapatra, 2013). The external velocity is directed along the negative y-axis of the plate, whereas the strain rate is applied horizontally (Salleh, 2011). Furthermore, stagnation point flow exists in two types: axisymmetrical and plane (Chu *et al.,* 2021).

The problem involving stagnation points was first explored by Hiemenz (1911). He also succeeded in solving the exact value of the Navier-Stokes equation. Due to his findings, it attracts researchers to further explore this topic, such as Chao and Jeng (1965), who discovered that the time needed to reach a stagnation line for the thermal boundary layer is inversely proportional to the velocity stream and directly proportional to the ¼ power of the Prandtl number of the fluid. This topic is also extended by considering suction and blowing (Sano, 1981). It was found that accurate results of heat transfer are achieved with a large Prandtl number compared to the moderate Prandtl number of asymptotic solutions. Salleh *et al.* (2009) investigate two-dimensional forced convection at a forward stagnation point with Newtonian heating effects. The Keller-Box method was used in this research for numerical analysis. An investigation of radiation and chemical reaction effects near the region of stagnation point of a micropolar fluid was executed by Chamkha *et al.* (2015). Their assumption for this research was free stream velocity, and the surface temperature and concentration are assumed to vary linearly with the distance along the surface. Mabood *et al.* (2016) also studied radiation and chemical reactions as well as viscous dissipation effects on water-based nanofluids (Cu and Al_2O_3) using the Runge-Kutta-Fehlberg method to solve numerical equations. Hamid *et al.* (2016) have pointed out that stagnation is often studied with stretching sheets. The next sub-topic will review previous literature that studies this matter. Thompson and Troian slip boundary conditions were included in the investigation of the stagnation point of Casson nanofluid with thermal radiation impact (Akaje & Olajuwon, 2021). It is found that the temperature increases linearly with thermal radiation, Eckert number, and Casson parameter. Sahoo (2022) found that the boundary layer for fluids with very small viscosities will not be affected by the viscous effect in the investigation of viscous fluid flow in stagnation point flow. The Buongiorno model was used by Mabood *et al.* (2022) to study the stagnation point flow of viscoelastic nanofluid. Other research on stagnation points was accomplished by Mabood *et al.* (2022), Abbasi *et al.* (2022), and Rehman *et al.* (2022). They have included various parameters, various surfaces, and fluid models in their research on stagnation point flow.

Waqas *et al.* (2021) conducts research on the behavior of a hybrid nanofluid, $Fe_3O_4 - CuO / H_2O$, in the presence of a magnetic field to improve heat transmission on a horizontally stretchable surface. The heat transfer in the absence of a magnetic field is boosted by the collision of nanoparticles of varying sizes in the base fluid. They found that incorporation of Fe_3O_4 and CuO into a water-based fluid greatly enhanced the process of heat transmission. Khan *et al.* (2014b) examines the stagnation point flow and heat transfer characteristics of three different types of ferroparticles: magnetite (Fe_3O_4), cobalt ferrite ($CoFe_2O_4$), and $Mn-Zn$ ferrite ($Mn-ZnFe_2O_4$), when combined with water and kerosene as standard base fluids. Yasin *et al.* (2020) researched the stagnation point flow of ferrofluid with the presence of Newtonian heating. Using the Keller-box method to solve the numerical equations, they recorded inclination of ferrofluid thermal conductivity as the magnetite volume fraction increases. They extend their research on lower stagnation points of ferrofluid with mixed convection. Using the same method, viscosity and temperature of fluid can influence the velocity of ferrofluid (Yasin *et al.,* 2021a). Khashi'ie *et al.* (2022b) used the bvp4c function to analyze the dynamic unsteady separated stagnation point (USSP) flow and thermal behavior of $Fe_3O_4 - CoFe_2O_4 / H_2O$ on a mobile plate under the influence of heat generation and MHD influences.

2.4 Stretching Sheet in Williamson Hybrid Ferrofluid

As mentioned in Section 2.2, stagnation points often relate to the stretching sheet effect. A stretching sheet is defined as the velocity at the boundary layer moving away from a fixed point (Ishak, 2011; Yahaya *et al.,* 2018; Mohd Nasir *et al.,* 2020). The pioneer in exploring the convection boundary layer flow on a stretching sheet was Crane (1970). He learned that the boundary layer for fluid velocity varied linearly when investigating the incompressible viscous fluid flow over a stretching sheet. Some researchers have obtained closed-form solutions when extending Crane's research (Kumaran *et al.,* 2009). Nazar *et al.* (2004) and Ishak *et al.,* (2006; 2008) used the combination of similarity transformation and Keller-box method (KBM) to study the characteristics of boundary layer flow in the stagnation point for stretching, vertical and continuous, and vertical and linearly sheet, respectively, using different types of fluid. Many researchers who are interested in this topic also extend it to viscous fluid, viscoelastic fluid, micropolar fluid, nanofluid, and hybrid fluid. The stretching sheet is often encountered in real-life problems, and it also plays significant roles in numerous engineering and industrial applications such as microelectronics, microfluidics, transportation, manufacturing, stretching of plastic films, etc. (Nadeem *et al.,* 2013c; Devi & Anjali Devi, 2016, 2017; Zeeshan *et al.,* 2016).

Bachok *et al.* (2011b) study three types of nanofluid stagnation point flow over a stretching sheet. They were using water as the base fluid for all the nanofluids. The homotopy analysis approach was used by Khan *et al.* (2012) to investigate the viscoelastic fluid model with stretching effects. Mohamed *et al.,* (2012a; 2012b) studied the presence of Newtonian heating on the flow over as a stretching sheet using the shooting and Keller-box methods, respectively. After that, Mohamed *et al.,* (2013a; 2014) extended their research to thermal radiation effects using the Keller-Box method for numerical solutions. They found that temperature boundary layer flow declines while the velocity profile increases as the stretching parameter increases. Another study by Mohamed *et al.* (2013b) also stated the same finding in their numerical investigation of flow over stretching sheets with convective boundary conditions. Yacob and Ishak (2012) studied micropolar fluid flow over a stretching sheet using the Runge-Kutta-Fehlberg method and shooting technique. They also concluded with the same findings. Vittal *et al.* (2017a) studied the stagnation point flow and heat transfer of magnetohydrodynamics (MHD) on a stretching sheet submerged in a thermal stratified medium. Then, Nadeem *et al.,* (2013a; 2013; 2014) investigate the Williamson fluid flow over a stretching sheet using the homotopy analysis method to solve the reduced equations analytically. Nadeem found that the Williamson parameter reduces the velocity profile. They also presented the plotted graph of shear stress against the deformation rate and apparent viscosity against the deformation rate of Williamson fluid, with the Williamson parameter being, $\lambda = 0.4$. From both graphs, they concluded that the behavior is similar to that of a pseudo-plastic fluid.

A recent study on this topic was accomplished by Abbasian Arani and Aberoumand (2021). They investigated flow of hybrid $Ag - CuO$/water nanofluids over the permeable stretching sheet using Runge-Kutta-Fehlberg (RKF45) method with shooting technique. Anuar *et al.* (2021) also study the effect of permeable stretching sheets of $Ag - MgO$ water hybrid nanofluid flow. Bvp4c function in MATLAB is used in this investigation, revealing that Ag nanoparticle volume fraction in MgO/water nanofluid declines the local Nusselt number. Another research of hybrid nanofluid with permeable stretching sheets was discussed by Zainal *et al.* (2021). They studied $Al_2O_3 - Cu$/water hybrid nanofluid using bvp4v function. Investigation of permeable stretching curved surface Williamson nanofluid was studied by Ahmed *et al.* (2021). They found that increasing the permeability parameter reduces the velocity profile due to the porosity of the surface increases. Kausar *et al.* (2022) concluded that Eckert number and radiation parameter increases the temperature in their study of micropolar nanofluid flow towards a permeable stretching sheet using Tiwari–Das nanofluid model. Dawar *et al.* (2023) researched the characteristics of copper nanofluid on the stagnation point flow with the effect of solar radiation. Other research that is reviewed included from Ullah

Awan *et al.* (2022), Jalili *et al.* (2022), Sinha and Sarma (2020), Mohamed *et al.* (2020a), and Khashi'ie *et al.* (2020a; 2020b).

Yasin *et al.* (2018a) and Mohamed *et al.* (2019b) both studied the stagnation point flow of ferrofluid with the effect of Newtonian heating and thermal radiation and stretching sheets with Newtonian heating, respectively. Imtiaz *et al.* (2017) investigate the movement of ferrofluid over a curved, stretched surface with heterogeneous responses. The wall surface undergoes heterogeneous reactions that follow isothermal cubic auto-catalator kinetics. They found that larger curvature values enhanced the magnitude of velocity. The effect of homogeneous-heterogeneous reactions on ferrofluid was studied by Nadeem *et al.* (2017). They discovered that fluid particle motion is slowed down by magneto-thermomechanical interaction, increasing skin friction and slowing down the rate of heat transfer at a cylinder's surface. Jalili *et al.* (2019) investigated the ferrofluid's microstructure and inertial properties throughout a stretching sheet. The governing equation was formulated based on the Tiwari-Das nanofluid model, where Fe_3O_4 as a nanoparticle and water as a base fluid. They discovered that the presence of the magnetic parameter causes an increase in the thickness of the thermal boundary layer using two semi-analytical methods: the homotopy perturbation method (HPM) and Akbari-Ganji's method (AGM). Rashad (2017) conducted a study on the effect of anisotropic slip on the transient three-dimensional magnetohydrodynamic (MHD) flow of cobalt-kerosene ferrofluid over an inclined radiating stretching surface. Rashad employed the Thomas algorithm, utilizing a finite-difference approach, to solve the governing partial differential equations in his work.

2.5 Moving Surface in Williamson Hybrid Ferrofluid

Studying the flow of the boundary layer on a plate or surface that is in motion is crucial due to its relevance in various technological processes. Examples of applications that use flow over a moving plate are metal and plastic extrusion, glass blowing hot rolling, and electro timing of copper wire (Raju, 2022). Sakiadis (1961) was the first to investigate the concept and formulation of boundary layer flow over a moving plate. He specifically examined the scenario when the plate was moving at a constant speed. This form of flow is characterized by the introduction of surrounding fluid, setting it apart from Blasius flow (Sravanthi *et al.,* 2022). In their study, Cao *et al.* (2016) examined the impact of a moving plate on a fractional Maxwell viscoelastic nanofluid. They achieved this by integrating the finite-difference approach with the L1-algorithm. In their study, Aladdin *et al.* (2020) found that the increment of shear stress for hybrid nanofluid is better than nanofluid. Reduction of temperature profile as moving parameter increases in an investigation of water hybrid nanofluid ($SiO_2 - MoS_2$) flow by Yaseen *et al.* (2021) using bvp4c method. Khashi'ie *et al.* (2022a) concluded that the inclusion of small-scale suction and magnetic field effects is recommended for cooling and heating industries to increase the heat transfer rate of hybrid nanofluid. Bachok *et al.* (2012) conducted an investigation on the features of three types of nanofluid, namely Copper (Cu), Alumina (Al_2O_3), and Titania (TiO_2), in their ability to expand the Blasius and Sakiadis problems. Asshaari *et al.* (2023) investigated the heat and mass transport properties of water-based nanofluids containing carbon nanotubes flowing between moving plates. They utilized the Tiwari and Das, and Buongiorno nanofluid model for their investigation. The effect of viscous dissipation with vertical moving plate of nanofluid was discussed by Mohamed *et al.* (2020c). Using the Keller-box method, Mohamed found that moving parameters reduce the thermal boundary layer flow. Megahed (2019) studies the effects of viscous dissipation and slip velocity on the Williamson fluid flow. They found that the heat transfer performance increased in slip velocity and viscosity parameter. Increasing Williamson fluid and suction/injection parameters, Khan *et al.* (2018) found that the velocity profile decreases in their paper analyzing relations of magneto-nanoparticles in Williamson fluid flow over convective oscillatory moving surface.

Ramli *et al.* (2017) utilized the shooting method to examine the slip impact of ferrofluid flow across a mobile flat plate. They studied three type of ferroparticles, magnetite (Fe_3O_4), cobalt ferrite ($CoFe_2O_4$) and Mangane-zinc ferrite ($Mn - ZnFe_2O_4$) with water-based fluid. Tripple solutions exist when moving parameter are applied in the research of stability analysis of mixed convection flow (Ramli & Ahmad, 2019). Sravanthi *et al.* (2022) examined the properties of a magnetite-water nano liquid in the presence of permeable moving plates. Idris *et al.* (2023) investigates the rheological properties and thermal conductivity characteristics of a hybrid ferrofluid

$Fe_3O_4 - CoFe_2O_4$/water flowing over a porous moving surface. By employing the bvp4pc approach, they found that the use of a 1% volume fraction of Fe_3O_4 and $CoFe_2O_4$ in the hybrid ferrofluid resulted in a higher convective heat transfer rate compared to both the mono-ferrofluid and water, with enhancements of 2.75% and 6.91% respectively. Kamis *et al.* (2023) examines the ferrohydrodynamic interaction of hybrid magnetic nanoparticles in a mixture of ethylene glycol and water flowing over an inclined stretched sheet, while considering the magnetic dipole effect. An increase in the inclination angle and mixed convective parameter was found to boost the velocity profile and Nusselt number, according to their assertion.

After reviewing previous research on Williamson hybrid ferrofluid from different aspects that presented in Section 2.2 to 2.5, it can be concluded that research on the Williamson fluid model on blood hybrid ferrofluid was not available during the time of executing this research. Therefore, this issue is new and relevant to be studied.

CHAPTER 3

METHODOLOGY

3.1 Introduction

This chapter outlines the process of deriving the fundamental equations that regulate the movement of Williamson hybrid ferrofluid. The derivation begins with the conservation equations, which are first written in vector form. In addition, this chapter will provide a comprehensive explanation of the process of solving the modified ordinary differential equations for the initial issue, which entails analyzing the flow of Williamson hybrid ferrofluid at a stagnation point across a stretched sheet. The Keller-box method, is an implicit finite difference technique, is implemented and programmed in MATLAB software. In Chapter 4, the discussion on the results of this problem with the Keller-box approach is continued. This numerical approach will also be employed in Chapter 5 and Chapter 6 to solve the numerical equations correspondingly.

3.2 Governing Equation

The fundamental equation in fluid dynamics is derived from the principles of conservation, namely the laws of mass, momentum, and energy conservation. Bejan (1984) provides the vector version of the governing equations for continuity, momentum, and energy for an incompressible viscous fluid:

Continuity equation

$$\frac{\partial \rho}{\partial t} + \nabla.\left(\rho \underline{u}\right) = 0 \qquad 3.1$$

Momentum equation

$$\rho\left(\frac{\partial v}{\partial t} + \frac{D\underline{u}}{Dt}\right) = -\nabla p + \nabla.S + \underline{F}, \qquad 3.2$$

Energy equation

$$\left(\rho C\right)_p \frac{DT}{Dt} = k\nabla^2 T + \mu\Phi, \qquad 3.3$$

with

$$\frac{D}{Dt} = \frac{\partial}{\partial t} + u.\nabla = \frac{\partial}{\partial t} + u\frac{\partial}{\partial x} + v\frac{\partial}{\partial y} + w\frac{\partial}{\partial z},$$

$$\nabla = \frac{\partial}{\partial x}\mathbf{i} + \frac{\partial}{\partial y}\mathbf{j} + \frac{\partial}{\partial z}\mathbf{k}, \qquad 3.4$$

where $\underline{u}$ represents a velocity component and $\underline{F}$ represents a force. Other definitions for other variables are as follows: ρ represents fluid density, p represents pressure, μ represents dynamic viscosity, t represents time, T represents temperature, C_p represents specific heat at constant pressure, k represents thermal conductivity, Cauchy stress tensor is denoted by the symbol S. Finally, x and y denote the Cartesian coordinates parallel and perpendicular to the surface, respectively. Φ refers to the viscous dissipation function, whereas the material derivative is represented by $\frac{D}{Dt}$. The omission of the viscous dissipation function, Φ in Equation 3.3, is justified due to the low flow velocities and the presence of free convection, as stated by Ozisik (1985) and Lok (2002).

This thesis investigates a steady two-dimensional flow in an incompressible fluid; consequently, the variable t is disregarded. The fluid properties, including specific heat, thermal conductivity, and viscosity, remain unchanged. The Equations 3.1 - 3.3, as discussed before, can be represented as (Nadeem & Hussain, 2013).

$$\frac{\partial u}{\partial x} + \frac{\partial v}{\partial y} = 0, \qquad 3.5$$

$$u\frac{\partial u}{\partial x} + v\frac{\partial u}{\partial y} = -\frac{1}{\rho}\frac{dp}{dx} + \frac{\partial \tau_{xx}}{\partial x} + \frac{\partial \tau_{xy}}{\partial y} + F_x, \qquad 3.6$$

$$u\frac{\partial v}{\partial x}+v\frac{\partial v}{\partial y}=-\frac{1}{\rho}\frac{dp}{dy}+\frac{\partial \tau_{yx}}{\partial x}+\frac{\partial \tau_{yy}}{\partial y}+F_y, \tag{3.7}$$

$$u\frac{\partial T}{\partial x}+v\frac{\partial T}{\partial y}=\frac{k}{(\rho C_p)}\left(\frac{\partial^2 T}{\partial x^2}+\frac{\partial^2 T}{\partial y^2}\right). \tag{3.8}$$

where u represents the velocity in the x direction, whereas v represents the velocity in the y direction. The body force per unit volume is composed of two components, F_x and F_y. Additionally, the thermal diffusivity is represented by the variable $\frac{k}{(\rho C_p)}$. τ_{xx}, τ_{yx}, τ_{xy}, and τ_{yy} defines as the extra stress tensor, which will be explained in Section 3.3.

3.3 Williamson Hybrid Ferrofluid Model

For an incompressible Williamson fluid model, the Cauchy stress tensor is given by (Nadeem & Hussain, 2013; 2013c; Kebede *et al.,* 2020; Ibrahim & Negera, 2020):

$$S=-\mathrm{pI}+\tau, \tag{3.9}$$

$$\tau=\left[\mu_\infty+\frac{(\mu_0-\mu_\infty)}{1-\Gamma\dot{\gamma}}\right]A_1, \tag{3.10}$$

where I represents the identity vector, p represents pressure, μ_0 and μ_∞ represent the limiting viscosities at zero and infinite shear rate respectively, Γ is a positive time constant, A_1 represents the first Rivlin-Erickson tensor, and $\dot{\gamma}$ is defined as follows (Nadeem & Hussain, 2013; 2013c):

$$\dot{\gamma}=\sqrt{\frac{1}{2}\pi},\ \pi=\mathrm{trace}\left(A_1^2\right), \tag{3.11}$$

$$\dot{\gamma}=\left[\left(\frac{\partial u}{\partial x}\right)^2+\frac{1}{2}\left(\frac{\partial u}{\partial y}+\frac{\partial v}{\partial x}\right)^2+\left(\frac{\partial v}{\partial y}\right)^2\right]^{\frac{1}{2}}. \tag{3.12}$$

π represents the second invariant of the strain tensor. Only the scenario when μ_∞ and μ_0 is equal to zero and $\Gamma\dot{\gamma}$ is less than one has been taken into account. Therefore, the additional stress tensor is expressed as (Nadeem & Hussain, 2013; 2013c; Kebede *et al.,* 2020):

$$\tau = \left[\frac{\mu_0}{1-\Gamma\dot{\gamma}}\right]A_1, \qquad 3.13$$

using binomial expansion we get:

$$\tau = \mu_0\left[1-\Gamma\dot{\gamma}\right]A_1. \qquad 3.14$$

The components of the extra stress tensor are:

$$\begin{aligned}
\tau_{xx} &= 2\mu_0\left[1+\Gamma\dot{\gamma}\right]\frac{\partial u}{\partial x}, \\
\tau_{xy} &= \tau_{yx} = \mu_0\left[1+\Gamma\dot{\gamma}\right]\left(\frac{\partial u}{\partial y}+\frac{\partial v}{\partial x}\right), \\
\tau_{yy} &= 2\mu_0\left[1+\Gamma\dot{\gamma}\right]\frac{\partial v}{\partial y}, \\
\tau_{xz} &= \tau_{yz} = \tau_{zx} = \tau_{zz} = 0.
\end{aligned} \qquad 3.15$$

Substitute Equation 3.12 and 3.15 into the components of tensor in x-momentum, Equation 3.6, and y-momentum, Equation 3.7, the components become (Nadeem, 2013):

$$
\begin{aligned}
u\frac{\partial u}{\partial x}+v\frac{\partial u}{\partial y}=&-\frac{1}{\rho_{hnf}}\frac{dp}{dx}\\
&+\frac{\partial}{\partial x}\left[\frac{2\mu_{hnf}}{\rho_{hnf}}\left\{\frac{\partial u}{\partial x}+\Gamma\frac{\partial u}{\partial x}\left\{\begin{matrix}\left(\frac{\partial u}{\partial x}\right)^{2}\\+\frac{1}{2}\left(\frac{\partial u}{\partial y}+\frac{\partial v}{\partial x}\right)^{2}\\+\left(\frac{\partial v}{\partial y}\right)^{2}\end{matrix}\right\}^{\frac{1}{2}}\right\}\right]\\
&+\frac{\partial}{\partial x}\left[\frac{\mu_{hnf}}{\rho_{hnf}}\left\{1+\Gamma\left\{\begin{matrix}\left(\frac{\partial u}{\partial x}\right)^{2}\\+\frac{1}{2}\left(\frac{\partial u}{\partial y}+\frac{\partial v}{\partial x}\right)^{2}\\+\left(\frac{\partial v}{\partial y}\right)^{2}\end{matrix}\right\}^{\frac{1}{2}}\right\}\left(\frac{\partial u}{\partial y}+\frac{\partial v}{\partial x}\right)\right]\\
&+F_{x},
\end{aligned}
\qquad 3.16
$$

$$
\begin{aligned}
u\frac{\partial v}{\partial x}+v\frac{\partial v}{\partial y} &= -\frac{1}{\rho_{hnf}}\frac{dp}{dy} \\
&+\frac{\partial}{\partial x}\left[\frac{\mu_{hnf}}{\rho_{hnf}}\left\{1+\Gamma\left\{\begin{array}{l}\left(\frac{\partial u}{\partial x}\right)^2\\ +\frac{1}{2}\left(\frac{\partial u}{\partial y}+\frac{\partial v}{\partial x}\right)^2\\ +\left(\frac{\partial v}{\partial y}\right)^2\end{array}\right\}^{\frac{1}{2}}\right\}\left(\frac{\partial u}{\partial y}+\frac{\partial v}{\partial x}\right)\right] \\
&+\frac{\partial}{\partial x}\left[\frac{2\mu_{hnf}}{\rho_{hnf}}\left\{\frac{\partial v}{\partial y}+\Gamma\frac{\partial v}{\partial y}\left\{\begin{array}{l}\left(\frac{\partial u}{\partial x}\right)^2\\ +\frac{1}{2}\left(\frac{\partial u}{\partial y}+\frac{\partial v}{\partial x}\right)^2\\ +\left(\frac{\partial v}{\partial y}\right)^2\end{array}\right\}^{\frac{1}{2}}\right\}\right] \\
&+F_y.
\end{aligned}
\tag{3.17}
$$

$$
u\frac{\partial T}{\partial x}+v\frac{\partial T}{\partial y}=\frac{k_{hnf}}{\left(\rho C_p\right)_{hnf}}\left(\frac{\partial^2 T}{\partial x^2}+\frac{\partial^2 T}{\partial y^2}\right),
\tag{3.18}
$$

where $\nu_{hnf}=\dfrac{\mu_{hnf}}{\rho_{hnf}}$ as the hybrid ferrofluid kinematic viscosity. The hybrid ferrofluid dynamic viscosity, and density are denoted as μ_{hnf} and ρ_{hnf} respectively. T is the temperature inside the boundary layer, $(\rho C_p)_{hnf}$ is the heat capacity of hybrid ferrofluid, and k_{hnf} is the thermal conductivity of Williamson hybrid ferrofluid. Next, B_0 is the magnetic field and σ is the electric conductivity.

Other properties related to base fluid and the nanoparticles are denoted with subscript bf and $s1$, s2 respectively (Devi & Anjali Devi, 2017) as shown in Equation 3.19:

$$
\begin{aligned}
&\nu_{hnf} = \frac{\mu_{hnf}}{\rho_{hnf}}, \qquad \mu_{hnf} = \frac{\mu_f}{(1-\phi_1)^{2.5}(1-\phi_2)^{2.5}}, \\
&\rho_{hnf} = (1-\phi_2)\left[(1-\phi_1)\rho_f + \phi_1\rho_{s1}\right] + \phi_2\rho_{s2}, \\
&\left(\rho C_p\right)_{hnf} = (1-\phi_2)\left[(1-\phi_1)\left(\rho C_p\right)_f + \phi_1\left(\rho C_p\right)_{s1}\right] + \phi_2\left(\rho C_p\right)_{s2}, \\
&\frac{k_{hnf}}{k_{bf}} = \frac{k_{s2} + 2k_{bf} - 2\phi_2(k_{bf} - k_{s2})}{k_{s2} + 2k_{bf} + \phi_2(k_{bf} - k_{s2})}, \\
&\frac{k_{bf}}{k_f} = \frac{k_{s1} + 2k_f - 2\phi_1(k_f - k_{s1})}{k_{s1} + 2k_f + \phi_1(k_f - k_{s1})}, \\
&\frac{\nu_{hnf}}{\nu_f} = \frac{1}{(1-\phi_1)^{2.5}(1-\phi_2)^{2.5}\left[(1-\phi_2) + \left[(1-\phi_1) + \phi_1\frac{\rho_{s1}}{\rho_f}\right] + \phi_2\frac{\rho_{s2}}{\rho_f}\right]}, \\
&\frac{\left(\rho C_p\right)_f}{\left(\rho C_p\right)_{hnf}} = \frac{1}{(1-\phi_2)\left[(1-\phi_1)\rho_f + \phi_1\frac{(\rho C_p)_{s1}}{(\rho C_p)_f}\right] + \phi_2\frac{(\rho C_p)_{s2}}{(\rho C_p)_f}},
\end{aligned} \tag{3.19}
$$

where ϕ_1, ϕ_2 are the nanoparticles volume fractions.

3.4 Volume Force

Volume force refers to the forces exerted on the flow of fluid. It is alternatively referred to as the long-range force. The magnitude of this force exhibits gradual variations and exerts a consistent effect on every component of a fluid motion. Examples of such forces include gravitational and magnetic forces from a momentum equation. According to Kasim (2014) and Ahmed *et al.* (2012) $F = \left(F_x, F_y, 0\right)$ is defined as

$$
F = \rho g + J \times B. \tag{3.20}
$$

J represents current density, g represents the gravitational field and B represents the external magnetic field. $\left(J \times B\right)$ represents the Lorentz force that arises from the interaction between the velocity of the fluid and the magnetic field that is applied. Cowling (1976) and Kasim (2014) asserted that the mechanical force $J \times B$ exerted by the electromagnetic force is at a right angle to the magnetic field. Therefore, the motion parallel to the field is unaffected. The current density may be determined by applying Ohm's law.

$$J = \sigma\left(E + V \times B\right). \qquad 3.21$$

σ represents the electrical conductivity of the fluid, E represents the electric field, $B = B_0 + b$ with $B_0 = \left(0, 0, B_0\right)$ represents the magnetic field, and b represents the induced magnetic field. Both the electric field and the induced magnetic field are disregarded in this study because of the minimal magnetic Reynolds number, as stated by Nihoul (1967) and Mangi (2013). Hence,

$$J = \sigma\left(V \times B_0\right). \qquad 3.22$$

Substituting Equation 3.22 into Equation 3.20, we obtain

$$F = \rho g + \sigma\left(V \times B_0\right) \times B_0. \qquad 3.23$$

Since

$$\left(V \times B_0\right) \times B_0 = \begin{vmatrix} i & j & k \\ u & v & 0 \\ 0 & 0 & B_0 \end{vmatrix} \times B_0, \qquad 3.24$$

the above expression is calculated and obtained as

$$\left(V \times B_0\right) \times B_0 = \left(-uB_0^2, -vB_0^2, 0\right). \qquad 3.25$$

Then the Equation 3.23 becomes

$$F = \rho g + \sigma\left(-uB_0^2, -vB_0^2, 0\right). \qquad 3.26$$

In the context of two-dimensional flows, the gravitational force is typically denoted as $g=\left(-g_x.-g_y,0\right)$. Equation 3.26 can be expressed as

$$F=\left(F_x,F_y,0\right)=\rho\left(-g_x.-g_y,0\right)+\sigma\left(-uB_0^2,-vB_0^2,0\right). \tag{3.27}$$

This research considered forced convection where $g=0$. Hence, the gravitational term can be disregarded. This is due to the little impact of gravity force on the fluid flow over a flat plate. Thus, Equation 3.16 and 3.17 can be expressed as

$$\begin{aligned}
u\frac{\partial u}{\partial x}+v\frac{\partial u}{\partial y}=&-\frac{1}{\rho_{hnf}}\frac{dp}{dx}\\
&+\frac{\partial}{\partial x}\left[\frac{2\mu_{hnf}}{\rho_{hnf}}\left\{\frac{\partial u}{\partial x}+\Gamma\frac{\partial u}{\partial x}\left\{\begin{array}{l}\left(\frac{\partial u}{\partial x}\right)^2\\+\frac{1}{2}\left(\frac{\partial u}{\partial y}+\frac{\partial v}{\partial x}\right)^2\\+\left(\frac{\partial v}{\partial y}\right)^2\end{array}\right\}^{\frac{1}{2}}\right\}\right]\\
&+\frac{\partial}{\partial x}\left[\frac{\mu_{hnf}}{\rho_{hnf}}\left\{1+\Gamma\left\{\begin{array}{l}\left(\frac{\partial u}{\partial x}\right)^2\\+\frac{1}{2}\left(\frac{\partial u}{\partial y}+\frac{\partial v}{\partial x}\right)^2\\+\left(\frac{\partial v}{\partial y}\right)^2\end{array}\right\}^{\frac{1}{2}}\right\}\left(\frac{\partial u}{\partial y}+\frac{\partial v}{\partial x}\right)\right]\\
&-\frac{\sigma u B_0^2}{\rho},
\end{aligned} \tag{3.28}$$

$$
\begin{aligned}
u\frac{\partial v}{\partial x}+v\frac{\partial v}{\partial y}=&-\frac{1}{\rho_{hnf}}\frac{dp}{dy}\\
&+\frac{\partial}{\partial x}\left[\frac{\mu_{hnf}}{\rho_{hnf}}\left\{1+\Gamma\left\{\begin{matrix}\left(\frac{\partial u}{\partial x}\right)^2\\ +\frac{1}{2}\left(\frac{\partial u}{\partial y}+\frac{\partial v}{\partial x}\right)^2\\ +\left(\frac{\partial v}{\partial y}\right)^2\end{matrix}\right\}^{\frac{1}{2}}\right\}\left(\frac{\partial u}{\partial y}+\frac{\partial v}{\partial x}\right)\right]\\
&+\frac{\partial}{\partial x}\left[\frac{2\mu_{hnf}}{\rho_{hnf}}\left\{\frac{\partial v}{\partial y}+\Gamma\frac{\partial v}{\partial y}\left\{\begin{matrix}\left(\frac{\partial u}{\partial x}\right)^2+\frac{1}{2}\left(\frac{\partial u}{\partial y}+\frac{\partial v}{\partial x}\right)^2\\ +\left(\frac{\partial v}{\partial y}\right)^2\end{matrix}\right\}^{\frac{1}{2}}\right\}\right]\\
&-\frac{\sigma v B_0^2}{\rho},
\end{aligned}
\tag{3.29}
$$

3.5 Order of Magnitude Analysis

The expansion of Equations 3.28 and 3.29 becomes intricate, resulting in an elliptical form similar to that in energy Equation 3.18, posing a challenge for resolution. The Equations 3.18, 3.28, and 3.29 can be transformed into a parabolic form by removing the second derivatives with regard to x or y. Solving parabolic partial differential equations is more manageable (Anderson *et al.,* 1997; Ishak, 2008).

In order to transform the elliptic equations into parabolic equations, it is important to eliminate one of the second derivative elements by assessing its magnitude. The smallest term in an equation will be deleted when compared to the other terms (Ahmad, 2009). This is due to the fact that tiny values have less impact and may be disregarded in the context of the boundary layer flow.

Considering the assumption by Nadeem and Hussain (2013), it is assumed that the boundary layer approximations to the components of the tensor, we find that the order of x, T and u is 1, whereas the order of Γ, y, and v is δ. Apply this on x-momentum Equation 3.28 it becomes:

$$
\begin{aligned}
u\frac{\partial u}{\partial x}+v\frac{\partial u}{\partial y} &= -\frac{1}{\rho_{hnf}}\frac{dp}{dx} \\
&+\frac{\partial}{\partial x}\left[\frac{2\mu_{hnf}}{\rho_{hnf}}\left\{\frac{\partial u}{\partial x}+\Gamma\frac{\partial u}{\partial x}\left\{\begin{matrix}\left(\frac{\partial u}{\partial x}\right)^2+\frac{1}{2}\left(\frac{\partial u}{\partial y}+\frac{\partial v}{\partial x}\right)^2 \\ +\left(\frac{\partial v}{\partial y}\right)^2\end{matrix}\right\}^{\frac{1}{2}}\right\}\right] \\
&+\frac{\partial}{\partial x}\left[\frac{\mu_{hnf}}{\rho_{hnf}}\left\{1+\Gamma\left\{\begin{matrix}\left(\frac{\partial u}{\partial x}\right)^2+\frac{1}{2}\left(\frac{\partial u}{\partial y}+\frac{\partial v}{\partial x}\right)^2 \\ +\left(\frac{\partial v}{\partial y}\right)^2\end{matrix}\right\}^{\frac{1}{2}}\right\}\left(\frac{\partial u}{\partial y}+\frac{\partial v}{\partial x}\right)\right] \qquad 3.30 \\
&-\frac{\sigma u B_0^2}{\rho}.
\end{aligned}
$$

$$
\begin{aligned}
&1 \quad 1 \quad 1 \\
&1\left[\delta^2 \quad \left\{1 \quad \delta^2 \quad \left\{1 \quad \frac{1}{\delta^2} \quad \delta^2 \quad 1\right\}^{1/2}\right\}\right] \\
&1\left[\delta^2\left\{1 \quad \delta\left\{1 \quad \frac{1}{\delta^2} \quad \delta^2 \quad 1\right\}^{1/2}\right\}\left(\frac{1}{\delta} \quad \delta\right)\right] \\
&1.
\end{aligned}
$$

Comparing the order of each term in Equation 3.28, the term with order 1 remains while the term with order dell will be eliminated. It is suggested that, all of the term in τ_{xx} are neglected except the term $\frac{\partial^2 u}{\partial y^2}$ and $\sqrt{2}\Gamma\frac{\partial u}{\partial y}\frac{\partial^2 u}{\partial y^2}$ in τ_{xy}.

For y-momentum Equation 3.29

$$
\begin{aligned}
u\frac{\partial v}{\partial x}+v\frac{\partial v}{\partial y} &= -\frac{1}{\rho_{hnf}}\frac{dp}{dy} \\
&\quad +\frac{\partial}{\partial x}\left[\frac{\mu_{hnf}}{\rho_{hnf}}\left\{1+\Gamma\left\{\begin{matrix}\left(\dfrac{\partial u}{\partial x}\right)^2 \\ +\dfrac{1}{2}\left(\dfrac{\partial u}{\partial y}+\dfrac{\partial v}{\partial x}\right)^2 \\ +\left(\dfrac{\partial v}{\partial y}\right)^2\end{matrix}\right\}^{\frac{1}{2}}\right\}\left(\frac{\partial u}{\partial y}+\frac{\partial v}{\partial x}\right)\right] \\
&\quad +\frac{\partial}{\partial x}\left[\frac{2\mu_{hnf}}{\rho_{hnf}}\left\{\frac{\partial v}{\partial y}+\Gamma\frac{\partial v}{\partial y}\left\{\begin{matrix}\left(\dfrac{\partial u}{\partial x}\right)^2 \\ +\dfrac{1}{2}\left(\dfrac{\partial u}{\partial y}+\dfrac{\partial v}{\partial x}\right)^2+\left(\dfrac{\partial v}{\partial y}\right)^2\end{matrix}\right\}^{\frac{1}{2}}\right\}\right] \\
&\quad -\frac{\sigma v B_0^2}{\rho},
\end{aligned}
\qquad 3.31
$$

$$
\begin{aligned}
&\delta \quad \delta \quad \frac{1}{\delta} \\
&1\left[\delta^2 \quad \left\{1 \quad \delta \quad \left\{1 \quad \frac{1}{\delta^2} \quad \delta^2 \quad 1\right\}^{1/2}\right\} \quad \left(\frac{1}{\delta} \quad \delta\right)\right] \\
&1\left[\delta^2 \quad \left\{1 \quad \delta \quad \left\{1 \quad \frac{1}{\delta^2} \quad \delta^2 \quad 1\right\}^{1/2}\right\}\right] \\
&\delta.
\end{aligned}
$$

Interestingly, all the term in this equation is neglected except for $-\frac{1}{\rho}\frac{dp}{dy}$. Lastly, for the energy equation, the order of magnitude analysis is as follows:

$$
\begin{aligned}
u\frac{\partial T}{\partial x} \quad + \quad v\frac{\partial T}{\partial y} \quad &= \quad \frac{k_{hnf}}{\left(\rho C_p\right)_{hnf}}\left(\frac{\partial^2 T}{\partial x^2}+\frac{\partial^2 T}{\partial y^2}\right), \\
1 \quad 1 \quad &\delta^2 \quad \left(1 \quad \frac{1}{\delta^2}\right).
\end{aligned}
\qquad 3.32
$$

From the order of magnitude analysis, the term $\frac{\partial^2 T}{\partial x^2}$ have a δ^2 order thus will be eliminated while $\frac{\partial^2 T}{\partial y^2}$ with order 1 will remained.

In overall, from the order of magnitude analysis, the governing equation of the boundary layer flow in Williamson hybrid ferrofluid can be written as:

$$\frac{\partial u}{\partial x}+\frac{\partial v}{\partial y}=0, \tag{3.33}$$

$$u\frac{\partial u}{\partial x}+v\frac{\partial u}{\partial y}=v_{hnf}\frac{\partial^2 u}{\partial y^2}-\frac{1}{\rho_{hnf}}\frac{dp}{dx}+\sqrt{2}v_{hnf}\Gamma\frac{\partial u}{\partial y}\frac{\partial^2 u}{\partial y^2}-\frac{1}{\rho_{hnf}}\sigma u B_0^2, \tag{3.34}$$

$$0=-\frac{1}{\rho_{hnf}}\frac{dp}{dy}, \tag{3.35}$$

$$u\frac{\partial T}{\partial x}+v\frac{\partial T}{\partial y}=\frac{k_{hnf}}{\left(\rho C_p\right)_{hnf}}\frac{\partial^2 T}{\partial y^2}. \tag{3.36}$$

3.6 Stagnation Point Flow of Williamson Hybrid Ferrofluid Over a Stretching Sheet

Considering the steady flow of a two-dimensional hybrid ferrofluid in blood on a stagnation point over a stretched sheet with ambient temperature, T_∞. Let's assume that u represents the velocity component along the $x-$ axis, whereas v represents the velocity component along the $y-$ axis. B_0 represents the magnetic field. It is assumed that the stretching velocity $u_w(x)=ax$ and the free stream velocity $U_\infty=bx$ can be expressed in linear forms, with a and b being positive constants (Mohamed *et al.,* 2012b).

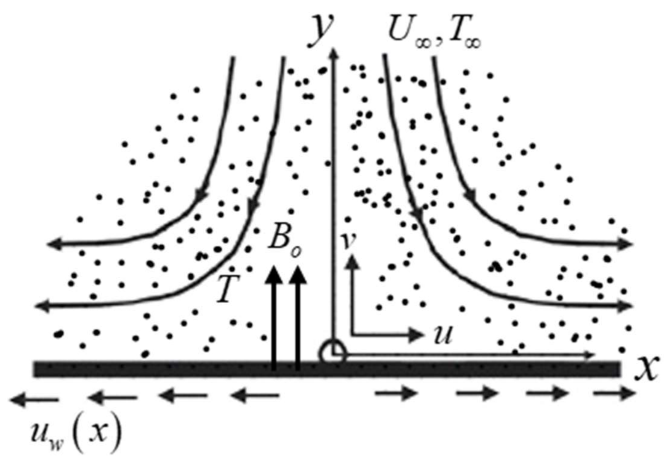

Figure 3.1 Physical model and the coordinate system of Williamson hybrid ferrofluid on a stagnation point of a stretching sheet

Under the assumption that the boundary layer is valid, the dimensional gov equation can be written in cartesian coordinates as in Equations 3.33-3.36 subjected to the boundary conditions.

$$
\begin{aligned}
u = u_w,\ v = 0,\ T = T_w \ \text{at}\ y = 0,\\
u = U_\infty,\ T \rightarrow T_\infty \ \text{as y} \rightarrow \infty.
\end{aligned}
\qquad 3.37
$$

From Equation 3.35, it can be shown that the pressure p is solely dependent on x. Consequently, the pressure gradient $\frac{dp}{dx}$ may be derived from Equation 3.34 and become:

$$\frac{1}{\rho_{hnf}}\frac{dp}{dx} = -U_\infty \frac{\partial U}{\partial x} - \frac{1}{\rho_{hnf}}\sigma B_0^2 U_\infty, \qquad 3.38$$

where U_∞ is the free stream velocity. By substituting Equation 3.38 into Equation 3.34, it becomes

$$u\frac{\partial u}{\partial x} + v\frac{\partial u}{\partial y} = v_{hnf}\frac{\partial^2 u}{\partial y^2} + U_\infty \frac{\partial U_\infty}{\partial x} + \sqrt{2}v_{hnf}\Gamma\frac{\partial u}{\partial y}\frac{\partial^2 u}{\partial y^2} - \frac{\sigma B_0^2}{\rho_{hnf}}\left(u - U_\infty\right). \qquad 3.39$$

3.7 Similarity Transformation

Equations 3.33, 3.36, and 3.39 are non-linear partial differential equations with several dependent and independent variables. Furthermore, it exists in many dimensions configurations, hence posing challenges in direct solutions. Thus, the method of similarity transformation is utilised. (Merkin, 1994; Lesnic *et al.,* 1999; Salleh *et al.,* 2010; Yacob & Ishak, 2012; Hashim *et al.,* 2015; Hashim *et al.,* 2019b; Sarif *et al.,* 2013):

$$\eta = \left(\frac{b}{\nu_f}\right)^{1/2} y, \quad \psi = \left(b\nu_f\right)^{1/2} xf(\eta), \quad \theta(\eta) = \frac{T - T_\infty}{T_w - T_\infty}, \qquad 3.40$$

Equation 3.40 presents the similarity variables where η and θ is a non-dimensional variable while ψ is the stream function where is the stream function defined as $u = \frac{\partial \psi}{\partial y}$ and $v = -\frac{\partial \psi}{\partial x}$. Then, u and v can be derived as

$$u = bxf'(\eta), \; v = -(b\nu_f)^{1/2} f(\eta),$$

with

$$\frac{\partial u}{\partial x} = bf'(\eta), \; \frac{\partial v}{\partial \eta} = -(b\nu_f)^{1/2} f'(\eta), \; \frac{\partial \eta}{\partial y} = \left(\frac{b}{\nu_f}\right)^{1/2}$$

3.7.1 Similarity Transformation of Continuity Equation

By inserting the above equation into Equation 3.33, then

$$\frac{\partial u}{\partial x}+\frac{\partial v}{\partial y}=0,$$
$$\frac{\partial u}{\partial x}+\frac{\partial v}{\partial \eta}\frac{\partial \eta}{\partial y}=0,$$
$$bf'(\eta)-\left(\left(b\nu_f\right)^{1/2}f'(\eta)\right)\left(\frac{b}{\nu_f}\right)^{1/2}=0$$
$$bf'(\eta)-bf'(\eta)=0,$$

and thus Equation 3.33 is satisfied.

3.7.2 Similarity Transformation of Momentum Equation

From the similarity Equation 3.40, it is found that

$$\frac{\partial u}{\partial x}=bf'(\eta),\ \frac{\partial \eta}{\partial y}=\left(\frac{b}{\nu_f}\right)^{1/2},\ \frac{\partial U_\infty}{\partial x}=b,$$
$$\frac{\partial u}{\partial y}=\frac{\partial u}{\partial \eta}\frac{\partial \eta}{\partial y}=bxf''(\eta)\left(\frac{b}{\nu_f}\right)^{1/2}$$
$$\frac{\partial^2 u}{\partial y^2}=\frac{\partial}{\partial y}\left(\frac{\partial u}{\partial y}\right)=\frac{\partial}{\partial \eta}\left(bxf''(\eta)\left(\frac{b}{\nu_f}\right)^{1/2}\right)\frac{\partial \eta}{\partial y}=$$
$$bxf'''(\eta)\left(\frac{b}{\nu_f}\right)^{1/2}\left(\frac{b}{\nu_f}\right)^{1/2}=\frac{b^2}{\nu_f}xf'''(\eta)$$

By substituting the above equation and Equation 3.40 into momentum Equation 3.39, then

$$u\frac{\partial u}{\partial x}+v\frac{\partial u}{\partial y}=U_\infty\frac{dU_\infty}{dx}+\nu_{hnf}\frac{\partial^2 u}{\partial y^2}+$$
$$\sqrt{2}\ \nu_{hnf}\,\Gamma\frac{\partial u}{\partial y}\frac{\partial^2 u}{\partial y^2}-\frac{\sigma B_o^2(x)}{\rho_{hnf}}(u-U_\infty),$$
$$\left[bxf'(\eta)\right]\left[bf'(\eta)\right]-\left[b\nu_f\right]^{1/2}\left[b^{3/2}\nu_f^{-1/2}xf''(\eta)f(\eta)\right]=$$
$$bx(b)+\nu_{hnf}\left(b^2\nu_f^{-1}xf'''\right)+\sqrt{2}\Gamma\nu_{hnf}\left(b^{3/2}\nu_f^{-1/2}xf''\right)\left(b^2\nu_f^{-1}xf'''\right)$$
$$-\frac{\sigma B_o^2(x)}{\rho_{hnf}}\left(bxf'-bx\right),$$

$$f'^2 - ff'' = 1 + \frac{\nu_{hnf}}{\nu_f} f''' + \frac{\nu_{hnf}}{\nu_f}\sqrt{\frac{2b^2}{\nu_f}}\Gamma x f'' f''' - \frac{\sigma B_0^2(x)}{b\rho_{hnf}}\left(f'-1\right),$$

$$\frac{\nu_{hnf}}{\nu_f} f''' + ff''' + \frac{\nu_{hnf}}{\nu_f}\lambda f'' f''' - f'^2 - M\left(f'-1\right) + 1 = 0, \qquad 3.41$$

$$\frac{\nu_{hnf}}{\nu_f}\left(f'' + \lambda f'' f'''\right) + ff'' - f'^2 - M(f'-1) + 1 = 0.$$

Let $\Gamma = \alpha x^{-1}$ where α is constant (Mohamed *et al.,* 2021a; Ishak, 2010). By definition, $\lambda = \alpha\sqrt{\frac{2b^3}{\nu_f}}$ is the Williamson fluid parameter, $M = \frac{\sigma B_o^2}{b\rho_{hnf}}$ is the magnetic parameter.

3.7.3 Similarity Transformation of Energy Equation

Below shows the energy equation after inserting similarity variables Equation 3.40,

$$\frac{\partial T}{\partial \eta} = \theta'(T_w - T_\infty), \quad \frac{\partial \eta}{\partial x} = 0, \quad \frac{\partial \eta}{\partial y} = \left(\frac{b}{\nu_f}\right)^{1/2}$$

$$\frac{\partial T}{\partial x} = \frac{\partial T}{\partial \eta}\frac{\partial \eta}{\partial x} = (\theta'(T_w - T_\infty))(0) = 0,$$

$$\frac{\partial T}{\partial y} = \frac{\partial T}{\partial \eta}\frac{\partial \eta}{\partial y} = (\theta'(T_w - T_\infty))\left(\frac{b}{\nu_f}\right)^{1/2},$$

$$\frac{\partial^2 T}{\partial y^2} = \left(\frac{\partial}{\partial y}\right)\left(\frac{\partial T}{\partial y}\right) = \left(\frac{\partial}{\partial y}\right)\left(\frac{\partial T}{\partial y}\right)\left(\frac{\partial \eta}{\partial y}\right) = (\theta'(T_w - T_\infty))\left(\frac{b}{\nu_f}\right)$$

Substituting above equation and Equation 3.19 into energy Equation 3.36 and become

$$u\frac{\partial T}{\partial x}+v\frac{\partial T}{\partial y}=\frac{k_{hnf}}{(pC_p)_f}\frac{\partial^2 T}{\partial y^2}$$

$$-(bv_f)^{1/2}f\left(\frac{b}{v_f}\right)^{1/2}\left[\theta'\left(T_w-T_\infty\right)\right]=\frac{k_{hnf}}{\left(pC_p\right)_{hnf}}\theta''\left(T_w-T_\infty\right)\left(\frac{b}{v_f}\right)$$

$$-v_f\theta' f=\frac{k_{hnf}}{(1-\phi_2)\left(pCp\right)_f\left[(1-\phi_1)+\phi_1\frac{\left(\rho C_p\right)_{s1}}{\left(\rho C_p\right)_f}\right]+\phi_2\frac{\left(\rho C_p\right)_{s2}}{\left(\rho C_p\right)_f}}\theta''$$

$$\frac{k_{hnf}/k_f}{(1-\phi_2)\left[(1-\phi_1)+\phi_1\frac{\left(\rho C_p\right)_{s1}}{\left(\rho C_p\right)_f}\right]+\phi_2\frac{\left(\rho C_p\right)_{s2}}{\left(\rho C_p\right)_f}}\theta''+\frac{v_f\left(pCp\right)_f}{k_f}\theta' f=0$$

$$\frac{k_{hnf}}{k_f}\frac{\left(\rho C_p\right)_f}{\left(\rho C_p\right)_{hnf}}\theta''+\Pr\theta' f=0 \qquad 3.42$$

$\Pr=\dfrac{v_f\left(\rho C_p\right)_f}{k_f}$ is the Prandtl number, and the value is $\Pr=21$, corresponds to human blood (Khalid *et al.,* 2018; Saeed *et al.,* 2021a; Mohamed *et al.,* 2021c). Equations 3.39 and 3.36 have been transformed into ordinary differential equations, namely Equations 3.41 and 3.42.

3.7.4 Similarity Transformation of Boundary Conditions

Considering the boundary condition stated in Equation 3.37, after transformation, it becomes:

$u=u_w$ $bxf'(\eta)=ax$ $f'(\eta)=\frac{a}{b}$ $f'(\eta)=\varepsilon,$	$v=0$ $-(bv_f)^{1/2}f(\eta)=0$ $f(\eta)=0,$

<table>
<tr><td colspan="2">$$\theta(\eta)=\frac{T-T_\infty}{T_w-T_\infty}$$ $$\theta(\eta)\left[T_w-T_\infty\right]+T_\infty=T$$ $$\theta(\eta)\left[T_w-T_\infty\right]+T_\infty=T_w$$ $$\theta(\eta)=\frac{T_w-T_\infty}{T_w-T_\infty}$$ $$\theta(\eta)=1,$$</td></tr>
<tr><td>$$u=U_\infty$$ $$bxf'(\eta)=bx$$ $$f'(\eta)\to 1,$$</td><td>$$\theta(\eta)=\frac{T-T_\infty}{T_w-T_\infty}$$ $$\theta(\eta)\left[T_w-T_\infty\right]+T_\infty=T$$ $$\theta(\eta)\left[T_w-T_\infty\right]+T_\infty=T_\infty$$ $$\theta(\eta)\to 0 \ as \ y\to 0.$$</td></tr>
</table>

$$f(0)=0,\ f'(0)=\varepsilon,\quad \theta(0)=1,$$
$$f'(\eta)\to 1,\quad \theta(\eta)\to 0 \ \text{ as } \ \eta\to\infty. \tag{3.43}$$

$\varepsilon=\dfrac{a}{b},(\varepsilon>0)$ is the stretching parameter and thus similarity transformation for continuity, momentum, energy and boundary conditions are completed.

3.8 Numerical Method: Keller Box Method

Overview of KBM has already been explained in Section 1.1.5.4. This section will discuss details on this numerical method that is used for this research. The transformed ordinary differential Equations 3.41 and 3.42 subjected to the boundary conditions, Equation 3.43, will be solved numerically by using the Keller-box method. The procedures of Keller-box method are discussed in this Section while the numerical results will be fully discussed in Chapter 4.

Chapter 4 discusses the problem of Williamson hybrid ferrofluid on a stagnation point flow over a stretching sheet, and in this chapter detailed explanation on the solution of boundary layer equation in Chapter 3 using the Keller-box method is explained. This method was also used for Chapter 5 and Chapter 6.

3.8.1 Finite Difference Method

The Keller-box technique involves the conversion of Equations 3.41 and 3.42 into a system of first-order differentiation equations:

$$f' = u, \qquad 3.44$$

$$u' = v, \qquad 3.45$$

$$s' = t, \qquad 3.46$$

where $\theta = s = s(\eta)$, $u = u(\eta)$, $v = v(\eta)$, $t = t(\eta)$ and (') is derivative with respect to η. With this definition, the Equations 3.41 and 3.42 can be written as

$$\frac{\nu_{hnf}}{\nu_f}(v' + \lambda v v') + fv - u^2 - M(f-1) + 1 = 0 \qquad 3.47$$

$$\frac{k_{hnf}}{k_f}\frac{\left(\rho C_p\right)_f}{\left(\rho C_p\right)_{hnf}} t' + \Pr ft = 0, \qquad 3.48$$

and the boundary condition Equation 3.43 become

$$\begin{aligned} &f(0) = 0,\ u(0) = \varepsilon,\ s(0) = 1 \\ &u(\eta) \to 1,\ s(\eta) \to 0,\ as\ \eta \to \infty. \end{aligned} \qquad 3.49$$

The net rectangle in the η plane shown in Figure 3.2 is considered. The net points are defined as below:

$$\begin{aligned} &\eta_0 = 0,\ \eta_{j-1} + h_j,\ j = 1, 2, ..., J, \\ &\eta_j \equiv \eta_{\infty}, \end{aligned} \qquad 3.50$$

where h_j is the $\Delta\eta_j$-spacing. Here j is not tensor indices or exponents. It is a sequence of numbers that denotes the coordinate position.

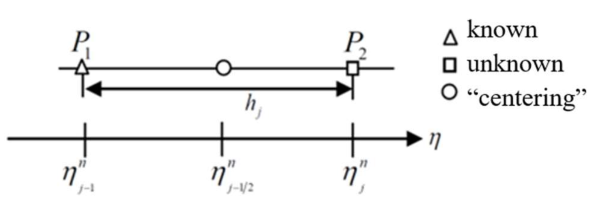

Figure 3.2 Net rectangle for difference approximations

The finite difference forms for any points are

$$(\ )^n_{j=1/2} = \frac{1}{2}\left[(\ )^n_j + (\ )^n_{j-1}\right], \tag{3.51}$$

$$\left(\frac{\partial u}{\partial \eta}\right)^{n-1/2}_{j-1/2} = \frac{u^{n-1/2}_j - u^{n-1/2}_{j-1}}{h_j} \tag{3.52}$$

The Equations 3.44 - 3.48 are modified by taking into account the net rectangle shown in Figure 3.2. The finite difference approximations for ordinary differential Equations 3.44 - 3.48 are derived by evaluating the midpoint $\eta^n_{j-1/2}$ of the segment P_1P_2 using central differences. Therefore, the following are acquired:

$$\frac{f^n_j - f^n_{j-1}}{h_j} = \frac{u^n_j + u^n_{j-1}}{2} = u^n_{j-1/2} \tag{3.53}$$

$$\frac{u^n_j - u^n_{j-1}}{h_j} = \frac{v^n_j + v^n_{j-1}}{2} = v^n_{j-1/2} \tag{3.54}$$

$$\frac{s^n_j - s^n_{j-1}}{h_j} = \frac{t^n_j + t^n_{j-1}}{2} = t^n_{j-1/2} \tag{3.55}$$

Equations 3.47 and 3.48 are shown as the finite centered differential equation at point $\eta_{j-1/2}$, specifically for line P_1P_2. The terms L_1 and L_2 correspond to the left-hand side of Equations 3.47 and 3.48, respectively. The finite difference equation may be expressed as follows:

$$\left(L_1\right)_{j-1/2}^{n-1/2} = 0 \quad 3.56$$

$$(L_2)_{j-1/2}^{n-1/2} = 0 \quad 3.57$$

Following the Equation 3.47, Equations 3.56 and 3.57 can be written as

$$(L_1)_{j-1/2}^{n} + (L_1)_{j-1/2}^{n-1} = 0, \quad 3.58$$

$$(L_2)_{j-1/2}^{n} + (L_2)_{j-1/2}^{n-1} = 0, \quad 3.59$$

with

$$\begin{aligned}(L_1)_{j-1/2}^{n} &= [H_1(v' + \lambda v v') + fv - u^2 + 1 - M(u-1)]_{j-1/2}^{n} \\ &= H_1\left(\frac{v_j^n - v_{j-1}^n}{h_j} + \lambda v_{j-1/2}^n \frac{v_j^n - v_{j-1}^n}{h_j}\right) + f_{j-1/2}^n v_{j-1/2}^n \\ &\quad -\left(u_{j-1/2}^n\right)^2 + 1 - M(u_{j-1/2}^n - 1)\end{aligned} \quad 3.60$$

$$\begin{aligned}(L_2)_{j-1/2}^{n} &= [H_2 t' + \Pr ft]_{j-1/2}^{n} \\ &= H_2\left(\frac{t_j^n - t_{j-1}^n}{h_j}\right) + \Pr f_{j-1/2}^n t_{j-1/2}^n\end{aligned} \quad 3.61$$

$$H_1 = \frac{v_{hnf}}{v_f}$$

$$H_2 = \frac{k_{hnf}}{k_f}\frac{\left(\rho C_p\right)_f}{\left(\rho C_p\right)_{hnf}}$$

The fluid properties variables in Equations 3.60 and 3.61 are denoted as H_1 and H_2 since it does not involve in the process and to ease the method.

$$H_1\left(\frac{v_j^n - v_{j-1}^n}{h_j} + \lambda v_{j-1/2}^n \frac{v_j^n - v_{j-1}^n}{h_j}\right) + f_{j-1/2}^n v_{j-1/2}^n - \left(u_{j-1/2}^n\right)^2$$
$$+1 - M(u_{j-1/2}^n - 1) + (L_1)_{j-1/2}^{n-1} = 0 \qquad 3.62$$
$$H_1\left(\frac{v_j^n - v_{j-1}^n}{h_j} + \lambda v_{j-1/2}^n \frac{v_j^n - v_{j-1}^n}{h_j}\right) + f_{j-1/2}^n v_{j-1/2}^n - \left(u_{j-1/2}^n\right)^2$$
$$+1 - M(u_{j-1/2}^n - 1) = -(L_1)_{j-1/2}^{n-1}$$

and

$$H_2\left(\frac{t_j^n - t_{j-1}^n}{h_j}\right) + \Pr f_{j-1/2}^n t_{j-1/2}^n + (L_2)_{j-1/2}^{n-1} = 0 \qquad 3.63$$
$$H_2\left(\frac{t_j^n - t_{j-1}^n}{h_j}\right) + \Pr f_{j-1/2}^n t_{j-1/2}^n = -(L_2)_{j-1/2}^{n-1}$$

Multiply h_j with Equations 3.53 – 3.55 and 3.62 – 3.63, therefore

$$f_j^n - f_{j-1}^n = \frac{h_j}{2}\left(u_j^n + u_{j-1}^n\right) \qquad 3.64$$

$$u_j^n - u_{j-1}^n = \frac{h_j}{2}\left(v_j^n + v_{j-1}^n\right) \qquad 3.65$$

$$s_j^n - s_{j-1}^n = \frac{h_j}{2}\left(t_j^n + t_{j-1}^n\right) \qquad 3.66$$

$$(R_1)_{j-1/2}^{n-1} = H_1\left(v_j^{n-1} - v_{j-1}^{n-1} + \lambda v_{j-1/2}^{n-1}\left(v_j^{n-1} - v_{j-1}^{n-1}\right)\right) + h_j f_{j-1/2}^{n-1} v_{j-1/2}^{n-1}$$
$$-h_j\left(u_{j-1/2}^{n-1}\right)^2 + h_j - h_j M(u_{j-1/2}^{n-1} - 1) \qquad 3.67$$

$$(R_2)_{j-1/2}^{n-1} = H_2\left(t_j^{n-1} - t_{j-1}^{n-1}\right) + h_j \Pr f_{j-1/2}^{n-1} t_{j-1/2}^{n-1} \qquad 3.68$$

where

$$(R_1)_{j-1/2}^{n-1} = -h_j (L_1)_{j-1/2}^{n-1}$$

$$(R_2)_{j-1/2}^{n-1} = -h_j (L_2)_{j-1/2}^{n-1}$$

The Equations 3.64 – 3.68 are for $j = 1, 2, \ldots J$ at the given n. Also, the boundary condition 3.49 become

$$f_0^n = 0,\; u_0^n = \varepsilon,\; s_0^n = 1,\; u_J^n = 1,\; s_J^n = 0 \tag{3.69}$$

3.8.2 Newton's Method

Equations 3.64 – 3.68 are then form a system equation for the solution of the unknown variable ($f_j^n,\, u_j^n,\, v_j^n,\, s_j^n,\, t_j^n$), $j = 1, 2, \ldots J$ due to the assumption that $f_j^{n-1},\, u_j^{n-1},\, v_j^{n-1},\, s_j^{n-1},\, t_j^{n-1}$ are known for $0 \le j \le J$ (Mohamed, 2013; Cebeci & Cousteix, 2005). Unknown variables ($f_j^n,\, u_j^n,\, v_j^n,\, s_j^n,\, t_j^n$) are revised as ($f_j,\, u_j,\, v_j,\, s_j,\, t_j$) to ease the process for this step. With Equation 3.52, Equations 3.64– 3.68 can be written as

$$f_j - f_{j-1} - \frac{h_j}{2}\left(u_j + u_{j-1}\right) = 0 \tag{3.70}$$

$$u_j - u_{j-1} - \frac{h_j}{2}\left(v_j + v_{j-1}\right) = 0 \tag{3.71}$$

$$s_j - s_{j-1} - \frac{h_j}{2}\left(t_j + t_{j-1}\right) = 0 \tag{3.72}$$

$$\begin{aligned}(R_1)_{j-1/2}^{n-1} = H_1\left(v_j - v_{j-1} + \frac{\lambda}{2}(v_j - v_{j-1})\left(v_j - v_{j-1}\right)\right) \\ + \frac{h_j}{4}\left(f_j - f_{j-1}\right)\left(v_j - v_{j-1}\right) \\ - \frac{h_j}{4}\left(u_j - u_{j-1}\right)^2 + h_j - h_j M\left(\frac{u_j - u_{j-1}}{2} - 1\right)\end{aligned} \tag{3.73}$$

$$(R_2)_{j-1/2}^{n-1} = H_2\left(t_j - t_{j-1}\right) + \frac{h_j}{4}\Pr\left(f_j - f_{j-1}\right)\left(t_j - t_{j-1}\right) \tag{3.74}$$

where

$$\left(R_1\right)_{j-1/2}^{n-1}=h_j\begin{bmatrix} H_1\left(\dfrac{v_j-v_{j-1}}{h_j}+\lambda v_{j-1/2}\left(\dfrac{v_j-v_{j-1}}{h_j}\right)\right)+f_{j-1/2}v_{j-1/2} \\ -\left(u_{j-1/2}\right)^2+1-M\left(u_{j-1/2}-1\right) \end{bmatrix}^{n-1},$$

$$\left(R_2\right)_{j-1/2}^{n-1}=h_j\left[H_2\left(\frac{t_j-t_{j-1}}{h_j}\right)+\Pr f_{j-1/2}t_{j-1/2}\right]^{n-1}$$

The nonlinear Equations 3.70 - 3.74 are resolved with Newton's technique. Therefore, the subsequent iterations are introduced. (Mohamed, 2013; Cebeci & Cousteix, 2005; Salleh *et al.,* 2010):

$$\begin{aligned} f_j^{(i+1)} &= f_j^{(i)}+\delta f_j^{(i)} \\ u_j^{(i+1)} &= u_j^{(i)}+\delta u_j^{(i)} \\ v_j^{(i+1)} &= v_j^{(i)}+\delta v_j^{(i)} \\ s_j^{(i+1)} &= s_j^{(i)}+\delta s_j^{(i)} \\ t_j^{(i+1)} &= t_j^{(i)}+\delta t_j^{(i)} \end{aligned} \tag{3.75}$$

Equation 3.75 is substituted into the system of Equations 3.70 – 3.74, and become

$$\left(f_j^{(i)}+\delta f_j^{(i)}\right)-\left(f_{j-1}^{(i)}+\delta f_{j-1}^{(i)}\right)-\frac{h_j}{2}\left(u_j^{(i)}+\delta u_j^{(i)}+f_{j-1}^{(i)}+\delta f_{j-1}^{(i)}\right)=0 \tag{3.76}$$

$$\left(u_j^{(i)}+\delta u_j^{(i)}\right)-\left(u_{j-1}^{(i)}+\delta u_{j-1}^{(i)}\right)-\frac{h_j}{2}\left(v_j^{(i)}+\delta v_j^{(i)}+v_{j-1}^{(i)}+\delta v_{j-1}^{(i)}\right)=0 \tag{3.77}$$

$$\left(s_j^{(i)}+\delta s_j^{(i)}\right)-\left(s_{j-1}^{(i)}+\delta s_{j-1}^{(i)}\right)-\frac{h_j}{2}\left(t_j^{(i)}+\delta t_j^{(i)}+t_{j-1}^{(i)}+\delta t_{j-1}^{(i)}\right)=0 \tag{3.78}$$

$$(R_1)_{j-1/2}^{n-1} = H_1 \begin{pmatrix} \left(v_j^{(i)} + \delta v_j^{(i)}\right) - \left(v_{j-1}^{(i)} + \delta v_{j-1}^{(i)}\right) \\ + \dfrac{\lambda}{2}\left(v_j^{(i)} + \delta v_j^{(i)} + v_{j-1}^{(i)} + \delta v_j^{(i)}\right) \begin{pmatrix} v_j^{(i)} + \delta v_j^{(i)} - v_{j-1}^{(i)} \\ -\delta v_{j-1}^{(i)} \end{pmatrix} \end{pmatrix}$$ 3.79

$$+\frac{h_j}{4}\left(f_j^{(i)} + \delta f_j^{(i)} + f_{j-1}^{(i)} + \delta f_{j-1}^{(i)}\right) \begin{pmatrix} v_j^{(i)} + \delta v_j^{(i)} + v_{j-1}^{(i)} \\ +\delta v_{j-1}^{(i)} \end{pmatrix}$$

$$-\frac{h_j}{4}\left(u_j^{(i)} + \delta u_j^{(i)} + u_{j-1}^{(i)} + \delta u_{j-1}^{(i)}\right)^2$$

$$+h_j - h_j M \left(\frac{u_j^{(i)} + \delta v_j^{(i)} + u_{j-1}^{(i)} + \delta u_{j-1}^{(i)}}{2} - 1\right)$$

$$(R_2)_{j-1/2}^{n-1} = H_2\left(t_j^{(i)} + \delta t_j^{(i)} - t_{j-1}^{(i)} - \delta t_{j-1}^{(i)}\right) + \frac{h_j}{4}\Pr\left(f_j^{(i)} + \delta f_j^{(i)} - f_{j-1}^{(i)} - \delta f_{j-1}^{(i)}\right)\left(t_j^{(i)} + \delta t_j^{(i)} - t_{j-1}^{(i)} - \delta t_{j-1}^{(i)}\right)$$ 3.80

The superscript i from iterates are eliminated for ease of operation and simplification. Subsequently, via a series of algebraic manipulations and disregarding the terms of higher order for $\delta f_j^{(i)}$, $\delta u_j^{(i)}$, $\delta v_j^{(i)}$, $\delta s_j^{(i)}$, $\delta t_j^{(i)}$, the system of equations can be expressed as follows:

$$\delta f_j - \delta f_{j-1} - \frac{h_j}{2}\left(\delta u_j + \delta u_{j-1}\right) = f_{j-1} - f_j + h_j u_{j-1/2}$$

$$\delta u_j - \delta u_{j-1} - \frac{h_j}{2}\left(\delta v_j + \delta v_{j-1}\right) = u_{j-1} - u_j + h_j v_{j-1/2}$$

$$\delta s_j - \delta s_{j-1} - \frac{h_j}{2}\left(\delta t_j + \delta t_{j-1}\right) = s_{j-1} - s_j + h_j t_{j-1/2}$$

$$(R_1)_{j-1/2}^{n-1} + H\left(v_{j-1} - v_j\right) - \frac{H\lambda}{2}\left(\left(v_j\right)^2 - \left(v_{j-1}\right)^2\right) - h_j f_{j-1/2} v_{j-1/2}$$

$$+h_j\left(u_{j-1/2}\right)^2 + Mh_j u_j - Mh_j - h_j = \delta v_j\left(H_1\left(1+\lambda v_j\right) + \frac{h_j}{2} f_{j-1/2}\right) +$$

$$\delta v_{j-1}\left(-H_1\left(1+\lambda v_{j-1}\right) + \frac{h_j}{2} f_{j-1/2}\right) + \delta f_j\left(\frac{h_j}{2} v_{j-1/2}\right) + \delta f_{j-1}\left(\frac{h_j}{2} v_{j-1/2}\right)$$

$$+\delta u_j\left(-h_j\left(u_{j-1/2} + \frac{M}{2}\right)\right) + \delta u_{j-1}\left(-h_j\left(u_{j-1/2} + \frac{M}{2}\right)\right)$$

$$\left(R_2\right)_{j-1/2}^{n-1} + H_2\left(t_{j-1} - t_j\right) - h_j \Pr f_{j-1/2} t_{j-1/2} = \delta t_j\left(H_2 + \frac{h_j \Pr}{2} f_j\right)$$

$$+\delta t_{j-1}\left(-H_2 + \frac{h_j \Pr}{2} f_{j-1/2}\right) + \delta f_j\left(\frac{h_j \Pr}{2} t_{j-1/2}\right) + \delta f_{j-1}\left(\frac{h_j \Pr}{2} t_{j-1/2}\right)$$

The above system of equations has been simplified to

$$\delta f_j - \delta f_{j-1} - \frac{h_j}{2}\left(\delta u_j + \delta u_{j-1}\right) = \left(r_1\right)_{j-1/2} \tag{3.81}$$

$$\delta u_j - \delta u_{j-1} - \frac{h_j}{2}\left(\delta v_j + \delta v_{j-1}\right) = \left(r_2\right)_{j-1/2} \tag{3.82}$$

$$\delta s_j - \delta s_{j-1} - \frac{h_j}{2}\left(\delta t_j + \delta t_{j-1}\right) = \left(r_3\right)_{j-1/2} \tag{3.83}$$

$$\begin{aligned}\left(r_4\right)_{j-1/2} = {} & \left(a_1\right)_j \delta v_j + \left(a_2\right)_j \delta v_{j-1} + \left(a_3\right)\delta f_j + \left(a_4\right)\delta f_{j-1} \\ & + \left(a_5\right)\delta u_j + \left(a_6\right)\delta u_{j-1}\end{aligned} \tag{3.84}$$

$$\left(r_5\right)_{j-1/2} = \left(b_1\right)\delta t_j + \left(b_2\right)\delta t_{j-1} + \left(b_3\right)\delta f_j + \left(b_4\right)\delta f_{j-1} \tag{3.85}$$

where

$$
\begin{aligned}
(a_1)_j &= H_1\left(1+\lambda v_j\right)+\frac{h_j}{2} f_{j-1/2} \\
(a_2)_j &= -H_1\left(1+\lambda v_{j-1}\right)+\frac{h_j}{2} f_{j-1/2} \\
(a_3)_j &= \frac{h_j}{2} v_{j-1/2}, \quad (\mathrm{a}_4)_j = (a_3)_j, \\
(a_5)_j &= -h_j\left(u_{j-1/2}+\frac{M}{2}\right), \quad (a_6)_j = (a_5)_j
\end{aligned} \tag{3.86}
$$

$$
\begin{aligned}
(b_1)_j &= H_2 + \frac{h_j \operatorname{Pr}}{2} f_{j-1/2} \\
(b_2)_j &= (b_1)_j - 2H_2 \\
(b_3)_j &= \frac{h_j \operatorname{Pr}}{2} t_{j-1/2}, \quad (b_4)_j = (b_3)_j
\end{aligned} \tag{3.87}
$$

$$
\begin{aligned}
(r_1)_{j-1/2} &= f_{j-1} - f_j + h_j u_{j-1/2} \\
(r_2)_{j-1/2} &= u_{j-1} - u_j + h_j v_{j-1/2} \\
(r_3)_{j-1/2} &= s_{j-1} - s_j + h_j t_{j-1/2} \\
(r_4)_{j-1/2} &= H_1\left(v_{j-1}-v_j\right) - \frac{H_1\lambda}{2}\left[\left(v_j\right)^2 - \left(v_{j-1}\right)^2\right] - h_j f_{j-1/2} v_{j-1/2} \\
&\quad + h_j\left(u_{j-1/2}\right)^2 + M h_j u_{j-1/2} - M h_j - h_j + (R_4)_{j-1/2} \\
(r_5)_{j-1/2} &= H_2\left(t_{j-1}-t_j\right) - h_j \operatorname{Pr} f_{j-1/2} t_{j-1/2} + (R)_{j-1/2}
\end{aligned} \tag{3.88}
$$

As stated by Cebeci and Bradshaw (1988), the boundary conditions given by Equation 3.69 may be met without the need for iteration. Thus, the boundary conditions can be expressed as:

$$
\delta f_0 = 0, \delta u_0 = 0, \delta s_0 = 0, \ \delta u_j = 0 \text{ and } \delta s_j = 0 \tag{3.89}
$$

3.8.3 The Block Elimination Technique

After the process of linearization from Newton's method, Equations 3.81 - 3.85 are solved with the block elimination technique (Na, 1979) due to the system consisting of three diagonal block structures.

A common three-diagonal block structure consists of variables or constants. Nevertheless, the Keller-box technique incorporates the use of block matrices. In order to solve the linearized difference Equations 3.81 to 3.85 using the block elimination approach, it is necessary to specify the elements of the block matrices. The blocks are specified by three situations, which is when $j=1,\ j=2,\ ....,j=J-1$ and $j=J$.

When $j=1$, the linearize difference Equations 3.81 - 3.85 become

$$(r_1)_{1-1/2} = \delta f_1 - \delta f_0 + \frac{1}{2} h_1 \left(\delta u_1 + \delta u_0\right)$$

$$(r_2)_{1-1/2} = \delta u_1 - \delta u_0 + \frac{1}{2} h_1 \left(\delta v_1 + \delta v_0\right)$$

$$(r_3)_{1-1/2} = \delta s_1 - \delta s_0 - \frac{h_j}{2} \left(\delta t_1 + \delta t_0\right)$$

$$(r_4)_{1-1/2} = (a_1)_1 \delta v_1 + (a_2)_1 \delta v_0 + (a_3)_1 \delta f_1 + (a_4)_1 \delta f_0 + (a_5)_1 \delta u_1 + (a_6)_1 \delta u_0$$

$$(r_5)_{1-1/2} = (b_1)_1 \delta t_1 + (b_2)_1 \delta t_0 + (b_3)_1 \delta f_1 + (b_4)_1 \delta f_0$$

Subjected to the boundary conditions 3.89, suitable matrices can be formed is

$$\begin{bmatrix} 0 & 0 & 1 & 0 & 0 \\ -\frac{1}{2}h_1 & 0 & 0 & -\frac{1}{2}h_1 & 0 \\ 0 & -\frac{1}{2}h_1 & 0 & 0 & -\frac{1}{2}h_1 \\ (a_2)_1 & 0 & (a_3)_1 & (a_1)_1 & 0 \\ 0 & (b_2)_1 & (b_3)_1 & 0 & (b_1)_1 \end{bmatrix} \begin{bmatrix} \delta v_0 \\ \delta t_0 \\ \delta f_1 \\ \delta v_1 \\ \delta t_1 \end{bmatrix} + \begin{bmatrix} -\frac{1}{2}h_1 & 0 & 0 & 0 & 0 \\ 1 & 0 & 0 & 0 & 0 \\ 0 & 1 & 0 & 0 & 0 \\ (a_5)_1 & 0 & 0 & 0 & 0 \\ 0 & 0 & 0 & 0 & 0 \end{bmatrix} \begin{bmatrix} \delta u_1 \\ \delta s_1 \\ \delta f_2 \\ \delta v_2 \\ \delta t_2 \end{bmatrix} = \begin{bmatrix} (r_1)_{1-1/2} \\ (r_2)_{1-1/2} \\ (r_3)_{1-1/2} \\ (r_4)_{1-1/2} \\ (r_5)_{1-1/2} \end{bmatrix}$$

Hence, for $j=1$, it can be written as

$$\left[A_1\right]\left[\delta_1\right]+\left[C_1\right]\left[\delta_2\right]=\left[r_1\right]$$

Next, when $j=2$ ...., $j=J-1$ the linearize difference Equations 3.81 - 3.85 become

$$\left(r_1\right)_{(J-1)-1/2}=\delta f_{J-1}-\delta f_{J-2}+\frac{1}{2}h_{J-1}\left(\delta u_{J-1}+\delta u_{J-2}\right)$$

$$\left(r_2\right)_{(J-1)-1/2}=\delta u_{J-1}-\delta u_{J-2}+\frac{1}{2}h_{J-1}\left(\delta v_{J-1}+\delta v_{J-2}\right)$$

$$\left(r_3\right)_{(J-1)-1/2}=\delta s_{J-1}-\delta s_{J-2}-\frac{h_j}{2}\left(\delta t_{J-1}+\delta t_{J-2}\right)$$

$$\begin{aligned}\left(r_4\right)_{(J-1)-1/2}=&\left(a_1\right)_{J-1}\delta v_{J-1}+\left(a_2\right)_{J-1}\delta v_{J-2}+\left(a_3\right)_{J-1}\delta f_{J-1}+\left(a_4\right)_{J-1}\delta f_{J-2}\\&+\left(a_5\right)_{J-1}\delta u_{J-2}+\left(a_6\right)_{J-1}\delta u_{J-2}\end{aligned}$$

$$\left(r_5\right)_{(J-1)-1/2}=\left(b_1\right)_{J-1}\delta t_{J-1}+\left(b_2\right)_{J-1}\delta t_{J-2}+\left(b_3\right)_{J-1}\delta f_{J-1}+\left(b_4\right)_{J-1}\delta f_{J-2}$$

Subjected to the boundary conditions 3.89, suitable matrices can be formed is

$$
\begin{bmatrix}
0 & 0 & -1 & 0 & 0 \\
0 & 0 & 0 & -\frac{1}{2}h_{J-1} & 0 \\
0 & 0 & 0 & 0 & -\frac{1}{2}h_{J-1} \\
0 & 0 & (a_4)_{J-1} & (a_2)_{J-1} & 0 \\
0 & 0 & (b_4)_{J-1} & 0 & (b_2)_{J-1}
\end{bmatrix}
\begin{bmatrix}
\delta u_{J-3} \\ \delta s_{J-3} \\ \delta f_{J-2} \\ \delta v_{J-2} \\ \delta t_{J-2}
\end{bmatrix} +
$$

$$
\begin{bmatrix}
-\frac{1}{2}h_{J-1} & 0 & 1 & 0 & 0 \\
-1 & 0 & 0 & -\frac{1}{2}h_{J-1} & 0 \\
0 & -1 & 0 & 0 & -\frac{1}{2}h_{J-1} \\
(a_6)_{J-1} & 0 & (a_3)_{J-1} & (a_1)_{J-1} & 0 \\
0 & 0 & (b_3)_{J-1} & 0 & (b_1)_{J-1}
\end{bmatrix}
\begin{bmatrix}
\delta u_{J-2} \\ \delta s_{J-2} \\ \delta f_{J-1} \\ \delta v_{J-1} \\ \delta t_{J-1}
\end{bmatrix}
$$

$$
+\begin{bmatrix}
-\frac{1}{2}h_{J-1} & 0 & 0 & 0 & 0 \\
1 & 0 & 0 & 0 & 0 \\
0 & -1 & 0 & 0 & 0 \\
(a_5)_{J-1} & 0 & 0 & 0 & 0 \\
0 & 0 & 0 & 0 & 0
\end{bmatrix}
\begin{bmatrix}
\delta u_{J-1} \\ \delta s_{J-1} \\ \delta f_{J} \\ \delta v_{J} \\ \delta t_{J}
\end{bmatrix}
=
\begin{bmatrix}
(r_1)_{(J-1)-1/2} \\ (r_2)_{(J-1)-1/2} \\ (r_3)_{(J-1)-1/2} \\ (r_4)_{(J-1)-1/2} \\ (r_5)_{(J-1)-1/2}
\end{bmatrix}
$$

hence, for $j = 2$ ...., $j = J-1$, it can be written as

$$
\left[r_j\right] = \left[B_j\right]\left[\delta_{j-1}\right] + \left[A_j\right]\left[\delta_{j+1}\right] + \left[C_j\right]\left[\delta_{j+1}\right]
$$

Lastly, when $j = J$, the linearize difference Equations 3.81 - 3.85 become

$$
(r_1)_{J-1/2} = \delta f_J - \delta f_{J-1} + \frac{1}{2}h_J\left(\delta u_J + \delta u_{J-1}\right)
$$

$$
(r_2)_{J-1/2} = \delta u_J - \delta u_{J-1} + \frac{1}{2}h_J\left(\delta v_J + \delta v_{J-1}\right)
$$

$$
(r_3)_{J-1/2} = \delta s_J - \delta s_{J-1} - \frac{1}{2}h_J\left(\delta t_J + \delta t_{J-1}\right)
$$

$$
(r_4)_{J-1/2} = (a_1)_J\,\delta v_J + (a_2)_J\,\delta v_{J-1} + (a_3)_J\,\delta f_J + (a_4)_J\,\delta f_{J-1} + (a_5)_J\,\delta u_J + (a_6)_J\,\delta u_{J-1}
$$

$$
(r_5)_{J-1/2} = (b_1)_J\,\delta t_J + (b_2)_J\,\delta t_{J-1} + (b_3)_J\,\delta f_J + (b_4)_J\,\delta f_{J-1}
$$

Subjected to the boundary conditions 3.89, the suitable matrices can be formed as

$$
\begin{bmatrix} 0 & 0 & -1 & 0 & 0 \\ 0 & 0 & 0 & -\frac{1}{2}h_J & 0 \\ 0 & 0 & 0 & 0 & -\frac{1}{2}h_J \\ 0 & 0 & (a_4)_J & (a_2)_J & 0 \\ 0 & 0 & (b_4)_J & 0 & (b_2)_J \end{bmatrix}
\begin{bmatrix} \delta u_{J-2} \\ \delta s_{J-2} \\ \delta f_{J-1} \\ \delta v_{J-1} \\ \delta t_{J-1} \end{bmatrix}
+\begin{bmatrix} -\frac{1}{2}h_J & 0 & 0 & 0 & 0 \\ -1 & 0 & 0 & -\frac{1}{2}h_J & 0 \\ 0 & -1 & 0 & 0 & -\frac{1}{2}h_J \\ (a_6)_J & 0 & (a_3)_J & (a_1)_J & 0 \\ 0 & 0 & (b_3)_J & 0 & 0 \end{bmatrix}
\begin{bmatrix} \delta u_{J-1} \\ \delta s_{J-1} \\ \delta f_J \\ \delta v_J \\ \delta t_J \end{bmatrix}
=\begin{bmatrix} (r_1)_{J-1/2} \\ (r_2)_{J-1/2} \\ (r_3)_{J-1/2} \\ (r_4)_{J-1/2} \\ (r_5)_{J-1/2} \end{bmatrix}
$$

hence, for $j = J$, it can be written as

$$[r_j] = [B_J][\delta_{J-1}] + [A_J][\delta_J]$$

Therefore, in overall, for $j = 1, 2, 3, \ldots., J-1, J$, the system of equations can be summarized as

$$
\begin{aligned}
j = 1 \quad &: [r_1] = [A_1][\delta_1] + [C_1][\delta_2], \\
j = 2 \quad &: [r_2] = [B_2][\delta_1] + [A_2][\delta_2] + [C_2][\delta_3], \\
j = 3 \quad &: [r_3] = [B_3][\delta_2] + [A_3][\delta_3] + [C_3][\delta_4], \\
&\vdots \\
j = J-1 &: [r_{J-1}] = [B_{J-1}][\delta_{J-2}] + [A_{J-1}][\delta_{J-1}] + [C_{j-1}][\delta_J] + \\
j = J \quad &: [r_J] = [B_J][\delta_{J-1}] + [A_J][\delta_J]
\end{aligned}
$$

Generally, in matrix vector form, the above system can be simplified as

$$A\delta = r, \qquad 3.90$$

with

$$
A=\begin{bmatrix}
[A_1] & [C_1] & & & & & \\
[B_2] & [A_2] & [C_2] & & & & \\
& & & \ddots & & & \\
& & & \ddots & & & \\
& & & \ddots & & & \\
& & & & [B_{J-1}] & [A_{J-1}] & [C_{J-1}] \\
& & & & & [B_J] & [A_J]
\end{bmatrix},\quad \delta=\begin{bmatrix}[\delta_1]\\ [\delta_2]\\ \vdots\\ \vdots\\ \vdots\\ [\delta_{J-1}]\\ [\delta_J]\end{bmatrix}
$$

and

$$
r=\begin{bmatrix}[r_1]\\ [r2]\\ \vdots\\ \vdots\\ \vdots\\ [r_{J-1}]\\ [r_J]\end{bmatrix}
$$

The elements of the matrices are

$$
[A_1]=\begin{bmatrix}
0 & 0 & 1 & 0 & 0\\
-\frac{1}{2}h_1 & 0 & 0 & -\frac{1}{2}h_1 & 0\\
0 & -\frac{1}{2}h_1 & 0 & 0 & -\frac{1}{2}h_1\\
(a_2)_1 & 0 & (a_3)_1 & (a_1)_1 & 0\\
0 & (b_2)_1 & (b_3)_1 & 0 & (b_1)_1
\end{bmatrix}, \qquad 3.91
$$

$$
A_j=\begin{bmatrix}
-\frac{1}{2}h_j & 0 & 0 & 0 & 0\\
-1 & 0 & 0 & -\frac{1}{2}h_j & 0\\
0 & -1 & 0 & 0 & -\frac{1}{2}h_j\\
(a_6)_j & 0 & (a_3)_j & (a_1)_j & 0\\
0 & 0 & (b_3)_j & 0 & (b_1)_j
\end{bmatrix},\ 2\le j\le J, \qquad 3.92
$$

$$[B_j] = \begin{bmatrix} 0 & 0 & -1 & 0 & 0 \\ 0 & 0 & 0 & -\frac{1}{2}h_j & 0 \\ 0 & 0 & 0 & 0 & -\frac{1}{2}h_j \\ 0 & 0 & (a_4)_j & (a_2)_j & 0 \\ 0 & 0 & (b_4)_j & 0 & (b_2)_j \end{bmatrix}, \; 2 < j < J, \qquad 3.93$$

$$[C_j] = \begin{bmatrix} -\frac{1}{2}h_j & 0 & 0 & 0 & 0 \\ 1 & 0 & 0 & 0 & 0 \\ 0 & 1 & 0 & 0 & 0 \\ (a_5)_j & 0 & 0 & 0 & 0 \\ 0 & 0 & 0 & 0 & 0 \end{bmatrix}, \; 2 \le j \le J \, [\qquad 3.94$$

$$[\delta_1] = \begin{bmatrix} \delta v_0 \\ \delta s_0 \\ \delta f_1 \\ \delta v_1 \\ \delta t_1 \end{bmatrix}, \quad [\delta_j] = \begin{bmatrix} \delta u_{j-1} \\ \delta s_{j-1} \\ \delta f_j \\ \delta v_j \\ \delta_j \end{bmatrix}, \quad 2 \le j \le J \qquad 3.95$$

and

$$[r_j] = \begin{bmatrix} (r_1)_{J-1/2} \\ (r_2)_{J-1/2} \\ (r_3)_{J-1/2} \\ (r_4)_{J-1/2} \\ (r_5)_{J-1/2} \end{bmatrix}, \; 1 \le \mathrm{j} \le J \qquad 3.96$$

Matrix A in Equation 3.90 is known as a tridiagonal matrix with zero elements, except at its main diagonal. Equation 3.90 can be solved by using a block elimination technique (Na, 1979) with the assumption that matrix A is non-singular and can be factored in the form of

$$A = LU, \qquad 3.97$$

with

$$L = \begin{bmatrix} [\alpha_1] & & & & \\ [B_2] & [\alpha_2] & & & \\ & & \ddots & & \\ & & \ddots & [\alpha_{J-1}] & \\ & & & [B_J] & [\alpha_J] \end{bmatrix} \text{ and}$$

$$U = \begin{bmatrix} [I] & [\Gamma_1] & & & & \\ & [I] & [\Gamma_2] & & & \\ & & & \ddots & & \\ & & & \ddots & & \\ & & & & [I] & [\Gamma_{J-1}] \\ & & & & & [I] \end{bmatrix}$$

where $[I]$ is the identity matrix of order 5 and $[\alpha_1]$, and $[\Gamma_i]$ are 5x5 matrices which elements are determined by the following equations:

$$[\alpha_1] = [A_1], \qquad 3.98$$

$$[A_1][\Gamma_1] = [C_1], \qquad 3.99$$

$$[\alpha_j] = [A_j] - [B_j][\Gamma_{j-1}], \quad j = 2,3,.....,J, \qquad 3.100$$

$$[\alpha_j][\Gamma_j] = [C_j], \quad j = 2,3,.....,J-1, \qquad 3.101$$

Then, Equation 3.97 is substituted into Equation 3.90, hence

$$LU\delta = r. \qquad 3.102$$

if

$$U\delta = W, \qquad 3.103$$

then the Equation 3.102 become

$$LW = r, \tag{3.104}$$

where

$$W = \begin{bmatrix} [W_1] \\ [W_2] \\ \vdots \\ [W_{J-1}] \\ [W_J] \end{bmatrix},$$

and $[W_j]$ are 5 x 1 column matrices. The elements W can be solved from Equation 3.103 which is

$$[\alpha_1][W_1] = [r_1] \tag{3.105}$$

$$[\alpha_j][W_j] = [r_j] - [B_j][W_{j-1}], \quad 2 \le j \le J. \tag{3.106}$$

The process of calculating Γ_j, α_j and W_j is often known as the forward sweep. After identifying the elements of W, the answer δ may be derived using Equation 3.103 in the backward sweep. The elements are determined using the following relationships:

$$[\delta_J] = [W_J], \tag{3.107}$$

$$[\delta_j] = [W_j] - [\Gamma_j][\delta_{j+1}], \quad 1 \le j \le J-1. \tag{3.108}$$

Once the constituents of δ are identified, Equation 3.81 - 3.85 can be utilised to get the ($i+1$)th iterates for Equation 3.75.

The computations are iterated until a convergence condition is met. The parameter $v(0)$, which represents the wall shear stress, is frequently employed as a convergence criteria in laminar boundary layer computations (Cebeci & Bradshaw, 1988). The likely explanation for this is the computations involving the boundary layer, where the most significant inaccuracies often arise in the parameter related to wall shear stress. Thus, the wall shear stress parameter is employed as the convergence criteria in this work. Calculations cease when

$$\left|\delta v_0^{(i)}\right| < \varepsilon_1, \qquad 3.109$$

where ε_1 is a predetermined, insufficient value. This study used $\varepsilon_1 = 0.00001$, which provides accurate data up to four decimal places, as recommended by Cebeci and Bradshaw (1988).

3.8.4 Initial Conditions and Thermophysical Properties

In order to ensure that the numerical results of the quantities of interest are not affected, it is necessary to select the appropriate step size $\Delta\eta$ and boundary layer thickness η_∞ for the numerical computation. The trial-and-error method is normally employed, commencing with the determination of the value of η_∞ by considering the velocity and temperature profile. Boundary layer thickness η_∞ that is either large or small may not satisfy the boundary condition $\eta \to \infty$. This study reveals that a boundary layer thickness, η_∞, ranging from 1 to 7 is optimal for obtaining precise numerical outcomes, depending on the specific challenges being addressed. Subsequently, once the value of η_∞ is ascertained, it is important to establish the appropriate value of $\Delta\eta$ (Nazar, 2003; Mohamed, 2013; Swalmeh *et al.,* 2018).

According to Nazar (2003), a step size between $\Delta\eta = 0.02$ and 0.07 is typically enough to provide precise numerical results. However, the specific value of the step size should not noticeably impact the final converged results. In order to get precise and convergent numerical findings, Mohamed *et al.* (2021b) defined the boundary layer thickness and step size as 7 and 0.02, respectively, across various parameters. In order to validate the precision of the numerical approach and MATLAB programming, the current result is compared to previously published results. The suitable way to verify the results is to compare them with other studies that use different methods of solving but has the same momentum and energy equation along with the same boundary condition to the present studies (Iqbal *et al.,* 2021; Yasin *et al.,* 2021a).

The are several types of fluid used in this research. The different types of fluid are use in this research is to evaluate the capabilities with the upgraded fluid. Table 3.1 below shows the thermophysical properties of fluid/ particles used for this research (Khalid *et al.,* 2018; Mohamed *et al.,* 2019a; 2019b; Waqas *et al.,* 2021; Ramli & Ahmad, 2019; Abu Bakar *et al.,* 2021; Khan *et al.,* 2022; Mohamed *et al.*2020b; 2021a):

Table 3.1 Thermophysical properties of fluid and particles that are used in this research.

Fluid/Particles	**Physical Properties**		
	ρ **(kg/m^3)**	C_p **(J/kg·K)**	***k*** **(W/m·K)**
Human blood	1053	3594	0.492
Magnetite (Fe_3O_4), ϕ_1	5180	670	9.7
Copper (Cu), ϕ_2	8933	385	400
Water	997	4179	0.613
Cobalt ferrite (*$CoFe_2O_4$*)	4907	700	3.7
Manganese-zinc ferrite (*$Mn\text{-}ZnFe_2O_4$*)	4900	800	5
Silver (*Ag*)	10500	235	429
Gold (*Au*)	19300	129	318

3.9 Initial Profiles

Initial guesses for the function and in the boundary layer flow is required to proceed the numerical computation. Since velocity and temperature distribution are both boundary conditions at and then the initial guesses will start with and for ease of process. Other functions will be defined after and with differentiation and integration. The selection of distribution curves has some possibilities as long as the boundary condition Equation 3.49 is satisfied. For the problem considered here, one possibility distribution curve for and suggested by Bejan (1984), and Bejan and Kraus (2003)

Prior to doing numerical computations, it is necessary to provide initial estimates for the variables f, u, v, s and t in the boundary layer flow. Given that the boundary conditions at points $\eta = 0$ and $\eta = \eta_\infty$ involve the velocity u and temperature distribution s, the initial guesses for the process will be u and s for simplicity. Functions f, v, and t will be defined subsequent to u and s using differentiation and integration. The choice of distribution curves is viable as long as the boundary constraint Equation 3.49 is met. Regarding the topic at hand, Bejan (1984) and Bejan and Kraus (2003) proposed a potential distribution curve for the variables u and s:

$$u(\eta) = \frac{df}{d\eta} = \frac{\eta}{\eta_\infty}\left(\frac{3}{2} - \frac{1}{2}\left(\frac{\eta}{\eta_\infty}\right)\right) + \varepsilon\left(1 - \left(\frac{\eta}{\eta_\infty}\right)^2\right), \tag{3.110}$$

$$s(\eta) = \theta(\eta) = \left(1 - \frac{\eta}{\eta_\infty}\right)^2 \tag{3.111}$$

Integrate Equation 3.110 with respect to η produce

$$\begin{aligned} f(\eta) = \int_{\eta=0}^{\eta=\eta_\infty} u\, d\eta = \frac{3}{4}\eta\left(\frac{\eta}{\eta_\infty}\right) - \frac{1}{8}\eta\left(\frac{\eta}{\eta_\infty}\right)\left(\frac{\eta}{\eta_\infty}\right)^2 \\ + \varepsilon\left(\eta - \frac{\eta}{3}\left(\frac{\eta}{\eta_\infty}\right)^2\right) \end{aligned} \tag{3.112}$$

and differentiate Equation 3.110 and Equation 3.111, respectively will produce

$$v(\eta) = \frac{du}{d\eta} = \frac{3}{2}\left(\frac{1}{\eta_\infty}\right)\left(1 - \left(\frac{\eta}{\eta_\infty}\right)^2\right) + \varepsilon\left(-2\left(\frac{1}{\eta_\infty}\right)\left(\frac{\eta}{\eta_\infty}\right)\right) \tag{3.113}$$

$$t(\eta) = \frac{ds}{d\eta} = 2\left(\frac{1}{\eta_\infty}\right)\left(\frac{\eta}{\eta_\infty}\right) \tag{3.114}$$

Chapter 4 will provide a comprehensive remedy for the problem addressed in this chapter. The Keller-box approach has been determined to yield precise outcomes for solving the stagnation point flow across the stretching sheet. Given its high level of precision, this method will also be employed for problem-solving purposes in Chapter 5 and Chapter 6. Figure 3.3 depicts the calculation flow diagram of the Keller-box approach, as it is utilized for the issues addressed in this thesis. The programming and numerical computations were performed using the MATLAB software. Appendix A contains a compilation of symbols utilized in the MATLAB program, whereas Appendix B showcases the comprehensive program for this particular problem.

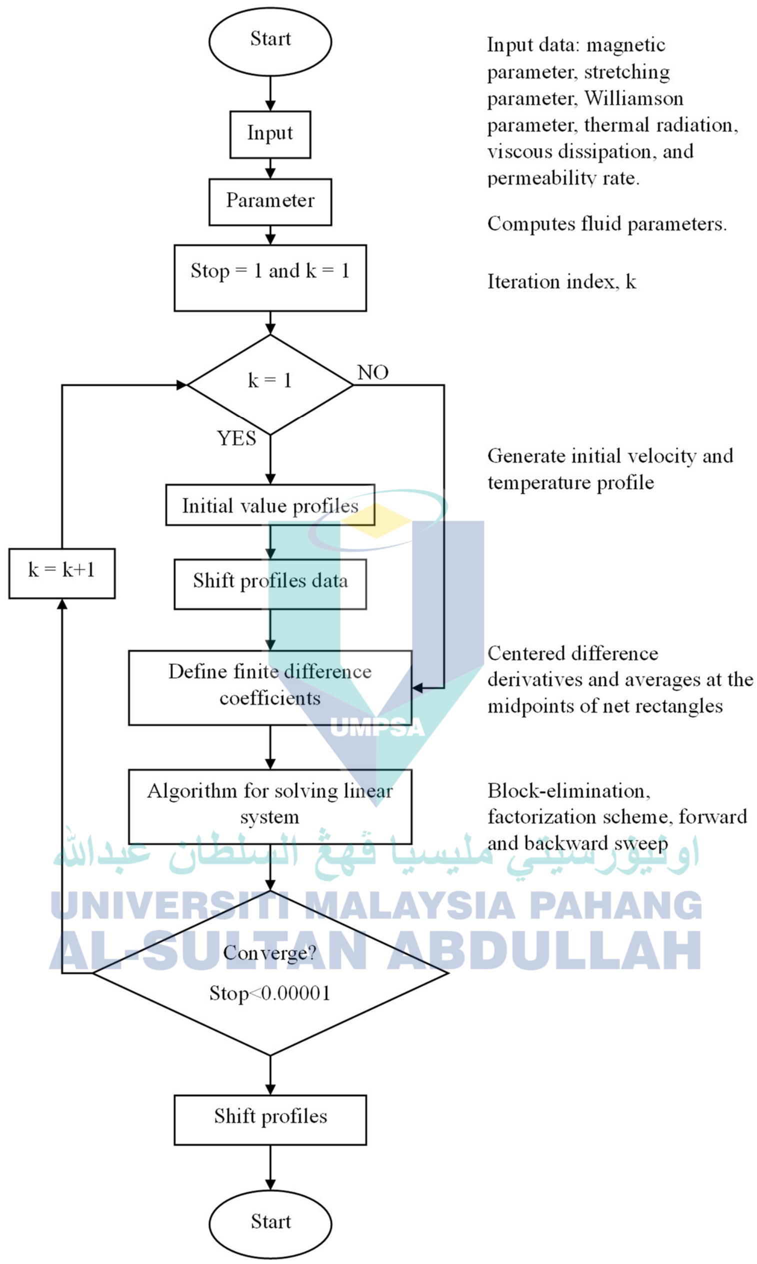

Figure 3.3 Keller-box method flow diagram

CHAPTER 4

STAGNATION POINT FLOW OF WILLIAMSON HYBRID FERROFLUID OVER A STRETCHING SHEET

4.1 Introduction

This chapter will explore the properties of convective boundary layer flow and heat transfer of a hybrid ferrofluid, with blood as based fluid, on a stagnation point flow over a stretching sheet. Specific cases for this problem are from Yasin *et al.,* (2018a; 2020) and Hashim *et al.* (2019b). Section 2.2 and Section 2.3 have provided information on stagnation point and stretching sheet, which is discussed in this research problem. In those two Sections, it can be concluded that there is a gap in studies for this new upgraded type of fluid. The formulation of the governing equations and the Keller-box algorithm for this problem has been discussed in Chapter 3. The boundary layer thickness and step size values inserted into the Keller-box method are 7 and 0.02, respectively. This chapter investigates the fluid flow properties and heat transmission of Williamson hybrid ferrofluid by examining a few relevant fluid parameters, including the magnetic parameter, Williamson parameter, and stretching parameter. The performance of the enhanced fluid is further evaluated by comparing it with various ferroparticle volume fractions. Section 4.3 examines and discusses the analysis of temperature distribution, velocity profiles, variation of the Nusselt number, and skin friction coefficient.

4.2 Mathematical Formulation

Considering a steady two-dimensional flow on a stagnation point over a stretching sheet with ambient temperature, as shown in Figure 3.1. A detailed discussion of the mathematical formulation has been covered in Chapter 3, Section 3.6, Equations 3.41 and 3.42 with boundary conditions in Equation 3.43. Below is the rewritten equation for this problem:

$$\frac{v_{hnf}}{v_f}\left(f''' + \lambda f'' f'''\right) + ff'' - f'^2 - M(f-1) + 1 = 0$$

$$\frac{k_{hnf}}{k_f}\frac{\left(\rho C_p\right)_f}{\left(\rho C_p\right)_{hnf}}\theta'' + \Pr\theta' f = 0$$

Other hybrid ferrofluid properties are mentioned in Equation 3.5. Subjected boundary conditions

$$\begin{gathered} f(0) = 0,\ f'(0) = \varepsilon,\ \theta(0) = 1, \\ f'(\eta) \to 1,\ \theta(\eta) \to 0,\ as\ y \to \infty \end{gathered}$$

The focus of this work is on two specific physical quantities: the skin friction coefficient C_f and the local Nusselt number Nu_x. Local skin coefficient, referred to as local dynamic pressure perceived as the shear stress of fluid on the surface (Kundu *et al.,* 2016). Local Nusselt number is referred to as the ratio of convection to conduction heat transfer under the same conditions (Astakhov, 2012). Both physical quantities are given (Salleh *et al.*, 2010; Bachok et al., 2011b; 2012; Yasin et al., 2018a; 2020):

$$C_f = \frac{\tau_w}{\rho_f U_\infty^2},\ Nu_x = \frac{xq_w}{k_f(T_w - T_\infty)} \qquad 4.1$$

with the surface shear stress τ_w and the surface heat flux q_w defined as (Asjad *et al.,* 2022; Lund *et al.,* 2019; Hashim *et al.,* 2016; 2019a; 2019b);

$$\tau_w = \mu_{hnf}\left(\frac{\partial u}{\partial y} + \frac{\Gamma}{\sqrt{2}}\left(\frac{\partial u}{\partial y}\right)^2\right)_{\bar{y}=0},\quad q_w = -k_{hnf}\left(\frac{\partial T}{\partial y}\right)_{y=0}. \qquad 4.2$$

Using variables in Equation 3.40 and Equation 4.1 give

$$C_f \mathrm{Re}_x^{1/2} = \frac{1}{(1-\phi_1)^{2.5}(1-\phi_2)^{2.5}}\left(f'' + \frac{\lambda}{2} f''^2 \right) \text{ and} \qquad 4.3$$

$$Nu_x \mathrm{Re}_x^{-1/2} = -\frac{k_{hnf}}{k_f}\theta'(0)$$

where $\mathrm{Re}_x = \dfrac{U_\infty x}{\nu_f}$ is the Reynold's number.

4.3 Results and Discussion

Numerical solutions were obtained for the non-linear ordinary differential Equation 3.41 and Equation 3.42, together with their corresponding boundary conditions 3.43, using the Keller-box technique implemented in MATLAB software. An analysis was conducted on the influence of physical factors, namely the stretching parameter ε, magnetic parameter M, and Williamson fluid parameter λ, on the velocity profiles, temperature profiles, reduced skin friction coefficient $C_f \mathrm{Re}_x^{1/2}$, and reduced Nusselt Number $Nu_x \mathrm{Re}_x^{-1/2}$. As mentioned before in Chapter 3, Prandtl number is set 21 throughout the results while (Fe_3O_4), and copper (Cu) are considered as the nanoparticle volume fraction, ϕ_1, and ϕ_2 respectively. The default nanoparticle volume fractions used for the hybrid ferrofluid fluid are $\phi_1 = 0.1$ and $\phi_2 = 0.06$ referenced from Devi and Anjali Devi (2017). The thermophysical characteristics of human blood, magnetite (Fe_3O_4), and copper (Cu) can be referred to Table 3.1. To authenticate the efficiency of the Keller-box used in this study, a comparison has been made that is shown in Table 4.1 with $\varepsilon = \phi_2 = \lambda = 0$ and $\Pr = 6.2$. The observed decrease in skin friction $C_f \mathrm{Re}_x^{1/2}$ is consistent with the findings of Yasin *et al.* (2018b), who also utilized the Keller-box approach.

Table 4.2 displays the lowered Nusselt number and skin friction values corresponding to the stretching parameter, $\Pr = 21$, M=0.5, and $\lambda = 0.1$. The parameter values for this parameter is referred from Bachok *et al.* (2011a). As the stretching parameter increases, the fluid's heat transmission capability improves. The skin friction values provide the opposite outcome. As the stretching parameter rises, the skin friction is significantly reduced until it reaches negative values after point $\varepsilon > 1$.

Figure 4.1 illustrate the distributions of $C_f \operatorname{Re}_x^{1/2}$ with λ for four types of fluid when $\Pr = 21$, $\varepsilon = 0.5$ and $M = 0.5$. Nadeem *et al.* (2013; 2013b; 2014) is the reference for the parameter values of λ. Figure 4.1 show that the hybrid ferrofluid produces the highest distributions of $C_f \operatorname{Re}_x^{1/2}$ as Williamson fluid parameter increases compared to the other types of fluid. The high distributions of $C_f \operatorname{Re}_x^{1/2}$ are due to the presence of Cu in the fluid mixture which has high particle density. Furthermore, the trend distributions of $C_f \operatorname{Re}_x^{1/2}$ are similar for all types of fluid in the figure. Increasing Williamson reduces the flow velocity as it increases the resistance of flow leading to increase of $C_f \operatorname{Re}_x^{1/2}$ values (Vittal *et al.*, 2017b). The distribution of $Nu_x \operatorname{Re}_x^{-1/2}$ is not considered as this parameter does not involve in the respective physical quantity which can be referred to Equation 4.3.

Figures 4.2 and 4.3 show the distributions of $Nu_x \operatorname{Re}_x^{-1/2}$ and $C_f \operatorname{Re}_x^{1/2}$ with M for four types of fluid when $\Pr = 21$, $\lambda = 0.1$, and $\varepsilon = 0.5$. The parameter values used for M is referred to Yasin *et al.* (2018b).There are four types of fluid involved in this study: blood ($\phi_1 = \phi_2 = 0$), 0.1 vol. of Fe_3O_4 /blood ferrofluid ($\phi_1 = 0.1, \phi_2 = 0$), 0.16 vol. of $Fe_3O_4 - Cu$ /blood hybrid ferrofluid ($\phi_1 = 0.1, \phi_2 = 0.06$), and 0.16 vol. of Fe_3O_4/blood ferrofluid ($\phi_1 = 0.16, \phi_2 = 0$). It is evident that in both figures, the increase of M and the volume of nanoparticles leads to an increase of $Nu_x \operatorname{Re}_x^{-1/2}$ and $C_f \operatorname{Re}_x^{1/2}$. $Fe_3O_4 - Cu$ /blood hybrid ferrofluid produces the highest values of $Nu_x \operatorname{Re}_x^{-1/2}$ and $C_f \operatorname{Re}_x^{1/2}$ compared to other types of fluid while blood-based fluid produces the lowest . $Nu_x \operatorname{Re}_x^{-1/2}$. and $C_f \operatorname{Re}_x^{1/2}$ value. The elevated values of $Nu_x \operatorname{Re}_x^{-1/2}$ in 0.16 volume of $Fe_3O_4 - Cu$ /blood hybrid ferrofluid are attributed to the exceptional heat conductivity of copper. Mathematically, it is determined that the values of $Nu_x \operatorname{Re}_x^{-1/2}$ may be enhanced by modifying the proportion of copper nanoparticle volume fraction that exceeds that of magnetite.

Figures 4.4 and 4.5 display the temperature profiles and velocity profiles for different values of the stretching parameter, ε. An increase in parameter ε indicates a greater influence of the stretching velocity ax on the free stream velocity bx, resulting in a reduction in the thickness of the thermal boundary layer in Figure 4.4. This observation aligns with the findings of Mohamed *et al.* (2019b). Finally, Figure 4.5 concludes that if the free stream velocity ($\varepsilon < 1$) is greater than the stretching velocity of the surface, it results in the flow having a boundary layer structure. Conversely, in the case of an inverted boundary layer flow, the thickness of the momentum boundary layer decreases with $\varepsilon > 1$ (Mohamed *et al.,* 2013b).

Table 4.1 Comparison values of $C_f \mathrm{Re}_x^{1/2}$ with previously published results.

ϕ_1	**Yasin *et al.* (2018a)**				**Present Result**			
	M=1	**M=2**	**M=5**	**M=10**	**M=1**	**M=2**	**M=5**	**M=10**
0.01	1.639	1.937	2.637	3.506	1.639	1.937	2.637	3.506
0.10	2.155	2.547	3.467	4.610	2.155	2.547	3.467	4.610
0.20	2.842	3.358	4.572	6.080	2.842	3.358	4.572	6.080

Table 4.2 The values of $Nu_x \mathrm{Re}_x^{-1/2}$ and $C_f \mathrm{Re}_x^{1/2}$ for various values of ε.

ε	$Nu_x \mathrm{Re}_x^{-1/2}$	$C_f \mathrm{Re}_x^{1/2}$
0	2.39742	2.41828
0.5	3.54431	1.34050
1	4.49063	0.00000
2	5.99939	-3.20462
2.5	6.62046	-4.94039

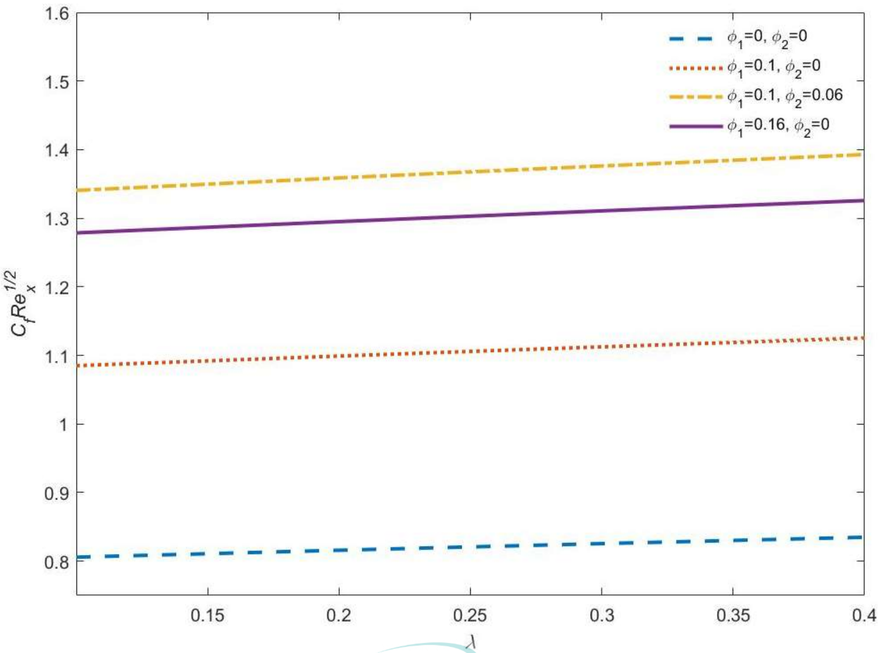

Figure 4.1 Distribution of $C_f \, \mathrm{Re}_x^{1/2}$ for various values of λ for different nano particle volume fractions.

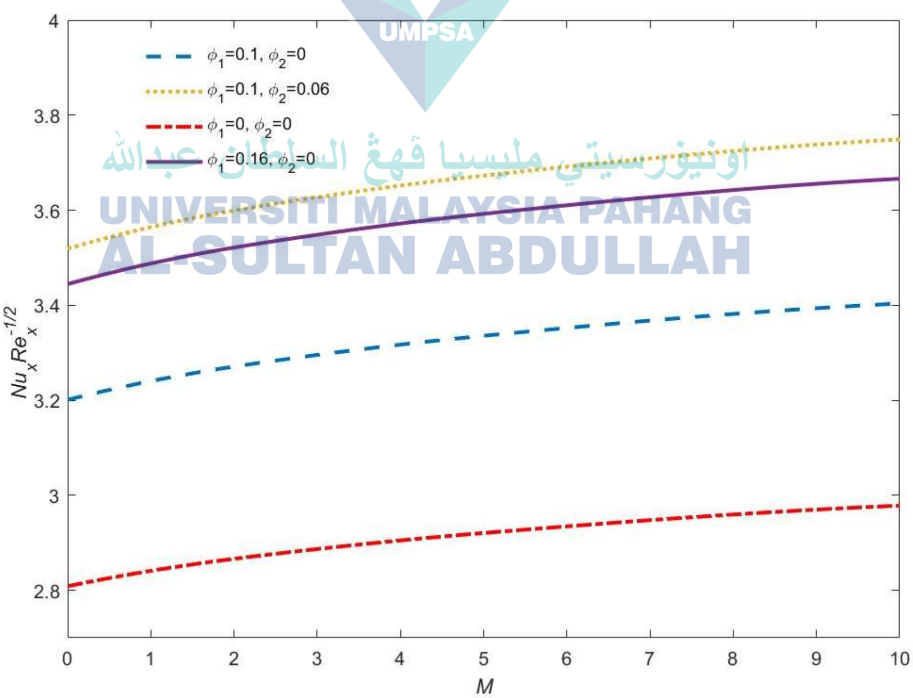

Figure 4.2 Distribution of $Nu_x \, \mathrm{Re}_x^{-1/2}$ with M for different nanoparticle volume fraction.

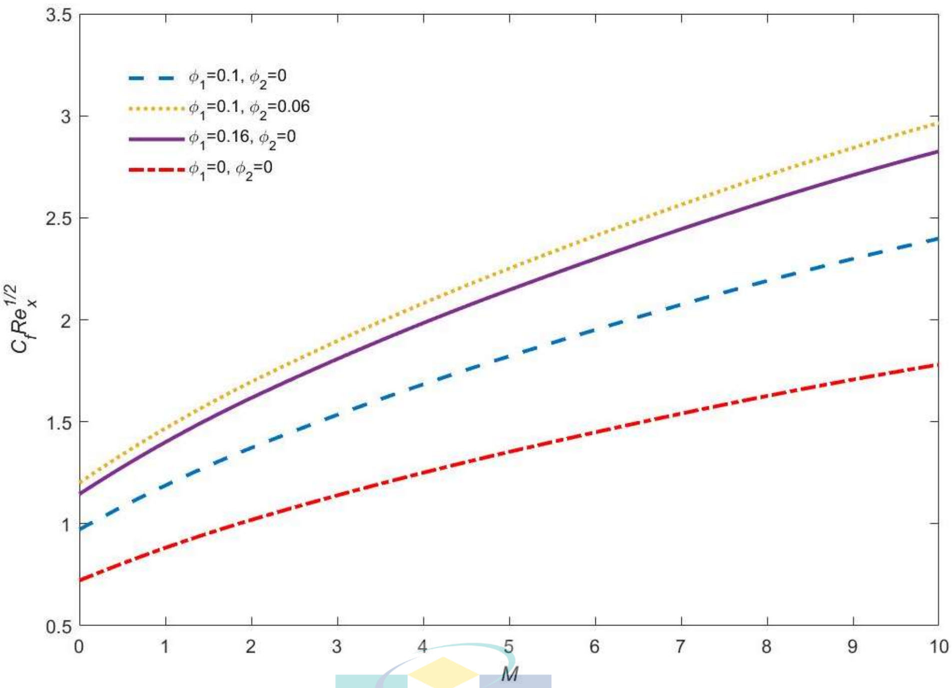

Figure 4.3 Distribution of $C_f \operatorname{Re}_x^{1/2}$ with M for different nanoparticle volume fraction.

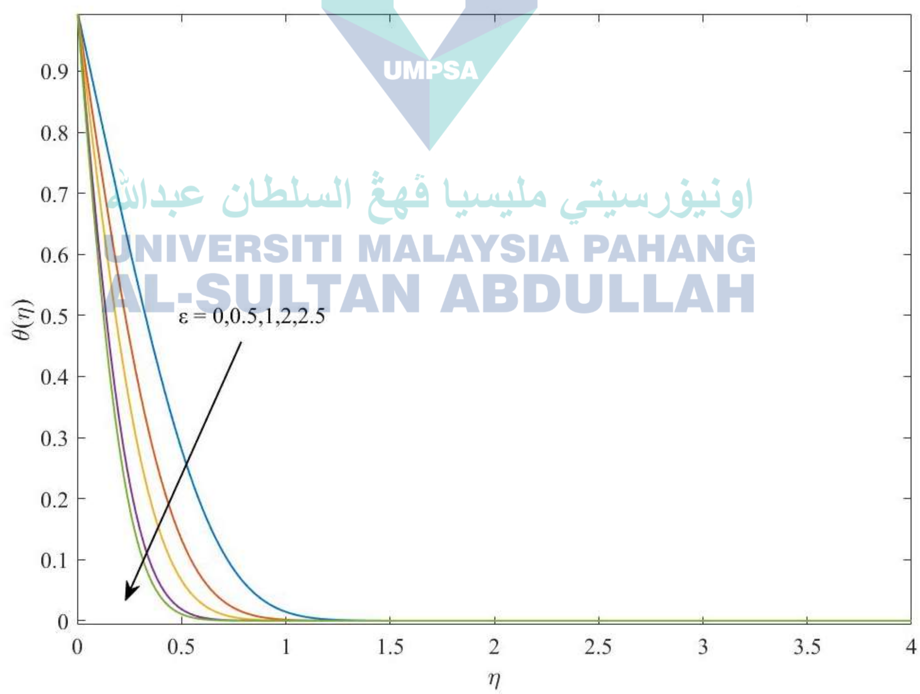

Figure 4.4 Temperature profiles for various values of ε.

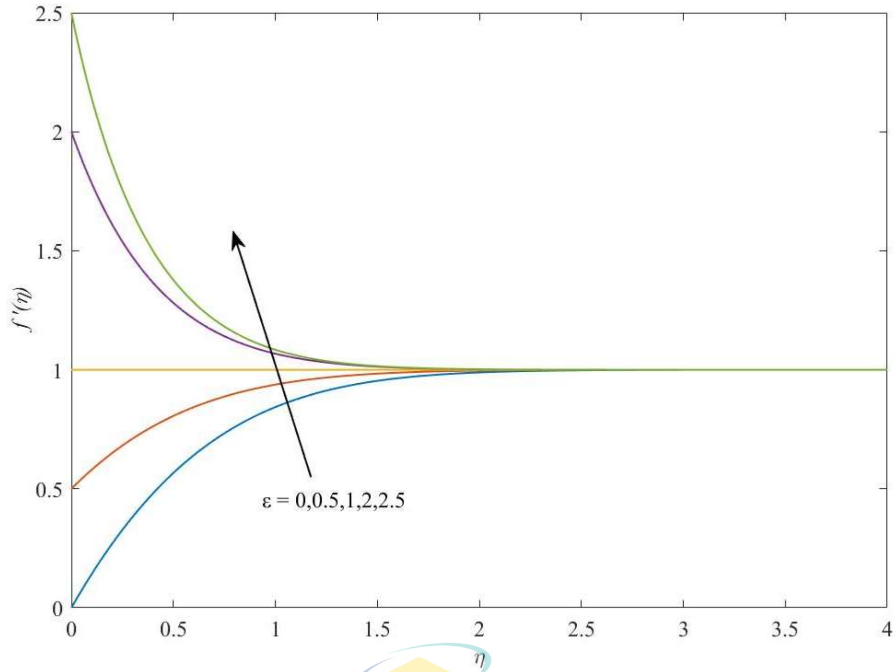

Figure 4.5 Velocity profiles for various values of ε.

4.4 Conclusion

This chapter has addressed the convective boundary layer flow and heat transfer of Williamson hybrid ferrofluid on a stagnation point towards a stretched sheet. The study demonstrated the impact of the magnetic parameter M, the Williamson fluid parameter λ, the stretching parameter ε, and the volume fractions of nanoparticles ϕ_1, ϕ_2 for Fe_3O_4 and Cu respectively on the temperature profiles, velocity profiles, reduced Nusselt number $Nu_x \mathrm{Re}_x^{-1/2}$, and skin friction $C_f \mathrm{Re}_x^{1/2}$. The research findings can be summarized as follows:

- The distribution of reduced Nusselt number and skin friction values for Williamson hybrid ferrofluid is the highest compared to other types of fluid that are compared.
- The Lorentz force, which opposes the fluid flow, leads to a rise in the skin friction coefficient as the magnetic parameter increases.
- As the stretching parameter increases, the thickness of the thermal and momentum boundary layer decreases.

CHAPTER 5

BOUNDARY LAYER FLOW OF WILLIAMSON HYBRID FERROFLUID OVER A PERMEABLE STRETCHING SHEET WITH THERMAL RADIATION EFFECTS

5.1 Introduction

This chapter investigated the mathematical model of a Williamson hybrid ferrofluid flow over a permeable stretching sheet with thermal radiation effects. The works from Salleh *et al.* (2010), Yasin *et al.* (2018a), and Mohamed *et al.* (2019a) are the specific cases of this problem. Crane (1970) has pioneered the research of the boundary layer flow on stretching sheets. Investigating incompressible viscous fluid flow over a stretching plate, Crane discovered that the boundary layer for fluid velocity varied linearly with the distance from a fixed point using an analytical solution. Kumaran *et al.* (2009) stated that the researchers extended Crane studies and obtained closed-form solutions. The liquid used for cooling and the rate of stretching are the two factors that would determine the desired fluid mechanical properties of such a process. Some applications in the industrial and manufacturing industries where stretching sheets play a major role in the quality of products are paper production, hot rolling, extrusion, metal spinning, and fiber making (Ahmed *et al.,* 2021). Other than conduction and convection, thermal radiation is another heat and energy transfer method, and it is the only heat transfer method that occurred without medium of transfer (vacuum). This method of heat and energy transfer influenced by a variety of physical systems, including heat, gas flow, and mass transit. The properties of thermal radiation in heat transfer processes become provocatively more apparent, especially at high temperatures. In engineering application thermal radiation plays role in process that involves high temperature such as nuclear power plants, polymer and glass productions, gas turbines, and so forth radiation mode contributes significantly (Saeed *et al.,* 2021b). Permeable surfaces through which the fluid is either injected or sucked received an interest from researchers due to their practical application towards boundary layer management and thermal protection of high energy flow by means of mass transfer. Jusoh *et al.* (2018) and Jalili *et al.* (2019) both study the characteristics of ferrofluid over a permeable stretching sheet. Mohamed *et al.* (2019a) compared three types of ferroparticles in their investigation of boundary layer flow and heat transfer over a permeable flat plate. His research on the permeability rate found that skin friction increased with suction rate but reduced with injection rate. The difference between this problem with Chapter 4 is that the exclusion of stagnation points flow, and the flow of the fluid are horizontal. Then this problem introduced additional parameter: permeability rate parameter and thermal radiation parameter. From Chapter 3 mathematical model, Chapter 5 will modify and extend the model to add two parameter which are the permeability rate and thermal radiation parameter and transformed into ordinary differential equation.

5.2 Mathematical Formulation

A steady two-dimensional Williamson hybrid ferrofluid flow on a permeable stretching sheet with ambient temperature is considered. As illustrated in Figure 5.1, assuming that $T = T_w$ is the wall temperature, u and v are the velocity components along the x and y axes, respectively. Next q_r is the radiative heat flux and B_0 is the uniform magnetic field of strength that is assumed to be applied the positive y - directional normal to the flat plate.

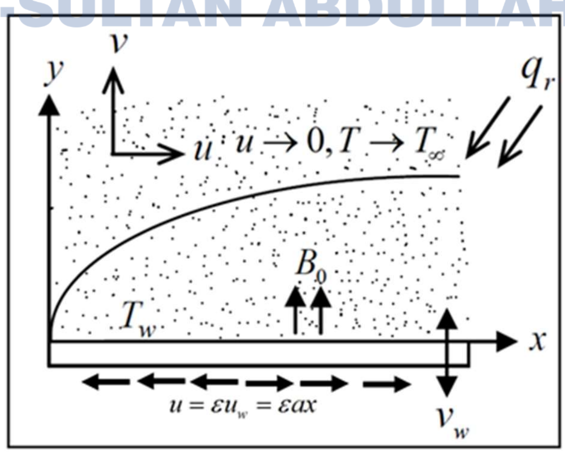

Figure 5.1 Physical model and the coordinate system of Williamson hybrid ferrofluid flow over a permeable stretching sheet.

The governing equations in the form of Navier-Stoke equations that can be formed are (Salleh *et al.,* 2010; Yasin *et al.,* 2018a; Hashim *et al.,* 2019b; Mohamed *et al.,* 2019a):

$$\frac{\partial u}{\partial x}+\frac{\partial v}{\partial y}=0, \tag{5.1}$$

$$u\frac{\partial u}{\partial x}+v\frac{\partial u}{\partial y}=\nu_{hnf}\frac{\partial^2 u}{\partial y^2}+\sqrt{2}\ \nu_{hnf}\,\Gamma\frac{\partial u}{\partial y}\frac{\partial^2 u}{\partial y^2}-\frac{\sigma B_o^2(x)}{\rho_{hnf}}u, \tag{5.2}$$

$$u\frac{\partial T}{\partial x}+v\frac{\partial T}{\partial y}=\frac{k_{hnf}}{\left(\rho C_p\right)_{hnf}}\frac{\partial^2 T}{\partial y^2}-\frac{1}{\left(\rho C_p\right)_{hnf}}\frac{\partial q_r}{\partial y}. \tag{5.3}$$

with boundary conditions:

$$\begin{gathered} u=\varepsilon u_w=\varepsilon ax,\ v=v_w,\ T=T_w \text{ at } y=0 \\ u\to 0,\quad T\to T_\infty,\ \text{as } y\to\infty \end{gathered} \tag{5.4}$$

ε is a stretching parameter and v_w is a plate permeability rate. Using the Rosseland approximation for radiation, the radiative heat flux is simplified as (Zheng *et al.,* 2013):

$$q_r=-\frac{4\sigma^*}{3k^*}\frac{\partial T^4}{\partial y} \tag{5.5}$$

where σ^* and k^* are the Stefan-Boltzmann constant and the mean absorption coefficient, respectively. The hybrid ferrofluid kinematic viscosity, a dynamic viscosity, a density, and electric conductivity are denoted as v_{hnf}, μ_{hnf}, ρ_{hnf} and σ , respectively. Furthermore, Γ, k_{hnf} and $(C_p)_{hnf}$ are the time constant, the thermal conductivity, and the heat capacity of Williamson hybrid ferrofluid, respectively. Other properties related to base fluid and the nanoparticles are denoted with subscript bf and $s1, s2$ respectively. We assume that the temperature differences within the flow through the fluid, such as that the term T^4 may be expressed as a linear function of temperature. Hence, expanding T^4 in a Taylor series about T_∞ and neglecting higher-order terms, we get:

$$T^4 \cong 4T_\infty^3 T - 3T_\infty^4 \qquad 5.6$$

In view of Equations 5.5 and 5.6, Equation 5.3 reduces to

$$u\frac{\partial T}{\partial x} + v\frac{\partial T}{\partial y} = \left(\frac{k_{hnf}}{\left(\rho C_p\right)_{hnf}} + \frac{16\sigma^* T_\infty^3}{3\left(\rho C_p\right)_{hnf} k^*} \right) \frac{\partial^2 T}{\partial y^2}. \qquad 5.7$$

The similarity variables considered are as follows (Salleh *et al.,* 2010):

$$\eta = \left(\frac{a}{\nu_f}\right)^{1/2} y,\ \ \psi = \left(a\nu_f\right)^{1/2} xf(\eta),\ \ \theta(\eta) = \frac{T - T_\infty}{T_w - T_\infty}, \qquad 5.9$$

where η, ψ and θ is a non-dimensional variable, dimensional stream function, and temperature, respectively. The similarity variables in Equation 5.9 satisfy the continuity Equation 5.1.

$$u = \frac{\partial \psi}{\partial y} \text{ and } v = -\frac{\partial \psi}{\partial x}. \qquad 5.10$$

Next, substitute the similarity variables Equations 5.9 and 5.10 into governing Equations 5.2 and 5.3, which gives the following transformed ordinary differential equations:

$$\frac{\nu_{hnf}}{\nu_f}\left(f''' + \lambda f'' f'''\right) + ff'' - f'^2 - Mf' = 0, \qquad 5.11$$

$$\frac{k_{hnf}}{k_f}\frac{\left(\rho C_p\right)_f}{\left(\rho C_p\right)_{hnf}}\left(1 + \frac{4}{3}N_R\right)\theta'' + \Pr f\theta' = 0. \qquad 5.12$$

The boundary conditions Equation 5.4 become

$$f(0)=S,\ \ f'(0)=\varepsilon,\ \ \theta(0)=1,$$
$$f'(\eta)\to 0,\ \ \theta(\eta)\to 0,\ \text{as}\ \eta\to\infty. \tag{5.13}$$

By definition, $S=-\dfrac{v_w}{(av_f)^{1/2}}$ is the permeability parameter at the plate surface, with S>0 and S<0 corresponding for suction and injection, respectively. $N_R=\dfrac{4\sigma^* T_\infty^3}{k^* k_{hnf}}$ is the thermal radiation parameter. Definitions for Pr, λ, ε, and M are mentioned in Chapter 4. Other quantities related to hybrid nanofluid are mentioned in Equation 3.19. The physical quantities of interest are the skin friction coefficient C_f and the local Nusselt number Nu_x. Skin friction coefficient is the same as in Equation 4.3. The local Nusselt number Nu_x is given by:

$$Nu_x=\frac{xq_w}{k_f(T_w-T_\infty)}, \tag{5.14}$$

with the surface heat flux q_w are given by

$$q_w=-k_{hnf}\left(\frac{\partial T}{\partial y}\right)_{\bar{y}=0}+q_r, \tag{5.15}$$

Using variables in Equation 3.40, Equation 5.14 give

$$Nu_x \operatorname{Re}_x^{-1/2}=-\frac{k_{hnf}}{k_f}\left[1+\frac{4}{3}N_R\right]\theta'(0) \tag{5.16}$$

5.3 Results and Discussion

The non-linear ordinary differential Equations 5.11 and. 5.12 with boundary conditions Equation 5.13 were solved using the Keller-box method with 6 physical parameters that will be considered, namely thermal radiation parameter, magnetic parameter, Williamson parameter, stretching parameter, permeability plate parameter, and nanoparticle volume fraction. The thermophysical properties of fluid and particles that are used for this research can be referred to Table 3.1. The nanoparticle volume fraction used for the hybrid ferrofluid is the same as in Chapter 4. A previously published result validates the efficiency of the method used in this study. Table 5.1 shows a comparison between present and previously published results, which also used the Keller-box method. Table 5.1 shows that the results obtained in this study are accurate with $\phi_1 = \phi_2 = M = \lambda = \varepsilon = N_R = S = 0$. Boundary layer thickness, step size, parameter M, ε and λ values inserted in KBM for this problem are the same as in Chapter 4.

Table 5.2 shows the result of $Nu_x \mathrm{Re}_x^{-1/2}$ and $C_f \mathrm{Re}_x^{1/2}$ for various values of magnetic parameter, M , with $\Pr = 21,\ \lambda = 1,\ \varepsilon = 0.5,\ N_R = 1,$ and $S = 0.5$. The increasing strength of magnetic effects causes `inclination of $C_f \mathrm{Re}_x^{1/2}$ values and reduction in $Nu_x \mathrm{Re}_x^{-1/2}$ values. Magnetic parameters induce Lorentz force, which slows down the fluid velocity via ferroparticles, thus opposing the flow and increasing the skin friction values.

Table 5.3 shows the effects of a stretching parameter ε on both $Nu_x \mathrm{Re}_x^{-1/2}$ and $C_f \mathrm{Re}_x^{1/2}$ with $\Pr = 21,\ M = 0.5,\ \lambda = 0.1,\ N_R = 1,$ and $S = 0.5$. As ε increases, it is observed that both $Nu_x \mathrm{Re}_x^{-1/2}$ and $C_f \mathrm{Re}_x^{1/2}$ increases. Physically, as ε increases, the stretching velocity increases, thus dragging the fluid together with the plate, which then reduces the skin friction of the fluid. This result is similar to the results from Hashim *et al.* (2019b).

Table 5.4 shows the effects of the permeability rate parameter S on both $Nu_x \mathrm{Re}_x^{-1/2}$ and $C_f \mathrm{Re}_x^{1/2}$ values with $\Pr = 21,\ M = 0.5,\ \varepsilon = 0.5,\ \lambda = 0.1,$ and $N_R = 1$. Gumber *et al.* (2022) and Ishak (2010) are the referenced for the parameter values. Noted that ($S < 0$) and ($S > 0$) are the injection and suction parameters, respectively. It can be concluded that increasing the S parameter results in an increase in both quantities. This result is in line with the claim from Jahan *et al.* (2018) and Naramgari and Sulochana (2016). The result for the permeability injection rate ($S < 0$) will be the opposite of permeability suction rate ($S > 0$) where skin friction and Nusselt number value are decreasing. Noticed that the large injection rate effect may promote the pure conduction heat transfer process ($Nu_x \mathrm{Re}_x^{-1/2} \simeq 0$).

Figures 5.2 illustrates the distributions of $C_f \mathrm{Re}_x^{1/2}$ with various values of λ parameter for different types of fluid with $\mathrm{Pr} = 21,\ M = 0.5,\ \varepsilon = 0.5,\ S = 0.5,$ and $N_R = 1$. Figure 5.2 shows the hybrid ferrofluid has the highest distributions of skin frictions values compared to other types of fluid similar to Figure 4.1. Different with Figure 4.1, the $C_f \mathrm{Re}_x^{1/2}$ is decreasing with an increase of λ for all types of fluid compared. This result is actually similar with the research from Nadeem *et al.,* (2013b; 2014). Nadeem mentioned that the skin friction is decreasing due to the values of $f''(0)$ being negative and skin friction equation, Equation 4.3, is the sum of $f''(0)$ and its square. The square being positive multiplied by a fraction (λ) less than 1, the difference is reduced as λ increases. Thus reduces the distributions of $C_f \mathrm{Re}_x^{1/2}$ as illustrated in Figure 5.2.

The effects of thermal radiation parameter N_R , as well as various nanoparticle volume fractions are illustrated in Figures 5.3 and 5 with the parameter values are referred from Zeeshan *et al.* (2016). From Figure 5.3, it shows that the $Fe_3O_4 - Cu$ /blood hybrid ferrofluid ($\phi_1 = 0.1, \phi_2 = 0.06$) scored the highest in $Nu_x \mathrm{Re}_x^{-1/2}$. Physically, $Fe_3O_4 - Cu$ /blood hybrid ferrofluid has better performance in heat transfer compared to blood-based viscous fluid ($\phi_1 = \phi_2 = 0$) and Fe_3O_4 /blood ferrofluid ($\phi_1 = 0.1, \phi_2 = 0$). Its performance is almost similar with the concentrated Fe_3O_4 /blood ferrofluid ($\phi_1 = 0.16, \phi_2 = 0$) as N_R increases. Figure 5.4 shows that the blood hybrid ferrofluid produces the highest skin friction compared to other fluids. This is due to the presence of copper in the fluid, which has high-density properties. Besides, it is found that the increase of N_R does not affect the skin friction of ferroparticle volume fractions, it produces constant $C_f \mathrm{Re}_x^{1/2}$ values throughout the parameter. This phenomenon is realistic where N_R has no relation with the velocity term in Equation 5.2.

Figures 5.5 and 5.6 illustrate the temperature and velocity for various magnetic parameters. Increasing the magnetic parameter reduces the boundary layer for velocity profiles in Figure 5.6 due to Lorentz force, as mentioned before. Due to the slow momentum of nanoparticles because of the magnetic presence, the thermal boundary layer increases with the rise of magnetic parameter.

The effects of stretching parameters for temperature and velocity profile are illustrated in Figure 5.7 and 5.8. The temperature profile shows a reduction of boundary layer while velocity profile shows the opposite characteristics when the stretching parameter increases.

Figures 5.9 and 5.10 showed significant changes of boundary layer with the permeability rate parameter. It can be seen in the temperature profile, Figure 5.9, when ($S > 0$) it starts to develop a boundary layer, and as the permeability rate increases, the thermal boundary layer is reduced. The momentum boundary layer in Figure 5.10 also decreases as the parameter increases. According to Devi and Anjali Devi (2016), an increase in suction parameters tends to force the fluid into a vacant space, which causes a reduction in temperature and velocity profile.

Table 5.1 Comparison values of $-\theta'(0)(CWT)$ with previously published result.

Pr	$-\theta'(0)$	
	Salleh *et al.* (2010)	**Present Result**
0.72	0.46317	0.46697
1	0.58198	0.58266
3	1.16522	1.16516
10	2.30821	2.30795

Table 5.2 Results $Nu_x \mathrm{Re}_x^{-1/2}$ and $C_f \mathrm{Re}_x^{1/2}$ for various values of M.

M	$Nu_x \mathrm{Re}_x^{-1/2}$	$C_f \mathrm{Re}_x^{1/2}$
0	12.44450	0.85161
1	12.27305	1.25583
2	12.15307	1.53795
5	11.95180	2.14104
10	11.74956	2.83803

Table 5.3 Results $Nu_x \mathrm{Re}_x^{-1/2}$ and $C_f \mathrm{Re}_x^{1/2}$ and for various values of ε.

ε	$Nu_x \mathrm{Re}_x^{-1/2}$	$C_f \mathrm{Re}_x^{1/2}$
0.6	12.65888	1.33770
0.8	13.23635	1.88913
1	13.76078	2.47926
1.2	14.24307	3.10163
1.4	14.69011	3.75022

Table 5.4 Results $Nu_x \mathrm{Re}_x^{-1/2}$ and $C_f \mathrm{Re}_x^{1/2}$ for various values of S.

S	$Nu_x \mathrm{Re}_x^{-1/2}$	$C_f \mathrm{Re}_x^{1/2}$
-0.8	0.00006	0.53796
-0.6	0.01754	0.59573
-0.4	0.34321	0.66201
-0.2	1.64054	0.73749
0	3.99166	0.82271
0.5	12.34609	1.07876
1	21.97220	1.39027
1.2	25.94791	1.52752
1.4	29.96149	1.67064

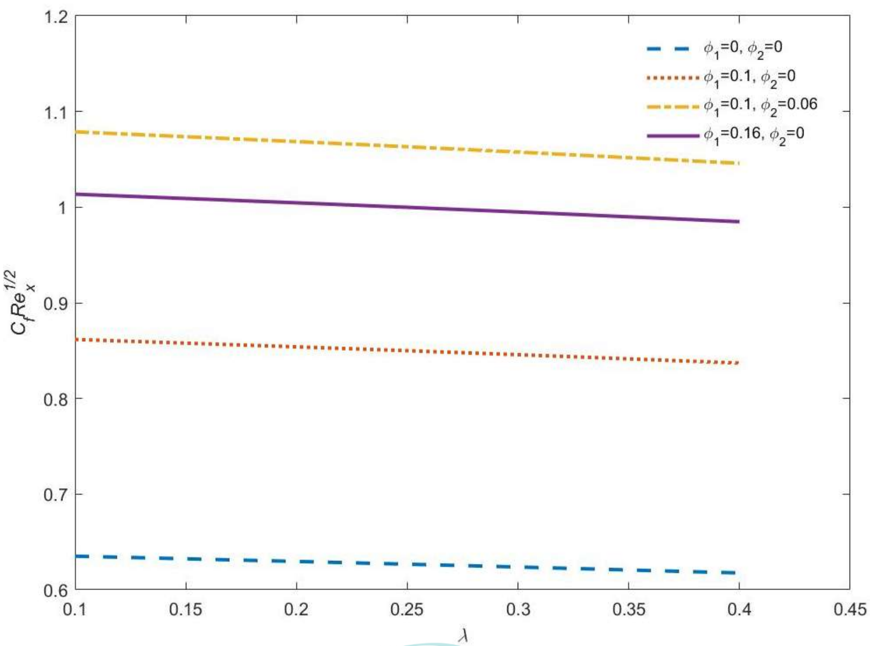

Figure 5.2 Velocity profiles for various values of λ for different nano particle volume fractions.

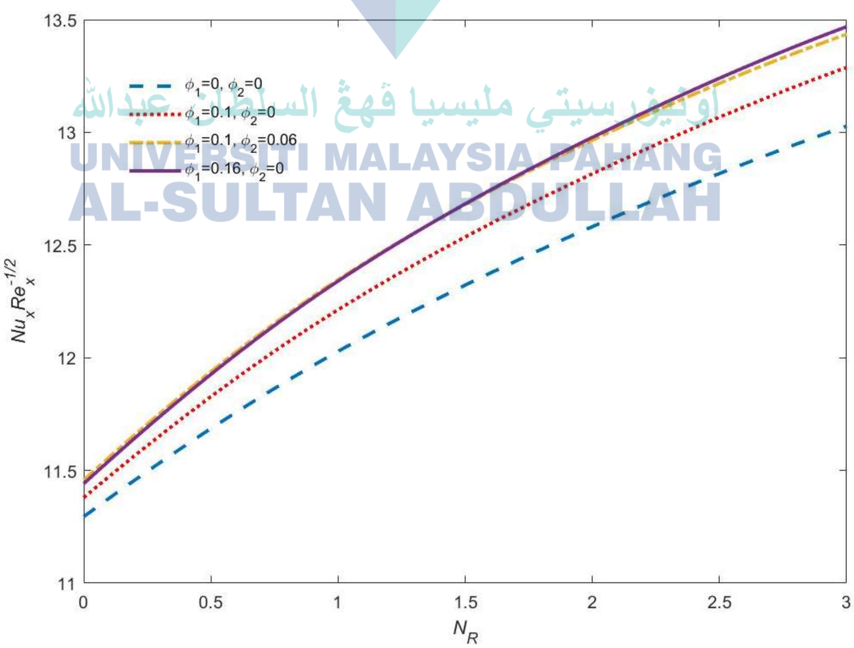

Figure 5.3 Distribution of $Nu_x \mathrm{Re}_x^{-1/2}$ with N_R for different nanoparticle volume fractions.

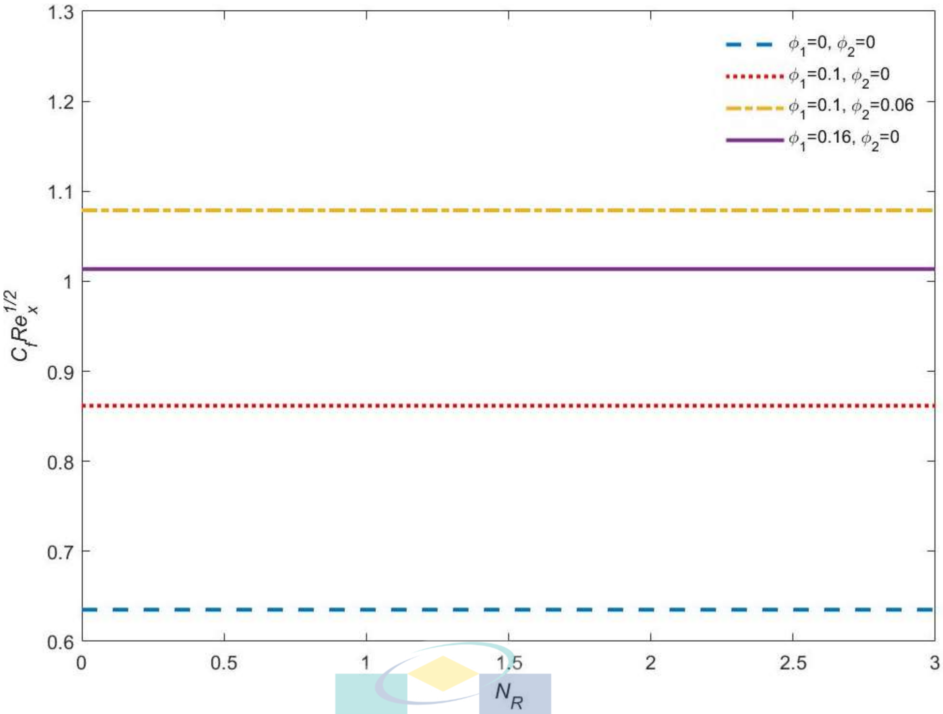

Figure 5.4 Distribution of $C_f \operatorname{Re}_x^{1/2}$ with N_R for different nanoparticle volume fractions.

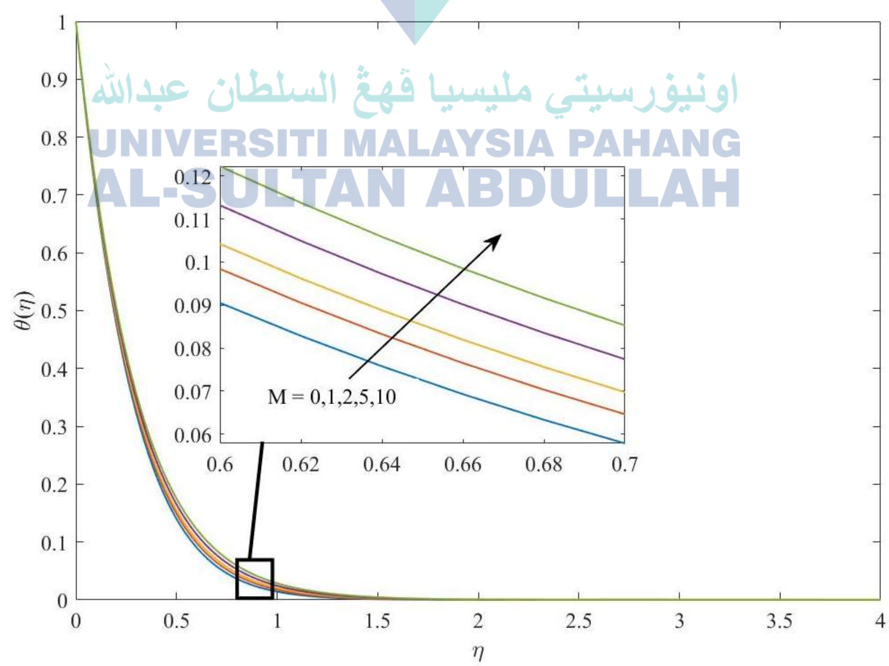

Figure 5.5 Temperature profiles for various values of M .

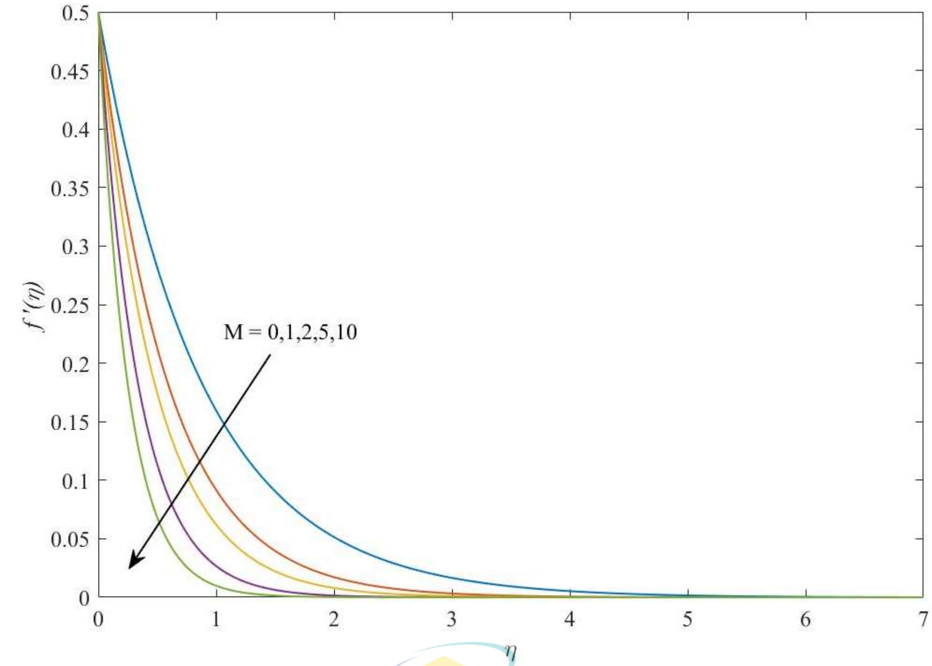

Figure 5.6 Velocity profiles for various values of M .

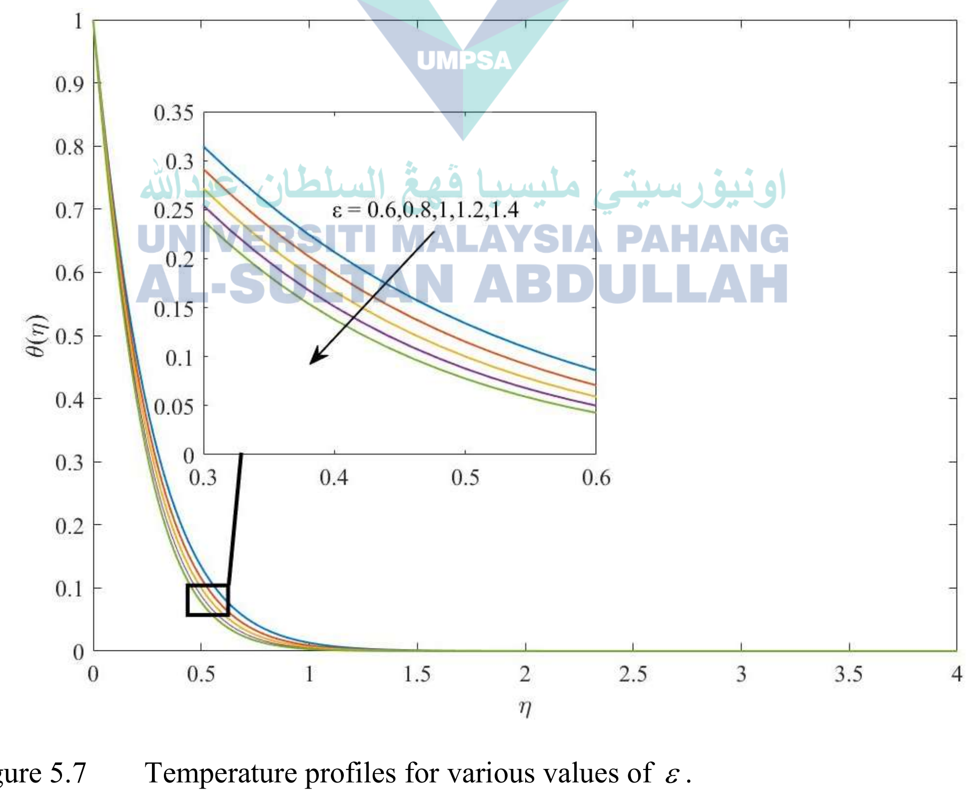

Figure 5.7 Temperature profiles for various values of ε .

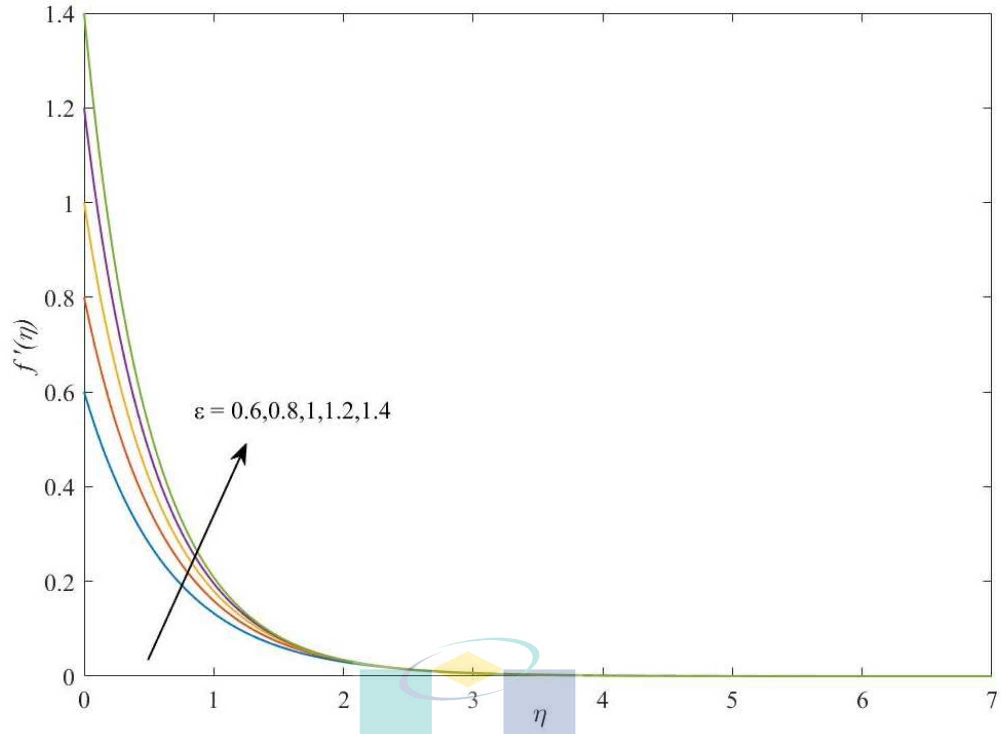

Figure 5.8 Velocity profiles for various values of ε.

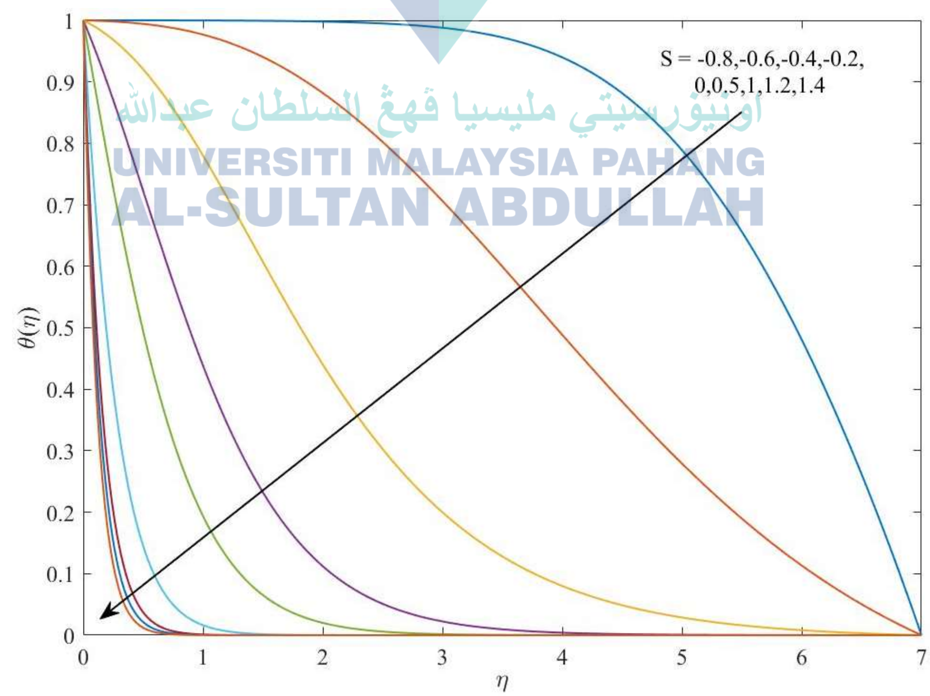

Figure 5.9 Temperature profiles for various values of S.

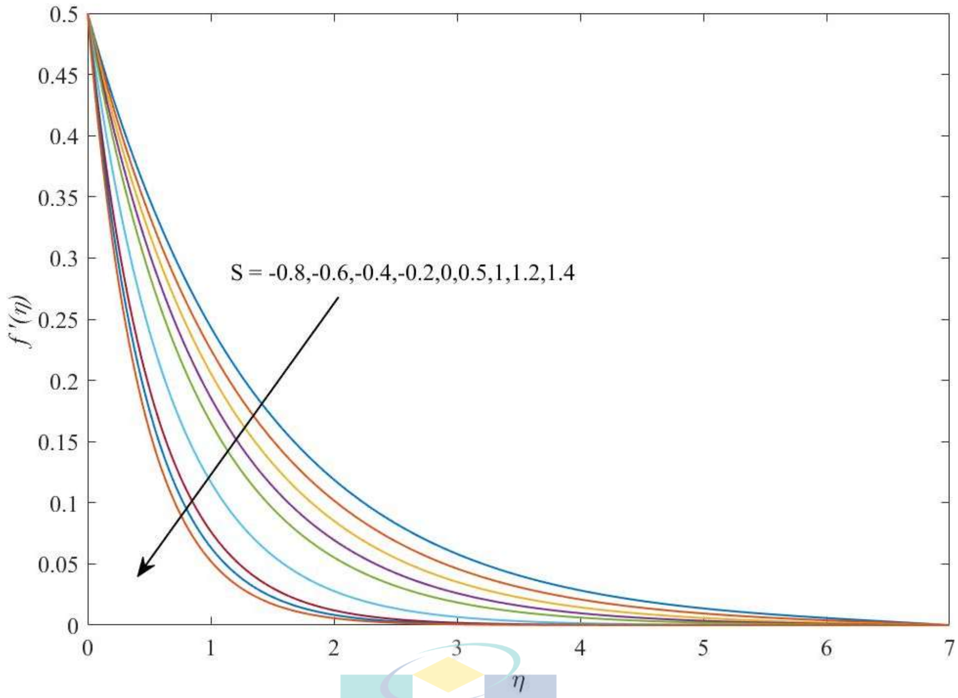

Figure 5.10 Velocity profiles for various values of S.

5.4 Conclusion

This chapter discusses the topic of convective boundary layer flow and heat transfer of Williamson hybrid ferrofluid om permeable stretching sheet with thermal radiation presents. The parameters involved in this research are similar to Chapter 4, with the addition of two new parameters. The effects of the magnetic parameter, M, Williamson parameter, λ, stretching parameter, ε, the permeability rate parameter, S, and the thermal radiation parameter, N_R, on the Nusselt number and the skin friction coefficient of Williamson hybrid ferrofluid is numerically studied. Below is the summary of the results:

- The blood hybrid ferrofluid has the same performance of heat transfer as ferrofluid with the same volume fraction of nanoparticle.
- The blood hybrid ferrofluid has the highest skin friction values when compared using the N_R and λ parameter to other types of ferroparticle volume fraction due to the presence of copper particles inside the fluid.

- The N_R parameter produces constant skin friction values due to the absence of respective parameter in the skin friction equation.
- Enhancing the stretching parameter and permeability rate parameter reduces the temperature profile while the magnetic parameter produces the opposite outcome.
- As Williamson parameter increase, distribution of $C_f \operatorname{Re}_x^{1/2}$ values are reduced due to $f''(0)$ values produce is negative.

CHAPTER 6

CONVECTIVE BOUNDARY LAYER FLOW OF WILLIAMSON HYBRID FERROFLUID OVER A MOVING PLATE WITH VISCOUS DISSIPATION

6.1 Introduction

This chapter investigates the convective boundary layer flow of a Williamson hybrid ferrofluid over a moving flat plate with viscous dissipation effects. Specific cases for this research are from Mohamed *et al.,* (2020c; 2021a; 2021c). The term "viscous dissipation" refers to how the kinetic energy produced by the fluid's motion is absorbed by the fluid's viscosity, then transformed into internal energy and heated by the fluid (Yap *et al.,* 2023). It controls the temperature profile during the heat transfer process and is crucial to the flow of energy. The reliability of viscous dissipation depends on the plate conditions whether it is frozen or heated. The effect of viscous dissipation on the thermal boundary layer was first identified by Gebhart (1962) and often ignored in unsteady conditions. From a practical point of view, this effect is important in several flow issues, and it is also the source of rising temperatures and geodynamic heating. In the behavior of dynamic temperature, which is equivalent to the attributed difference in heat transfer temperature, the impact of viscous dissipation cannot be ignored except for the lower velocity method due to the small temperature profile. Gebhart also pointed out that if the influence of viscous dissipation is neglected, then the natural convection flow is incomplete (Kausar *et al.,* 2022). This chapter differs from Chapter 4 and 5 where moving plate parameters and viscous dissipation are introduced. In addition, this chapter also discusses the comparison between blood hybrid ferrofluid with different types of hybrid ferrofluid.

6.2 Mathematical Formulation

A two-dimensional moving flat plate immersed in a steady Williamson hybrid ferrofluid with ambient temperature as (T_∞) is illustrated in Figure 6.1 below. It is assumed that the wall temperature, and velocity components along the x and y axes are defined as u and v. U_∞ defined as the free stream while $u = \Omega U_\infty$ is the moving plate velocity with Ω and B_0 as the plate velocity parameter and magnetic field strength proportional to $y-$ directional normal to the moving flat plate.

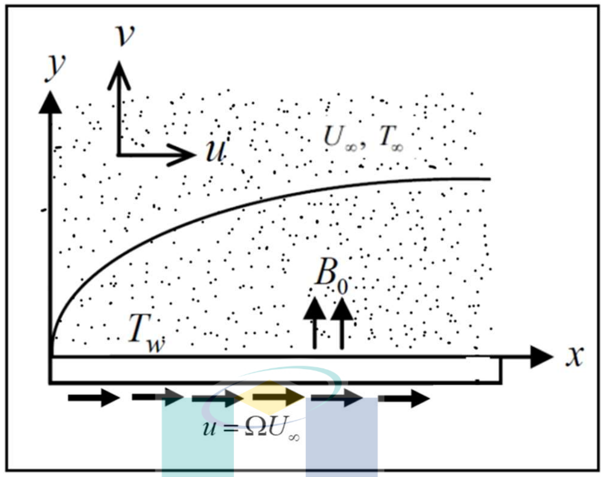

Figure 6.1 Physical model and the coordinate system of Williamson hybrid ferrofluid flow over a moving flat plate with viscous dissipation.

From Figure 6.1 above, the boundary layer equation that can be formed (Mohamed *et al.,* 2020c; 2021a; 2021c):

$$\frac{\partial u}{\partial x} + \frac{\partial v}{\partial y} = 0, \tag{6.1}$$

$$u\frac{\partial u}{\partial x} + v\frac{\partial u}{\partial y} = \nu_{hnf}\frac{\partial^2 u}{\partial y^2} + \sqrt{2}\,\nu_{hnf}\,\Gamma\frac{\partial u}{\partial y}\frac{\partial^2 u}{\partial y^2} - \frac{\sigma B_o^2(x)}{\rho_{hnf}}u, \tag{6.2}$$

$$u\frac{\partial T}{\partial x} + v\frac{\partial T}{\partial y} = \frac{k_{hnf}}{\left(\rho C_p\right)_{hnf}}\frac{\partial^2 T}{\partial y^2} + \frac{\mu_{hnf}}{\left(\rho C_p\right)_{hnf}}\left(\frac{\partial u}{\partial y}\right)^2. \tag{6.3}$$

with boundary conditions

$$\begin{gathered} u = \Omega U_\infty,\ v = 0,\ T = T_w \text{ at } y = 0 \\ u \to U_\infty,\quad T \to T_\infty, \text{ as } y \to \infty \end{gathered} \tag{6.4}$$

The hybrid ferrofluid kinematic viscosity, a dynamic viscosity, a density, and electric conductivity are denoted as $v_{hnf}, \mu_{hnf}, \rho_{hnf}$ and σ , respectively. Furthermore, Γ, k_{hnf} and $(C_p)_{hnf}$ are the time constant, the thermal conductivity, and the heat capacity of Williamson hybrid ferrofluid, respectively. Other properties related to base fluid and the nanoparticles are denoted with subscript bf and $s1$, $s2$ respectively. The hybrid ferrofluid properties are given as (Bachok *et al.,* 2012; Devi & Anjali Devi, 2017):

$$\eta = \left(\frac{U_\infty}{\nu x}\right)^{1/2} y, \;\; \psi = \left(U_\infty \nu x\right)^{1/2} f(\eta), \;\; \theta(\eta) = \frac{T - T_\infty}{T_w - T_\infty}, \qquad 6.5$$

where η, ψ and θ is a non-dimensional variable, dimensional stream function, and temperature, respectively. The similarity variables (6) satisfy the continuity equation (1) by definition:

$$u = \frac{\partial \psi}{\partial y} \text{ and } v = -\frac{\partial \psi}{\partial x}. \qquad 6.6$$

Next, substitute the similarity variables equations (6.2) and (6.3) into governing equations (6.5) and (6.6) gives the following transformed ordinary differential equations:

$$\frac{v_{hnf}}{v_f}\left(f''' + \lambda f'' f'''\right) + \frac{1}{2} ff'' - M\left(f' - 1\right) = 0, \qquad 6.7$$

$$\frac{1}{\Pr} \frac{k_{hnf}}{k_f} \frac{\left(\rho C_p\right)_f}{\left(\rho C_p\right)_{hnf}} \theta'' + \frac{1}{2} f \theta' + \frac{v_{hnf}}{v_f} \frac{\rho_{hnf}\left(C_p\right)_f}{\left(\rho C_p\right)_{hnf}} E_C f^{2''} = 0. \qquad 6.8$$

The boundary conditions (6.4) become

$$f(0) = 0, \;\; f'(0) = \Omega, \;\; \theta(0) = 1, \qquad 6.9$$

$$f'(\eta) \to 1, \;\; \theta(\eta) \to 0, \text{ as } \eta \to \infty.$$

By definition, $E_C = \dfrac{U_\infty^2}{\left(C_p\right)_f \left(T_w - T\infty\right)}$ is an Eckert number. Other parameter definitions for Pr, M and λ are similar to Chapter 4 and 5. Other quantities related to hybrid nanofluid are stated in Equation 3.19. The physical quantities of interest are the skin friction coefficient C_f and the local Nusselt number Nu_x. Skin friction coefficient C_f and the local Nusselt number Nu_x for this problem are similar with Equation 4.3.

6.3 Results and Discussion

This sub-section will discuss the results of Equations 6.7 and 6.8 as well as boundary conditions, Equation 6.9, numerically solved using the Keller-box method programmed in MATLAB software. The effects of physical parameters that are tested for this chapter are Eckert number E_C, magnetic M, Williamson λ, and moving plate parameter Ω. As mentioned earlier, this research includes a comparison of Williamson hybrid ferrofluid with various types of hybrids ferrofluid and different ferroparticle volume fractions. Thermophysical properties for blood, magnetite, and copper can be referred to Table 3.1. Other thermophysical properties of fluid and particles that are used for this research are also provided in Table 3.1. The nanoparticle volume fraction used for the hybrid ferrofluid is the same as in Chapter 4 and 5. The accuracy of numerical method is validated by comparing it with the previous numerical shown in Table 6.1 using copper-water fluid, $\Pr = 6.2$ with $\phi_1 = M = \lambda = \varepsilon = E_C = 0$. The method used for numerical solutions in previous studies was the shooting method. Comparison with both previous results achieved good agreement. Boundary layer thickness, step size, parameter M, and λ values inserted in KBM for this problem are the same as in Chapter 4 and 5.

Table 6.2 shows the values of $Nu_x \operatorname{Re}_x^{-1/2}$ and $C_f \operatorname{Re}_x^{1/2}$ change significantly as moving plate parameter increase with $\Pr = 21,\ \lambda = 0.1,\ \mathrm{M} = 0.5,\ E_C = 0.1$. As the moving plate parameter increases, $Nu_x \operatorname{Re}_x^{-1/2}$ values increase while $C_f \operatorname{Re}_x^{1/2}$ values decrease and produce negative values when $\Omega > 1$. When $\Omega = 1$ the fluid flowing on the moving surface experiences zero skin friction.

Distributions of $C_f \operatorname{Re}_x^{1/2}$ values with the influence of λ for several types of fluid is illustrated in Figure 6.2 with $\Pr = 21,\ \Omega = 0.5,\ \mathrm{M} = 0.5,\ E_C = 0.1$. Parameter values used for this parameter is same as in Chapter 4 and 5. It is seen that the Distributions of $C_f \operatorname{Re}_x^{1/2}$ values are still the highest compared to the other type of fluid compared similar to result in Figure 4.1 and 5.2. The trend distributions of $C_f \operatorname{Re}_x^{1/2}$ in Figure 6.2 is similar to the result from Figure 4.1 where the distributions are increasing.

Figures 6.3 and 6.4 illustrated the distributions of $Nu_x \operatorname{Re}_x^{-1/2}$ and $C_f \operatorname{Re}_x^{1/2}$ for four different ferroparticle volume fraction with the influence of viscous dissipation parameter known as Eckert number, E_C with $\Pr = 21,\ M = 0.5,\ \Omega = 0.1,\ \lambda = 0.1$. Mohamed *et al.,* (2020c; 2021a; 2021b) are the referenced used for the parameter values. Blood ($\phi_1 = \phi_2 = 0$), 0.1 vol. of Fe_3O_4/blood ferrofluid (s), 0.16 vol. of $Fe_3O_4 - Cu$ /blood hybrid ferrofluid ($\phi_1 = 0.1, \phi_2 = 0.06$), and 0.16 vol. of Fe_3O_4/blood ferrofluid ($\phi_1 = 0.16, \phi_2 = 0$) are the four ferroparticle volume fraction that is tested. Analyzing the results in Figures 6.3 and 6.4, the increase of E_C parameter reduces the performance of convective heat transfer but does not affect skin friction of the fluid. This result is similar with previous research done by Hasanuzzaman *et al.* (2023). When comparing different ferroparticle volume fractions, Figure 6.4 illustrates that blood hybrid ferrofluid produces the highest skin friction compared to other ferroparticle volume fractions. Blood has the lowest skin friction due to the absence of nanoparticles in the fluid, that resist the fluid flow. Considering the heat transfer performance, the 0.16 vol. of $Fe_3O_4 - Cu$ /blood hybrid ferrofluid has the best convective heat transfer performance as $E_C = 0$. The presence of E_C has eliminated the nanoparticle volume fraction effects, thus high E_c producing similar performance in convective heat transfer capabilities. It is clearly seen in Figure 6.4 that the values of $Nu_x \operatorname{Re}_x^{-1/2}$ become similar with the other volume fractions as E_C increases.

Figure 6.5 and 6.6 shows the distribution of $Nu_x \operatorname{Re}_x^{-1/2}$ and $C_f \operatorname{Re}_x^{1/2}$ for three types of blood-based hybrid ferrofluid with the influence of magnetic parameter, *M* with

$\Pr = 21,\ \lambda = 0.5,\ \Omega = 0.1,\ E_C = 0.1$. The three types of hybrids ferrofluid tested are blood with copper ferrite ($Fe_3O_4 - Cu$ /blood), cobalt ferrite with silver ($CoFe_2O_4 - Ag$ /blood) and manganese zinc ferrite with gold ($Mn - ZnFe_2O_4 - Au$ /blood). The ferroparticle volume is kept constant ($\phi_1 = 0.1, \phi_2 = 0.06$). Figure 6.5 illustrates that $Fe_3O_4 - Cu$ /blood has the highest convective heat transfer performance compared to $CoFe_2O_4 - Ag$ /blood and $Mn - ZnFe_2O_4 - Au$ /blood. It is noted that, the increase of magnetic parameter reduced the values of $Nu_x \operatorname{Re}_x^{-1/2}$. Physically, the increase in M , enhanced the magnetic force that attracts the hybrid ferrofluid to the plate surface, thus promoting the conductive heat transfer process, which translates into reducing the convective heat transfer capabilities. From Figure 6.6, it is found that the increase in magnetic parameters M enhanced the skin friction coefficient. The Lorentz force increases as the magnetic parameter increases, thus retarding the fluid flow and resisting the fluid flow for the hybrid ferrofluid tested. It is also found that the $Mn - ZnFe_2O_4 - Au$ /blood hybrid ferrofluid has the highest $C_f \operatorname{Re}_x^{1/2}$ values than $CoFe_2O_4 - Ag$ /blood and $Fe_3O_4 - Cu$ /blood hybrid ferrofluid. It is due to the high density of gold in the fluid, thus producing high resistance in fluid flow.

The effects of moving plate parameters on a temperature and velocity profile are illustrated in Figure 6.7 and 6.8. Parameter values are referred from Bachok *et al.* (2012) and Mohamed *et al.* (2020c). Respectively while in Figure 6.7, the boundary layer for the temperature profile decreases as the moving plate parameter increases. The area of boundary layer decreases due to the increase of $Nu_x \operatorname{Re}_x^{-1/2}$ values, which then promotes the convective heat transfer capabilities in the fluid. This trend is similar to the results from Mohamed *et al.* (2020c). In Figure 6.8, the velocity gradient is in inverted structure as $\Omega > 1$ and momentum boundary layer thickness decreases with the moving plate parameter. As $\Omega < 1$, the flow has the boundary layer structured, which is formed from the high plate velocity compared to the free stream velocity. It is observed that the boundary layer thickness increases with Ω. This pattern of boundary layer is similar to the findings of Mohamed *et al.* (2013b).

Table 6.1 Comparison values of $f''(0)$ with previously published result.

ϕ_2	$f''(0)$	
	Bachok *et al.* (2012)	**Present Result**
0	0.3321	0.3321
0.1	0.3901	0.3901
0.2	0.4045	0.4045

Table 6.2 Values of $Nu_x \mathrm{Re}_x^{-1/2}$ and $C_f \mathrm{Re}_x^{1/2}$ for various values of Ω.

Ω	$Nu_x \mathrm{Re}_x^{-1/2}$	$C_f \mathrm{Re}_x^{1/2}$
0	0.7231	1.2988
0.5	2.2283	0.6952
1	3.1745	0.0000
1.5	3.5172	-0.7728
2	3.1826	-1.6098

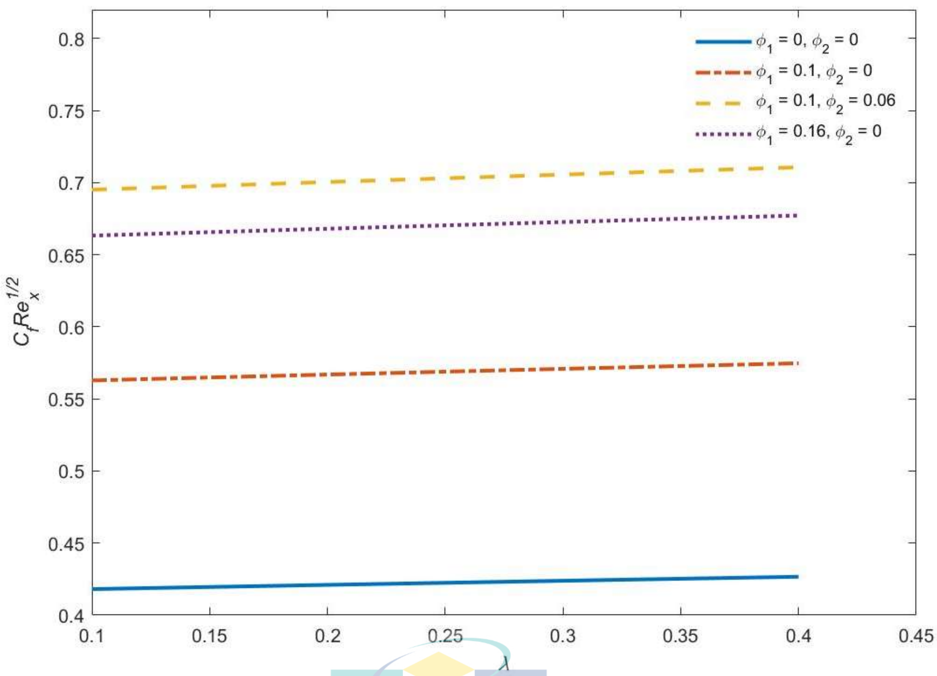

Figure 6.2 Velocity profiles for various values of λ for different nano particle volume fractions.

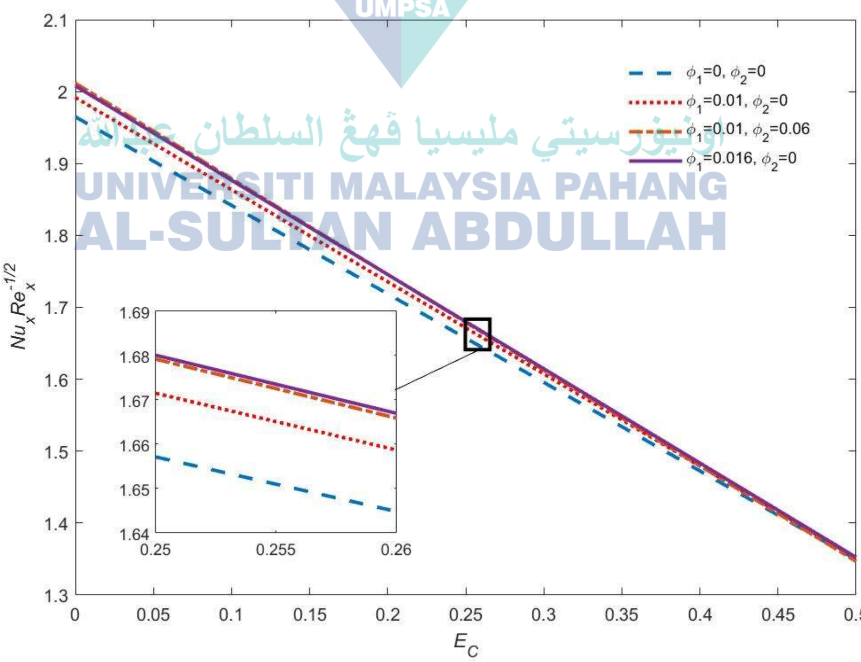

Figure 6.3 Distribution of $Nu_x \mathrm{Re}_x^{-1/2}$ with E_C for different nano particle volume fractions.

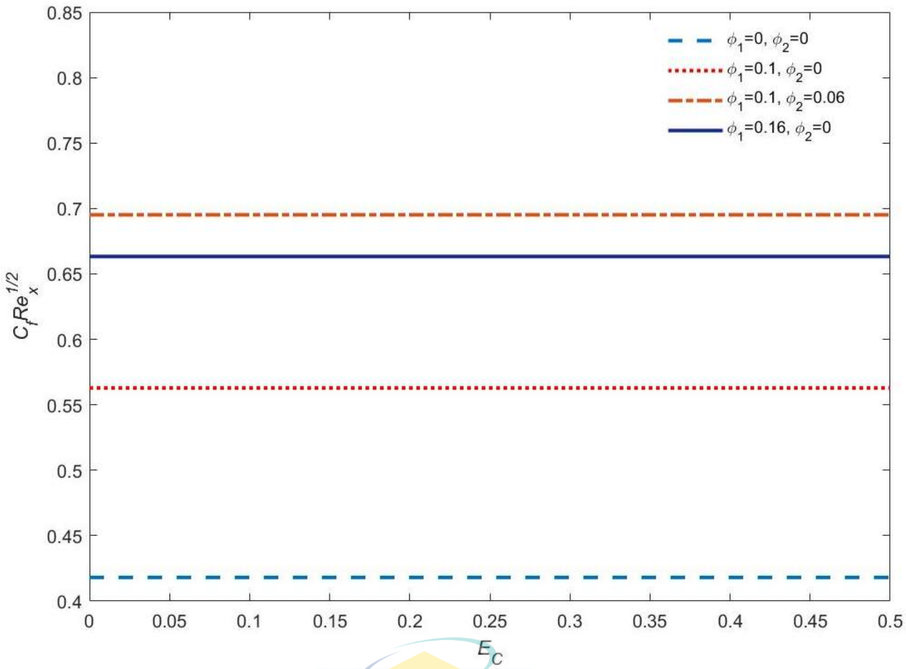

Figure 6.4 Distribution of $C_f \,\mathrm{Re}_x^{1/2}$ with E_C for different nano particle volume fractions.

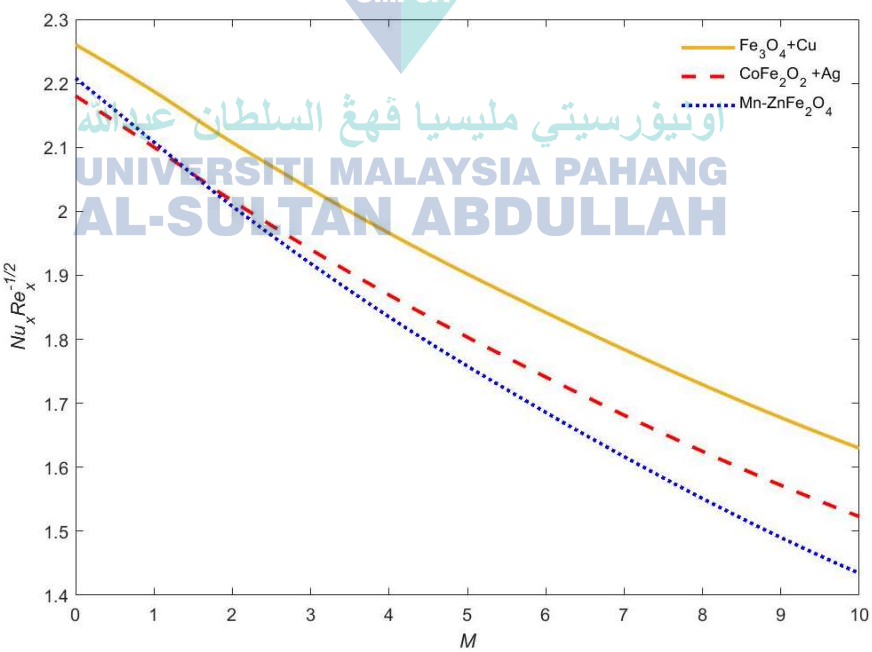

Figure 6.5 Distribution of $Nu_x \,\mathrm{Re}_x^{-1/2}$ with M for different types of hybrid ferrofluid.

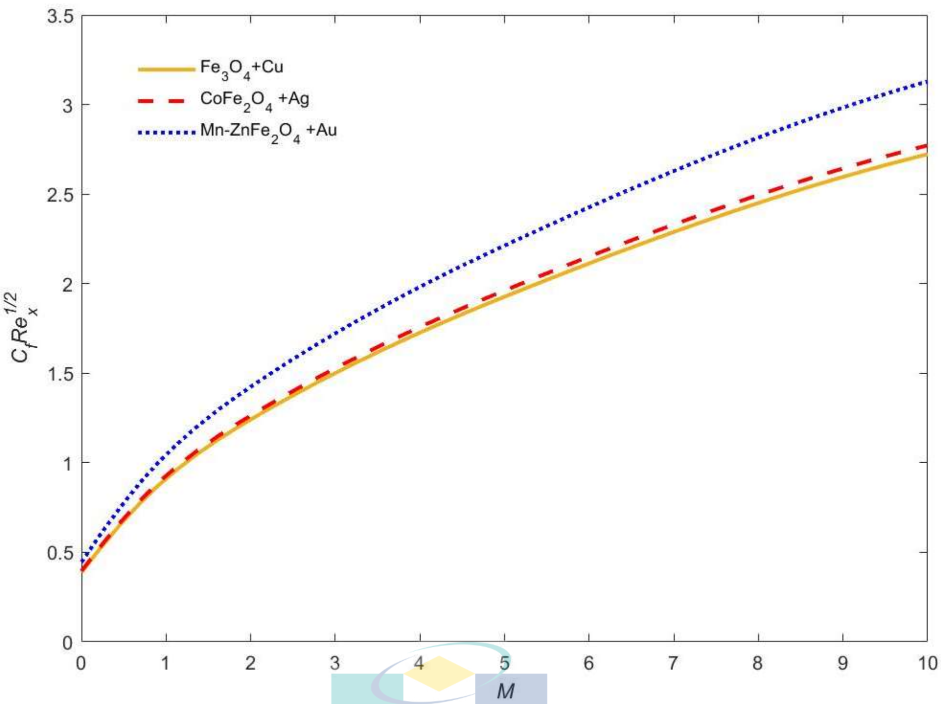

Figure 6.6 Distribution of $C_f \mathrm{Re}_x^{1/2}$ with M for different types of hybrid ferrofluid.

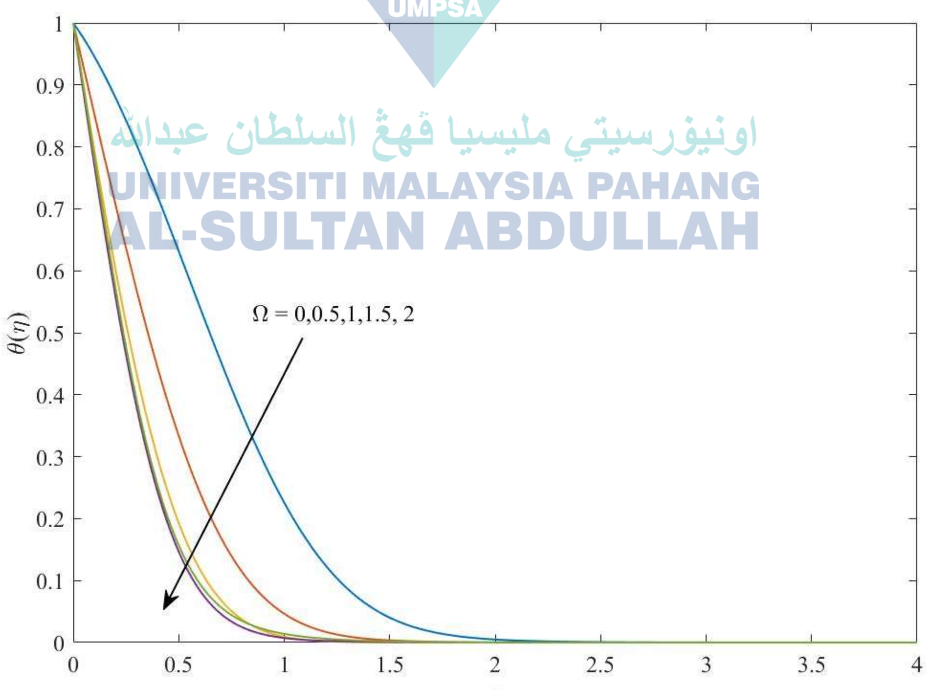

Figure 6.7 Temperature profiles for various values of Ω.

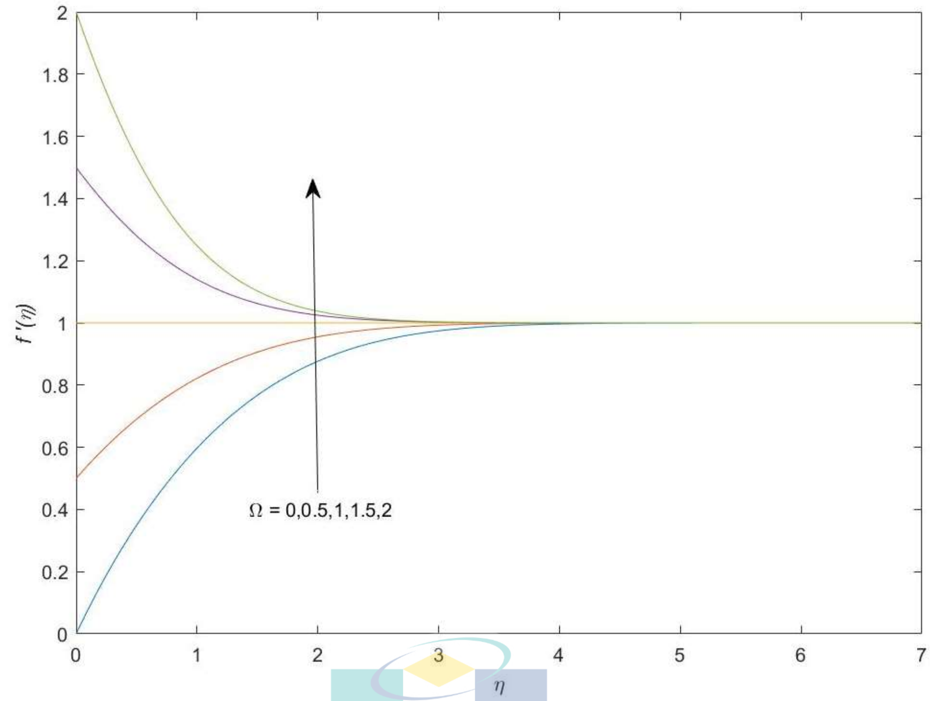

Figure 6.8 Velocity profiles for various values of Ω.

6.4 Conclusion

The convective boundary layer flow of Williamson hybrid ferrofluid over a moving flat with viscous dissipation were numerically studied. The present numerical method is validated with the sample result from Bachok *et al.* (2012), and the comparison achieved good agreement. Four parameters were tested in this chapter: Eckert number, E_C, magnetic parameter, M, Williamson parameter, λ, and moving plate parameter, Ω. Eckert number and magnetic parameter were tested with various ferroparticle volume fractions and different types of hybrids ferrofluid, respectively. The summarization of the results is as follows:

- Williamson hybrid ferrofluid produces slightly better convective heat transfer performance as viscous dissipation is neglected.
- Increase in magnetic parameters results in a decrease in $Nu_x \mathrm{Re}_x^{-1/2}$ but increase in $C_f \mathrm{Re}_x^{1/2}$ value.

- Ω parameters reduced the temperature profile while increasing the velocity profile.

- Heat transfer performance for different types of fluid tested becomes similar as viscous dissipation parameters increases and also does not effect the skin friction of the fluids tested.

- Distributions of $C_f \operatorname{Re}_x^{1/2}$ values increase as Williamson parameter is induced similar to the result in Chapter 4.

CHAPTER 7

CONCLUSION

7.1 Summary

This present thesis has numerically investigated the convective boundary layer flow in a Williamson hybrid ferrofluid. Considering 3 problems, which are stagnation point flow over a stretching sheet, convective boundary layer over a permeable stretching sheet with the presence of thermal radiation, and convective boundary layer flow over a moving plate with convective viscous dissipation, the three problems are subjected to the constant wall temperature.

It can be concluded that all of the three research objectives mentioned in Section 1.3 were successfully achieved. All the problems studied have been extended to hybrid ferrofluid mathematical model, numerical algorithm and analyzation of numerical result. For problem 1 the ferrofluid mathematical model is extended to Williamson hybrid ferrofluid model with the presence of stretching sheet, magnetic and Williamson effects. Meanwhile, problems 2 and 3, the Williamson hybrid ferrofluid model is extended with the presence of thermal radiation, suction and injection, moving plate and viscous dissipation effects. The mathematical formulations for each problem are in the form of non-linear partial differential equations. Using similarity transformation, the equations are then transformed into ordinary differential equations. The algorithm to solve the ODE using the KBM is developed for each problem and then coded into MATLAB software for numerical calculations. These transformation and numerical solutions are discussed in Chapter 3 Methodology. The results are then analyzed in Chapter 4, 5 and 6 for each problem respectively with the Nusselt number, $Nu_x \mathrm{Re}_x^{-1/2}$, and skin friction, $C_f \mathrm{Re}_x^{1/2}$ values.

In conclusion, when comparing the hybrid ferrofluid with different ferroparticle volume fraction using magnetic parameter, blood hybrid ferrofluid produced the highest

$Nu_x \mathrm{Re}_x^{-1/2}$ and $C_f \mathrm{Re}_x^{1/2}$. The presence of copper improves the heat transfer performance of the fluid, but due to its high density, it causes the fluid to exert more drag on the surface. Furthermore, when comparing with different types of hybrids ferrofluid using the same parameter, Williamson hybrid ferrofluid has the highest distributions of $Nu_x \mathrm{Re}_x^{-1/2}$ and the lowest distributions of $C_f \mathrm{Re}_x^{1/2}$ compared to the other types of hybrids ferrofluid. This accomplishes the objectives of proposing a hybrid ferrofluid with enhanced thermal conductivity and reduced skin friction characteristics.

The main parameter that is focused on Chapter 4 is stretching parameter. The result shows that when the stretching parameter increases, the values of $Nu_x \mathrm{Re}_x^{-1/2}$ increase while the values of $C_f \mathrm{Re}_x^{1/2}$ decreases. This results in the reduction of thermal boundary layer flow and inclination of momentum boundary layer flow, respectively. The stretching parameter increases the surface stretching sheet, which causes the fluid to move with the surface, thus reducing skin friction.

Chapter 5 introduces two main parameters that focus on thermal radiation and permeability rate parameters. The thermal radiation parameter induces $Nu_x \mathrm{Re}_x^{-1/2}$ values but has no effect on $C_f \mathrm{Re}_x^{1/2}$ values. This is because Nr parameter does not have relations with $C_f \mathrm{Re}_x^{1/2}$ equations. For permeability rate parameter, the results show that it increases $Nu_x \mathrm{Re}_x^{-1/2}$ and $C_f \mathrm{Re}_x^{1/2}$ values. When this parameter increases, forcing the fluid into a vacant space, resulting in the reduction of thermal and momentum boundary layer flow.

Viscous dissipation and moving plate parameters are introduced in Chapter 6. The viscous dissipation parameter, which is defined as Eckert number, E_C, inhibits the convective heat transfer of fluid as the parameter reduces $Nu_x \mathrm{Re}_x^{-1/2}$ values. This parameter does not affect the skin friction of the fluid. Furthermore, moving plate parameters causes the surface to increase in velocity. This results in the inclination of $Nu_x \mathrm{Re}_x^{-1/2}$ and reduction of $C_f \mathrm{Re}_x^{1/2}$. The thermal boundary layer flow is declining while the momentum boundary layer is increasing.

Since all the problems studied in this research have produced results and been completed, it can be concluded that the objectives of this study have been achieved. Mathematical modelling for all the problems is developed, tested, and compared with previous results. All the numerical algorithms developed show good agreement with previous studies, which indicates that they can produce reliable results. It is noted that the problems studied for this hybrid ferrofluid in this research are new during the time of doing research and have not been considered before. This research does not produce the product or physical outcome. This research provides mathematical modelling for hybrid ferrofluid, which can be used for future reference and comparison in future studies.

7.2 Future Studies

This research only covers convective boundary layer flow in Williamson hybrid ferrofluid with constant wall temperature. Many other aspects can be covered for future studies:

1. Type of geometries: cylinder, stretching cylinder, sphere, curved, thin needle, cavity, horizontal plate, incline surface, wedge, cone, rotating channel, aligned angle, moving surface, and vertical plate.
2. Physical effects: heat generation and absorption, chemical reaction as well as porosity effect, and temperature jump.
3. Boundary conditions: slip condition, peristaltic flow, unsteady flow with mixed thermal boundary condition.
4. Method of numerical solution: homotopy perturbation method (HPM), homotopy analysis method (HAM), shooting method bvp4c, and Spectral-relaxation method.

REFERENCES

Abbasi, A., Khan, S. U., Al-Khaled, K., Ijaz Khan, M., Farooq, W., Galal, A. M., . . . Malik, M. Y. (2022). Thermal Prospective Of Casson Nano-Materials In Radiative Binary Reactive Flow Near Oblique Stagnation Point Flow With Activation Energy Applications. Chemical Physics Letters, 786. doi:10.1016/j.cplett.2021.139172

Abbasian Arani, A. A., & Aberoumand, H. (2021). Stagnation-Point Flow Of Ag-Cuo/Water Hybrid Nanofluids Over A Permeable Stretching/Shrinking Sheet With Temporal Stability Analysis. Powder Technology, 380, 152-163. doi:10.1016/j.powtec.2020.11.043

Abu Bakar, S., Md Arifin, N., Bachok, N., & Md Ali, F. (2021). Effect Of Thermal Radiation And MHD On Hybrid Ag–Tio2/H2O Nanofluid Past A Permeable Porous Medium With Heat Generation. Case Studies in Thermal Engineering, 28. doi:10.1016/j.csite.2021.101681

Ahmad, S. (2009). *Convection Boundary Layer Flows Over Needles and Cylinders in Viscous Fluids.* Retrieved from http://psasir.upm.edu.my/id/eprint/7239/1/IPM_2009_4.pdf

Ahmed, K., Akbar, T., Muhammad, T., & Alghamdi, M. (2021). Heat Transfer Characteristics Of MHD Flow Of Williamson Nanofluid Over An Exponential Permeable Stretching Curved Surface With Variable Thermal Conductivity. Case Studies in Thermal Engineering, 28. doi:10.1016/j.csite.2021.101544

Ahmed, N., Sharma, D., & Deka, H. (2012). MHD Mixed Convection And Mass Transfer From An Infinite Vertical Porous Plate With Chemical Reaction In Presence Of A Heat Source. Applied Mathematical Sciences, 6(21), 1011-1020.

Akaje, T. W., & Olajuwon, B. I. (2021). Impacts of Nonlinear Thermal Radiation on a Stagnation Point of an Aligned MHD Casson Nanofluid Flow with Thompson and Troian Slip Boundary Condition. Journal of Advanced Research in Experimental Fluid Mechanics and Heat Transfer, 6(1), 1-15. Retrieved from https://www.akademiabaru.com/submit/index.php/arefmht/article/view/3911

Al-Sankoor, K., Al-Gayyim, H., Al-Musaedi, S., Asadi, Z., & Ganji, D. D. (2021). Analytically Investigating Of Heat Transfer Parameters With Presence Of Graphene Oxide Nanoparticles In Williamson-Magnetic Fluid By Agm And Hpm Methods. Case Studies in Thermal Engineering, 27. doi:10.1016/j.csite.2021.101236

Al-Zahrani, A. A., Adnan, Mahmood, I., Ur Rahman, K., Bani-Fwaz, M. Z., & Tag-Eldin, E. (2023). Analytical Study of (Ag-Graphene)/Blood Hybrid Nanofluid Influenced by (Platelets-Cylindrical)(nanoparticles) and Joule Heating via VIM. ACS Omega, 8(22), 19926-19938. doi:10.1021/acsomega.3c01903

Aladdin, N. A. L., Bachok, N., & Pop, I. (2020). Cu-Al2O3/Water Hybrid Nanofluid Flow Over A Permeable Moving Surface In Presence Of Hydromagnetic And Suction Effects. Alexandria Engineering Journal, 59(2), 657-666. doi:10.1016/j.aej.2020.01.028

Almaneea, A. (2022). Numerical Study On Heat And Mass Transport Enhancement In MHD Williamson Fluid Via Hybrid Nanoparticles. Alexandria Engineering Journal, 61(10), 8343-8354. doi:10.1016/j.aej.2022.01.041

Almeida, F., Venkatesh, P., Gireesha, B., & Krishnamurthy, M. Slip And Convective Flow Of Williamson Nanofluid Influenced By Brownian Motion And Thermophoresis Mechanism In A Horizontal Microchannel. Proceedings of the Institution of Mechanical Engineers, Part N: Journal of Nanomaterials, Nanoengineering and Nanosystems, 0(0), 23977914231177340. doi:10.1177/23977914231177340

Almeida, F., Venkatesh, P., Gireesha, B., & M.R, K. (2023). Slip and convective flow of Williamson nanofluid influenced by Brownian motion and thermophoresis mechanism in a horizontal microchannel. Proceedings of the Institution of Mechanical Engineers, Part N: Journal of Nanomaterials, Nanoengineering and Nanosystems, 239779142311773. doi:10.1177/23977914231177340

Anantha Kumar, K., Sandeep, N., Sugunamma, V., & Animasaun, I. L. (2019). Effect Of Irregular Heat Source/Sink On The Radiative Thin Film Flow Of MHD Hybrid Ferrofluid. Journal of Thermal Analysis and Calorimetry, 139(3), 2145-2153. doi:10.1007/s10973-019-08628-4

Anderson, D. A., Tannehill, J. C., & Pletcher, R. H. (1997). Computational Fluid Mechanics and Heat Transfer: Taylor & Francis.

Anderson, J. (2005). Ludwig Prandtl's Boundary Layer. Physics Today, 58. doi:10.1063/1.2169443

Anuar, N. S., Bachok, N., & Pop, I. (2021). Influence Of Buoyancy Force On Ag-Mgo/Water Hybrid Nanofluid Flow In An Inclined Permeable Stretching/Shrinking Sheet. International Communications in Heat and Mass Transfer, 123. doi:10.1016/j.icheatmasstransfer.2021.105236

API, A. P. I. (2010). Rheology and Hydraulics of Oil-well Drilling Fluids: American Petroleum Institute.

Asjad, M. I., Zahid, M., Inc, M., Baleanu, D., & Almohsen, B. (2022). Impact Of Activation Energy And MHD On Williamson Fluid Flow In The Presence Of Bioconvection. Alexandria Engineering Journal, 61(11), 8715-8727. doi:10.1016/j.aej.2022.02.013

Asshaari, I., Jedi, A., & Abdullah, S. (2023). Brownian Motion And Thermophoresis Effects In Co-Flowing Carbon Nanotubes Towards A Moving Plate. Results in Physics, 44. doi:10.1016/j.rinp.2022.106165

Astakhov, V. P. (2012). 4 - Environmentally friendly near-dry machining of metals. In V. P. Astakhov & S. Joksch (Eds.), Metalworking Fluids (MWFs) for Cutting and Grinding (pp. 135-200): Woodhead Publishing.

Bachok, N., Ishak, A., & Pop, I. (2011a). Stagnation-Point Flow Over A Stretching/Shrinking Sheet In A Nanofluid. Nanoscale Research Letters, 6(1), 623. doi:10.1186/1556-276X-6-623

Bachok, N., Ishak, A., & Pop, I. (2011b). Stagnation-Point Flow Over A Stretching/Shrinking Sheet In A Nanofluid. Nanoscale Research Letters. doi:10.1186/1556-276X-6-623

Bachok, N., Ishak, A., & Pop, I. (2012). Flow And Heat Transfer Characteristics On A Moving

Plate In A Nanofluid. International Journal of Heat and Mass Transfer, 55(4), 642-648. doi:10.1016/j.ijheatmasstransfer.2011.10.047

Basha, H. T., Rajagopal, K., Ahammad, N. A., Sathish, S., Gunakala, S. R., & Kutlu, M. C. (2022). Finite Difference Computation of Au-Cu/Magneto-Bio-Hybrid Nanofluid Flow in an Inclined Uneven Stenosis Artery. Complexity, 2022, 1-18. doi:10.1155/2022/2078372

Bejan, A. (1984). Convection Heat Transfer.

Bejan, A., & Kraus. (2003). Heat Transfer Handbooks. New York: John Wiley & Sons.

Blair, K. B. (2007). 3 - Materials and design for sports apparel. In A. Subic (Ed.), Materials in Sports Equipment (Vol. 2, pp. 60-86): Woodhead Publishing.

Caket, A. G., Wang, C., Nugroho, M. A., Celik, H., & Mobedi, M. (2022). Recent Studies on 3D Lattice Metal Frame Technique for Enhancement of Heat Transfer: Discovering Trends and Reasons. Renewable and Sustainable Energy Reviews, 167, 112697. doi:https://doi.org/10.1016/j.rser.2022.112697

Cao, Z., Zhao, J., Wang, Z., Liu, F., & Zheng, L. (2016). MHD Flow And Heat Transfer Of Fractional Maxwell Viscoelastic Nanofluid Over A Moving Plate. Journal of Molecular Liquids, 222, 1121-1127. doi:10.1016/j.molliq.2016.08.012

Cebeci, T., & Bradshaw, P. (1988). Physical and Computational Aspects of Convective Heat Transfer. Springer Berlin Heidelberg. doi:10.1007/978-3-662-02411-9

Cebeci, T., & Cousteix, J. (2005). Modeling And Computation Of Boundary-Layer Flows.

Chamkha, A. J., EL-Kabeir, S. M. M., & Rashad, A. M. (2015). Unsteady coupled heat and mass transfer by mixed convection flow of a micropolar fluid near the stagnation point on a vertical surface in the presence of radiation and chemical reaction. Progress in Computational Fluid Dynamics, 15(3). doi:10.1504/PCFD.2015.069576

Chao, B. T., & Jeng, D. R. (1965). Unsteady Stagnation Point Heat Transfer. Journal of Heat Transfer, 87(2). doi:10.1115/1.3689076

Choi, S. U. S. E., J A. (1995). Enhancing Thermal Conductivity Of Fluids With Nanoparticles. Paper presented at the American Society of Mechanical Engineers, Fluids Engineering Division. https://www.osti.gov/servlets/purl/196525.

Chu, Y., Khan, M. I., Rehman, M. I. U., Kadry, S., Qayyum, S., & Waqas, M. (2021). Stability Analysis And Modeling For The Three-Dimensional Darcy-Forchheimer Stagnation Point Nanofluid Flow Towards A Moving Surface. Applied Mathematics and Mechanics, 42(3), 357-370. doi:10.1007/s10483-021-2700-7

Cowling, T. G. (1976). Magnetohydrodynamics.

Cramer, S. D., & Marchello, J. M. (1968). Numerical Evaluation of Models Describing Non-Newtonian Behavior. AIChE Journal, 14(6), 980-983. doi:10.1002/aic.690140632

Crane, L. J. (1970). Flow Past a Stretching Plate. Zeitschrift für angewandte Mathematik und Physik ZAMP, 21(4). doi:10.1007/bf01587695

Daprà, I., & Scarpi, G. (2007). Perturbation Solution For Pulsatile Flow Of A Non-Newtonian Williamson Fluid In A Rock Fracture. International Journal of Rock Mechanics and Mining Sciences, 44(2), 271-278. doi:10.1016/j.ijrmms.2006.07.003

Dawar, A., Shah, Z., Islam, S., Deebani, W., & Shutaywi, M. (2023). MHD Stagnation Point Flow Of A Water-Based Copper Nanofluid Past A Flat Plate With Solar Radiation Effect. Journal of Petroleum Science and Engineering, 220. doi:10.1016/j.petrol.2022.111148

Devi, S. U., & Anjali Devi, S. P. (2016). Numerical Investigation of Hydromagnetic Hybrid Cu – Al2O3/Water Nanofluid Flow over a Permeable Stretching Sheet with Suction. International Journal of Nonlinear Sciences and Numerical Simulation, 17(5), 249-257. doi:10.1515/ijnsns-2016-0037

Devi, S. U., & Anjali Devi, S. P. (2017). Heat Transfer Enhancement of Cu-Al2O3/Water Hybrid Nanofluid Flow Over a Stretching Sheet. Journal of the Nigerian Mathematical Society, 36(2), 419-433.

Dincer, I., & Siddiqui, O. (2018). 1.10 Heat Transfer Aspects of Energy. In I. Dincer (Ed.), Comprehensive Energy Systems (pp. 422-477). Oxford: Elsevier.

Eckert, M. (2017). Ludwig Prandtl And The Growth Of Fluid Mechanics In Germany. Comptes Rendus Mécanique, 345(7), 467-476. doi:https://doi.org/10.1016/j.crme.2017.05.005

Gebhart, B. (1962). Effects Of Viscous Dissipation In Natural Convection. Journal of Fluid Mechanics, 14(2), 225-232. doi:10.1017/S0022112062001196

Geropp, D. (1969). Der turbulente Wärmeübergang am rotierenden Zylinder. Ingenieur-Archiv, 38(4), 195-203. doi:10.1007/BF00536164

Gschwendtner, M. A. (2004). The Eckert Number Phenomenon: Experimental Investigations On The Heat Transfer From a Moving Wall in The Case of a Rotating Cylinder. Heat and Mass Transfer, 40(6), 551-559. doi:10.1007/s00231-003-0437-9

Gul, T., Ali, B., Alghamdi, W., Nasir, S., Saeed, A., Kumam, P., . . . Jawad, M. (2021). Mixed convection stagnation point flow of the blood based hybrid nanofluid around a rotating sphere. Sci Rep, 11(1), 7460. doi:10.1038/s41598-021-86868-x

Gumber, P., Yaseen, M., Rawat, S. K., & Kumar, M. (2022). Heat Transfer In Micropolar Hybrid Nanofluid Flow Past A Vertical Plate In The Presence Of Thermal Radiation And Suction/Injection Effects. Partial Differential Equations in Applied Mathematics, 5. doi:10.1016/j.padiff.2021.100240

Guo, B., & Ghalambor, A. (2005). Chapter 11 - Transportation. In B. Guo & A. Ghalambor (Eds.), Natural Gas Engineering Handbook (Second Edition) (pp. 219-262): Gulf Publishing Company.

Haider, I., Nazir, U., Nawaz, M., Alharbi, S. O., & Khan, I. (2021). Numerical Thermal Study On Performance Of Hybrid Nano-Williamson Fluid With Memory Effects Using Novel Heat Flux Model. Case Studies in Thermal Engineering, 26. doi:10.1016/j.csite.2021.101070

Hamid, R. A., Nazar, R., & Pop, I. (2016). The Non-Alignment Stagnation-Point Flow Towards

A Permeable Stretching/Shrinking Sheet In A Nanofluid Using Buongiorno'S Model: A Revised Model. Zeitschrift für Naturforschung A, 71(1), 81-89.

Hasanuzzaman, M., Akter, S., Sharin, S., Hossain, M. M., Miyara, A., & Hossain, M. A. (2023). Viscous Dissipation Effect On Unsteady Magneto-Convective Heat-Mass Transport Passing In A Vertical Porous Plate With Thermal Radiation. Heliyon, 9(3), e14207. doi:10.1016/j.heliyon.2023.e14207

Hashim, Hamid, A., Khan, M., & Khan, U. (2018). Thermal Radiation Effects On Williamson Fluid Flow Due To An Expanding/Contracting Cylinder With Nanomaterials: Dual Solutions. Physics Letters A, 382(30), 1982-1991. doi:10.1016/j.physleta.2018.04.057

Hashim, H., Md Sarif, N., Salleh, M. Z., & Mohamed, M. K. A. (2019a). Aligned Magnetic Field on Williamson Fluid over a Stretching Sheet with Newtonian Heating. Journal of Physics: Conference Series. doi:10.1088/1742-6596/1529/5/052085

Hashim, H., Mohamed, M. K. A., Hussanan, A., Ishak, N., Md Sarif, N., & Salleh, M. Z. (2015). The Effects Of Slip Conditions And Viscous Dissipation On The Stagnation Point Flow Over A Stretching Sheet. Paper presented at the Innovation And Analytics Conference And Exhibition (IACE 2015): Proceedings of the 2nd Innovation and Analytics Conference & Exhibition.

Hashim, H., Mohamed, M. K. A., Hussanan, A., Ishak, N., Sarif, N., & Salleh, M. Z. (2016). Flow and Heat Transfer Analysis of Williamson Viscous Fluid on the Stagnation Point Past a Stretching Surface with Viscous Dissipation and Slip Conditions.

Hashim, H., Mohamed, M. K. A., Ishak, N., Md Sarif, N., & Salleh, M. Z. (2019b). Thermal Radiation Effect on MHD Stagnation Point Flow of Williamson Fluid over a Stretching Surface. Journal of Physics: Conference Series, 1366(1). doi:10.1088/1742-6596/1366/1/012011

Herwig, H. (2016). What Exactly is the Nusselt Number in Convective Heat Transfer Problems and are There Alternatives? Entropy, 18(5). doi:10.3390/e18050198

Hiemenz, K. (1911). Die Grenzschicht An Einem In Den Gleichförmigen Flüssigkeitsstrom Eingetauchten Geraden Kreiszylinder: [s.n.].

Ibrahim, W., & Negera, M. (2020). Viscous Dissipation Effect on Williamson Nanofluid Over Stretching/Shrinking Wedge with Thermal Radiation and Chemical Reaction. Journal of Physics Communications, 4(4). doi:10.1088/2399-6528/ab8a68

Idris, S., Jamaludin, A., Nazar, R., & Pop, I. (2023). Heat transfer characteristics of magnetized hybrid ferrofluid flow over a permeable moving surface with viscous dissipation effect. Heliyon, 9(5), e15907. doi:10.1016/j.heliyon.2023.e15907

Ilias, M. R., Rawi, N. A., & Shafie, S. (2017). Natural Convection Of Ferrofluid From A Fixed Vertical Plate With Aligned Magnetic Field And Convective Boundary Condition. Malaysian Journal of Fundamental and Applied Sciences, 13(3), 223-228. doi:10.11113/mjfas.v13n3.651

Imtiaz, M., Hayat, T., & Alsaedi, A. (2017). Convective Flow of Ferrofluid Due To a Curved Stretching Surface With Homogeneous-Heterogeneous Reactions. Powder Technology, 310, 154-162. doi:10.1016/j.powtec.2017.01.029

Iqbal, M. S., Ghaffari, A., Riaz, A., Mustafa, I., & Raza, M. (2021). Nanofluid Transport Through a Complex Wavy Geometry with Magnetic and Permeability Effects. Inventions, 7(1). doi:10.3390/inventions7010007

Ishak, A. (2010). Similarity Solutions for Flow and Heat Transfer Over a Permeable Surface with Convective Boundary Condition. Applied Mathematics and Computation, 217(2), 837-842. doi:10.1016/j.amc.2010.06.026

Ishak, A. (2011). MHD boundary layer flow due to an exponentially stretching sheet with radiation effect. Sains Malaysiana, 40(4), 391-395.

Ishak, A., Nazar, R., & Pop, I. (2006). Mixed Convection Boundary Layers In The Stagnation-Point Flow Toward A Stretching Vertical Sheet. Meccanica, 41(5), 509-518. doi:10.1007/s11012-006-0009-4

Ishak, A., Nazar, R., & Pop, I. (2008). Post-Stagnation-Point Boundary Layer Flow And Mixed Convection Heat Transfer Over A Vertical, Linearly Stretching Sheet. Archives of Mechanics, 60.

Ishak, A. M. (2008). *Penyelesaian Keserupaan Bagi Aliran Lapisan Sempadan Olakan Terhadap Permukaan Dalam Bendalir Likat.* Fakulti Sains Dan Teknologi, Universiti Kebangsaan Malaysia, Bangi.

Jahan, S., Sakidin, H., Nazar, R., & Pop, I. (2018). Analysis of heat transfer in nanofluid past a convectively heated permeable stretching/shrinking sheet with regression and stability analyses. Results in Physics, 10, 395-405. doi:10.1016/j.rinp.2018.06.021

Jain, S., & Parmar, A. (2018). Radiation Effect on MHD Williamson Fluid Flow over Stretching Cylinder Through Porous Medium with Heat Source. In Applications of Fluid Dynamics (pp. 61-78).

Jalili, B., Ganji, A. D., Jalili, P., Salman Nourazar, S., & Ganji, D. D. (2022). Thermal Analysis Of Williamson Fluid Flow With Lorentz Force On The Stretching Plate. Case Studies in Thermal Engineering, 39. doi:10.1016/j.csite.2022.102374

Jalili, B., Sadighi, S., Jalili, P., & Ganji, D. D. (2019). Characteristics Of Ferrofluid Flow Over A Stretching Sheet With Suction And Injection. Case Studies in Thermal Engineering, 14. doi:10.1016/j.csite.2019.100470

Jamaludin, A., Naganthran, K., Nazar, R., & Pop, I. (2020). Thermal Radiation And MHD Effects in the Mixed Convection Flow of Fe_3O_4–Water Ferrofluid towards a Nonlinearly Moving Surface. Processes, 8(1). doi:10.3390/pr8010095

Jusoh, R., Nazar, R., & Pop, I. (2018). Magnetohydrodynamic Rotating Flow And Heat Transfer Of Ferrofluid Due To An Exponentially Permeable Stretching/Shrinking Sheet. Journal of Magnetism and Magnetic Materials, 465, 365-374. doi:10.1016/j.jmmm.2018.06.020

Kamis, N. I., Jiann, L. Y., Shafie, S., & Rawi, N. A. (2023). Numerical Simulation of Convection Hybrid Ferrofluid With Magnetic Dipole Effect On An Inclined Stretching Sheet. Alexandria Engineering Journal, 76, 19-33. doi:10.1016/j.aej.2023.06.030

Kasim, A. R. M. (2014). *Convective Boundary Layer Flow of Viscoelastic Fluid.* University

Teknologi Malaysia,

Kausar, M. S., Hussanan, A., Waqas, M., & Mamat, M. (2022). Boundary Layer Flow Of Micropolar Nanofluid Towards A Permeable Stretching Sheet In The Presence Of Porous Medium With Thermal Radiation And Viscous Dissipation. Chinese Journal of Physics, 78, 435-452. doi:10.1016/j.cjph.2022.06.027

Kebede, T., Haile, E., Awgichew, G., & Walelign, T. (2020). Heat and Mass Transfer in Unsteady Boundary Layer Flow of Williamson Nanofluids. Journal of Applied Mathematics, 2020, 1-13. doi:10.1155/2020/1890972

Keller, H. B. (1971). A New Difference Scheme for Parabolic Problems. In B. Hubbard (Ed.), Numerical Solution of Partial Differential Equations–II (pp. 327-350): Academic Press.

Keller, H. B. (1978). Numerical Methods in Boundary Layer Theory. Annu Rev Fluid Mech, 10, 417-433. doi:10.1146/annurev.fl.10.010178.002221

Khalid, A., Khan, I., Khan, A., Shafie, S., & Tlili, I. (2018). Case Study Of MHD Blood Flow In A Porous Medium With CNTS and Thermal Analysis. Case Studies in Thermal Engineering, 12, 374-380. doi:10.1016/j.csite.2018.04.004

Khan, M. S., Rahman, M. M., Arifuzzaman, S. M., Biswas, P., & Karim, I. (2017). Williamson Fluid Flow Behaviour of MHD Convective-Radiative Cattaneo–Christov Heat Flux Type over a Linearly Stretched-Surface with Heat Generation and Thermal-Diffusion. Frontiers in Heat and Mass Transfer, 9. doi:10.5098/hmt.9.15

Khan, N. A., Khan, S., & Riaz, F. (2014a). Boundary Layer Flow of Williamson Fluid with Chemically Reactive Species using Scaling Transformation and Homotopy Analysis Method. Mathematical Sciences Letters, 3(3), 199-205. doi:10.12785/msl/030311

Khan, S. U., Shehzad, S. A., & Ali, N. (2018). Interaction of Magneto-Nanoparticles in Williamson Fluid Flow Over Convective Oscillatory Moving Surface. Journal of the Brazilian Society of Mechanical Sciences and Engineering, 40(4). doi:10.1007/s40430-018-1126-4

Khan, U., Zaib, A., Ishak, A., Bakar, S. A., Animasaun, I. L., & Yook, S.-J. (2022). Insights Into The Dynamics Of Blood Conveying Gold Nanoparticles On A Curved Surface When Suction, Thermal Radiation, And Lorentz Force Are Significant: The Case Of Non-Newtonian Williamson Fluid. Mathematics and Computers in Simulation, 193, 250-268. doi:10.1016/j.matcom.2021.10.014

Khan, Y., Hussain, A., & Faraz, N. (2012). Unsteady Linear Viscoelastic Fluid Model Over A Stretching/Shrinking Sheet In The Region Of Stagnation Point Flows. Scientia Iranica, 19(6), 1541-1549. doi:10.1016/j.scient.2012.10.019

Khan, Z. H., Khan, W. A., Qasim, M., & Shah, I. A. (2014b). MHD Stagnation Point Ferrofluid Flow and Heat Transfer Toward a Stretching Sheet. IEEE Transactions on Nanotechnology, 13(1), 35-40. doi:10.1109/tnano.2013.2286991

Khashi'ie, N. S., Arifin, N. M., Nazar, R., Hafidzuddin, E. H., Wahi, N., & Pop, I. (2020a). Magnetohydrodynamics (MHD) Axisymmetric Flow And Heat Transfer Of A Hybrid Nanofluid Past A Radially Permeable Stretching/Shrinking Sheet With Joule Heating. Chinese Journal of Physics, 64, 251-263. doi:10.1016/j.cjph.2019.11.008

Khashi'ie, N. S., Arifin, N. M., & Pop, I. (2022a). Magnetohydrodynamics (MHD) Boundary Layer Flow Of Hybrid Nanofluid Over A Moving Plate With Joule Heating. Alexandria Engineering Journal, 61(3), 1938-1945. doi:10.1016/j.aej.2021.07.032

Khashi'ie, N. S., Arifin, N. M., Pop, I., Nazar, R., Hafidzuddin, E. H., & Wahi, N. (2020b). Three-Dimensional Hybrid Nanofluid Flow and Heat Transfer past a Permeable Stretching/Shrinking Sheet with Velocity Slip and Convective Condition. Chinese Journal of Physics, 66, 157-171. doi:10.1016/j.cjph.2020.03.032

Khashi'ie, N. S., Waini, I., Zainal, N. A., Hamzah, K. B., Kasim, A. R. M., Arifin, N. M., & Pop, I. (2022b). Thermal Progress of Unsteady Separated Stagnation Point Flow with Magnetic Field and Heat Generation in Hybrid Ferrofluid. Nanomaterials (Basel), 12(18). doi:10.3390/nano12183205

Kho, Y. B., Hussanan, A., Mohamed, M. K. A., & Salleh, M. Z. (2019). Heat And Mass Transfer Analysis On Flow Of Williamson Nanofluid With Thermal And Velocity Slips: Buongiorno Model. Propulsion and Power Research, 8(3), 243-252. doi:10.1016/j.jppr.2019.01.011

Kho, Y. B., Hussanan, A., Mohamed, M. K. A., Sarif, N. M., Ismail, Z., & Salleh, M. Z. (2017). Thermal Radiation Effect On Mhd Flow And Heat Transfer Analysis Of Williamson Nanofluid Past Over A Stretching Sheet With Constant Wall Temperature. Journal of Physics: Conference Series, 890. doi:10.1088/1742-6596/890/1/012034

Krishnamurthy, M. R., Prasannakumara, B. C., Gireesha, B. J., & Gorla, R. S. R. (2016). Effect Of Chemical Reaction On MHD Boundary Layer Flow And Melting Heat Transfer Of Williamson Nanofluid In Porous Medium. Engineering Science and Technology, an International Journal, 19(1), 53-61. doi:10.1016/j.jestch.2015.06.010

Kumar, A., & Panda, U. (2022). Chapter 12 - Microfluidics-Based Devices and Their Role On Point-Of-Care Testing. In R. Khan, A. Parihar, & S. K. Sanghi (Eds.), Biosensor Based Advanced Cancer Diagnostics (pp. 197-224): Academic Press.

Kumaran, V., Banerjee, A. K., Vanav Kumar, A., & Vajravelu, K. (2009). MHD Flow Past A Stretching Permeable Sheet. Applied Mathematics and Computation, 210(1), 26-32. doi:10.1016/j.amc.2008.10.025

Kundu, P. K., Cohen, I. M., & Dowling, D. R. (2016). Chapter 10 - Boundary Layers and Related Topics. In P. K. Kundu, I. M. Cohen, & D. R. Dowling (Eds.), Fluid Mechanics (Sixth Edition) (pp. 469-532). Boston: Academic Press.

LaNasa, P. J., & Upp, E. L. (2014). 2 - Basic Flow Measurement Laws. In P. J. LaNasa & E. L. Upp (Eds.), Fluid Flow Measurement (Third Edition) (pp. 19-29). Oxford: Butterworth-Heinemann.

Lesnic, D., Ingham, D. B., & Pop, I. (1999). Free Convection Boundary-Layer Flow Along A Vertical Surface In A Porous Medium With Newtonian Heating. International Journal of Heat and Mass Transfer, 42(14), 2621-2627. doi:https://doi.org/10.1016/S0017-9310(98)00251-8

Loganathan, P., & Sangeetha, S. (2022). Effect Of Williamson Parameter On Cu-Water Williamson Nanofluid Over A Vertical Plate. International Communications in Heat and Mass Transfer, 137. doi:10.1016/j.icheatmasstransfer.2022.106273

Lok, Y. Y. (2002). *Nonisothermal Free Convection Boundary Layer Over A Vertical Flat Plate.* Retrieved from http://eprints.utm.my/id/eprint/43282/

Lund, L. A., Omar, Z., & Khan, I. (2019). Analysis Of Dual Solution For MHD Flow Of Williamson Fluid With Slippage. Heliyon, 5(3), e01345. doi:10.1016/j.heliyon.2019.e01345

Lyubimov, D. V., & Perminov, A. V. (2002). Motion Of A Thin Oblique Layer Of A Pseudoplastic Fluid. Journal of Engineering Physics and Thermophysics, 75. doi:https://doi.org/10.1023/A:1020371203799.

Mabood, F., Abbasi, A., Farooq, W., Hussain, Z., & Badruddin, I. A. (2022). Effects Of Non-Linear Radiation And Chemical Reaction On Oldroyd - B Nanofluid Near Oblique Stagnation Point Flow. Chinese Journal of Physics, 77, 1197-1208. doi:10.1016/j.cjph.2022.03.049

Mabood, F., Shateyi, S., Rashidi, M. M., Momoniat, E., & Freidoonimehr, N. (2016). MHD Stagnation Point Flow Heat And Mass Transfer Of Nanofluids In Porous Medium With Radiation, Viscous Dissipation And Chemical Reaction. Advanced Powder Technology, 27(2), 742-749. doi:10.1016/j.apt.2016.02.033

Mahesh, R., Mahabaleshwar, U. S., Kumar, P. N. V., Öztop, H. F., & Abu-Hamdeh, N. (2023). Impact Of Radiation On The MHD Couple Stress Hybrid Nanofluid Flow Over A Porous Sheet With Viscous Dissipation. Results in Engineering, 17. doi:10.1016/j.rineng.2023.100905

Mangi, A. (2013). *Unsteady Magnetohydrodynamics Flow Of A Micropolar Fluid With Heat And Mass Transfer.* Retrieved from http://eprints.utm.my/id/eprint/33855/5/AurangzaibMangiPFS2013.pdf

Maxwell, J. C. (2010). A Treatise on Electricity and Magnetism (Vol. 1). Cambridge: Cambridge University Press.

Megahed, A. M. (2019). Steady Flow of MHD Williamson Fluid Due To a Continuously Moving Surface with Viscous Dissipation and Slip Velocity. International Journal of Modern Physics C, 31(01). doi:10.1142/s0129183120500199

Merkin, J. H. (1994). Natural-Convection Boundary-Layer Flow On A Vertical Surface With Newtonian Heating. International Journal of Heat and Fluid Flow, 15(5), 392-398. doi:https://doi.org/10.1016/0142-727X(94)90053-1

Mohamed, M. (2018). Keller-Box Method Partial Differential Equations In Boundary Layer Flow Of Nanofluid. DRB-HICOM University Publisher, Pekan.

Mohamed, M., Salleh, M. Z., Nazar, R., & Ishak, A. (2012a). Stagnation Point Flow over a Stretching Sheet with Newtonian Heating. Sains Malaysiana, 41(11), 1467-1473.

Mohamed, M. K. A. (2013). *Mathematical Modeling For The Convection Boundary Layer Flow In A Viscous Fluid With Newtonian Heating And Convective Boundary Conditions.* UMP,

Mohamed, M. K. A., Abas, F. N., & Salleh, M. Z. (2019a). MHD Boundary Layer Flow Over a Permeable Flat Plate In a Ferrofluid with Thermal Radiation Effect. Journal of Physics:

Conference Series. doi:10.1088/1742-6596/1366/1/012014

Mohamed, M. K. A., Anwar, M. I., Shafie, S., Salleh, M. Z., & Ishak, A. (2013a). Magnetohydrodynamic Effects On Stagnation Point Flow Past A Stretching Sheet In Presence Of Thermal Radiation With Convective Boundary Conditions.

Mohamed, M. K. A., Anwar, M. I., Shafie, S., Salleh, M. Z., & Ishak, A. (2014). Effects of Magnetohydrodynamic on the Stagnation Point Flow past a Stretching Sheet in the Presence of Thermal Radiation with Newtonian Heating. In International Conference on Mathematical Sciences and Statistics 2013 (pp. 155-163).

Mohamed, M. K. A., Hussanan, A., Alkasasbeh, H. T., Widodo, B., & Salleh, M. Z. (2021a). Boundary Layer Flow On Permeable Flat Surface In Ag-Al2O3/Water Hybrid Nanofluid With Viscous Dissipation. Data Analytics and Applied Mathematics (DAAM), 2(1), 11-19. doi:10.15282/daam.v2i1.6431

Mohamed, M. K. A., Ismail, N. A., Hashim, N., M. Shah, N., & Salleh, M. Z. (2019b). MHD Slip Flow and Heat Transfer on Stagnation Point of a Magnetite (Fe3O4) Ferrofluid towards a Stretching Sheet with Newtonian Heating. CFD Letters, 11(1).

Mohamed, M. K. A., Md. Noar, N. A. Z., Salleh, M. Z., & Ishak, A. (2019c). Free Convection Boundary Layer Flow on a Solid Sphere in a Nanofluid with Viscous Dissipation. Malaysian Journal of Fundamental and Applied Sciences, 15(3). doi:https://doi.org/10.11113/mjfas.v15n3.1183

Mohamed, M. K. A., Nasir, N. M., Khasi'ie, N. S., Jusoh, R., Moslim, N. H., Zaihidee, E. M., & Salleh, M. Z. (2012b). Numerical Investigation Of Stagnation Point Flow Over A Stretching Sheet With Newtonian Heating.

Mohamed, M. K. A., Noar, N. A. Z. M., Salleh, M. Z., & Ishak, A. (2016a). Free Convection Boundary Layer Flow on a Horizontal Circular Cylinder in a Nanofluid with Viscous Dissipation. Sains Malaysiana, 45(2), 289-296. Retrieved from http://www.scopus.com/

Mohamed, M. K. A., Ong, H. R., Alkasasbeh, H. T., & Salleh, M. Z. (2020a). Heat Transfer Of Ag-Al2O3/Water Hybrid Nanofluid On A Stagnation Point Flow Over A Stretching Sheet With Newtonian Heating. Paper presented at the Journal of Physics: Conference Series.

Mohamed, M. K. A., Ong, H. R., Alkasasbeh, H. T., & Salleh, M. Z. (2020b). Heat Transfer of Ag-Al2O3/Water Hybrid Nanofluid on a Stagnation Point Flow over a Stretching Sheet with Newtonian Heating. 2020, 1529(4), 42-85. doi:10.1088/1742-6596/1529/4/042085

Mohamed, M. K. A., Salleh, M. Z., & Ishak, A. (2020c). Effects of Viscous Dissipation on Mixed Convection Boundary Layer Flow Past a Vertical Moving Plate in a Nanofluid. Journal of Advanced Research in Fluid Mechanics and Thermal Sciences, 69(2), 1-18. doi:10.37934/arfmts.69.2.118

Mohamed, M. K. A., Salleh, M. Z., Jamil, F. C., & Ong, H. R. (2021b). Free Convection Boundary Layer Flow Over A Horizontal Circular Cylinder In Al2O3-Ag/Water Hybrid Nanofluid With Viscous Dissipation. Malaysian Journal of Fundamental and Applied Sciences, 17(1), 20-25.

Mohamed, M. K. A., Salleh, M. Z., Md Noar, N. A. Z., & Ishak, A. (2016b). The Viscous

Dissipation Effects on the Mixed Convection Boundary Layer Flow on a Horizontal Circular Cylinder. Jurnal Teknologi, 78(4), 73-79. doi:10.11113/jt.v78.8304

Mohamed, M. K. A., Salleh, M. Z., Nazar, R., & Ishak, A. (2013b). Numerical Investigation Of Stagnation Point Flow Over A Stretching Sheet With Convective Boundary Conditions. Boundary Value Problems, 2013(1). doi:10.1186/1687-2770-2013-4

Mohamed, M. K. A., Yasin, S. H. M., & Salleh, M. Z. (2021c). Slip Effects on MHD Boundary Layer Flow over a Flat Plate in Casson Ferrofluid. Journal of Advanced Research in Fluid Mechanics and Thermal Sciences, 88(1), 49-57. doi:10.37934/arfmts.88.1.4957

Mohamed, M. K. A., Yasin, S. H. M. Y., Salleh, M. Z., & Alkasasbeh, H. T. (2021d). MHD Stagnation Point Flow and Heat Transfer Over a Stretching Sheet in a Blood-Based Casson Ferrofluid With Newtonian Heating. Journal of Advanced Research in Fluid Mechanics and Thermal Sciences, 82(1), 1-11. doi:10.37934/arfmts.82.1.111

Mohd Nasir, N. A. A., Ishak, A., & Pop, I. (2020). Magnetohydrodynamic Flow and Heat Transfer Induced by a Shrinking Sheet. Mathematics, 8(7). doi:10.3390/math8071175

Müller, M. (2019). 2.12 - Heat Transfer in Bioreactors. In M. Moo-Young (Ed.), Comprehensive Biotechnology (Third Edition) (pp. 133-150). Oxford: Pergamon.

Na, T. Y. (1979). Computational Methods in Engineering Boundary Value Problems (1 ed.). New York: Academic Press.

Nadeem, S., & Akbar, N. S. (2011). Numerical Solutions Of Peristaltic Flow Of Williamson Fluid With Radially Varying MHD In An Endoscope. International Journal for Numerical Methods in Fluids, 66(2), 212-220. doi:10.1002/fld.2253

Nadeem, S., & Akram, S. (2010a). Influence Of Inclined Magnetic Field On Peristaltic Flow Of A Williamson Fluid Model In An Inclined Symmetric Or Asymmetric Channel. Mathematical and Computer Modelling, 52(1-2), 107-119. doi:10.1016/j.mcm.2010.02.001

Nadeem, S., & Akram, S. (2010b). Peristaltic Flow Of A Williamson Fluid In An Asymmetric Channel. Communications in Nonlinear Science and Numerical Simulation, 15(7), 1705-1716. doi:10.1016/j.cnsns.2009.07.026

Nadeem, S., Hussain, S., & Lee, C. (2013a). Flow of a Williamson Fluid Over a Stretching Sheet. Brazilian Journal of Chemical Engineering, 30, 619-625. doi:10.1590/S0104-66322013000300019

Nadeem, S., & Hussain, S. T. (2013). Flow And Heat Transfer Analysis Of Williamson Nanofluid. Applied Nanoscience, 4(8), 1005-1012. doi:10.1007/s13204-013-0282-1

Nadeem, S., & Hussain, S. T. (2014). Heat Transfer Analysis Of Williamson Fluid Over Exponentially Stretching Surface. Applied Mathematics and Mechanics, 35(4), 489-502. doi:10.1007/s10483-014-1807-6

Nadeem, S., Hussain, S. T., & Lee, C. (2013b). Flow of a Williamson Fluid Over a Stretching Sheet. Brazilian Journal of Chemical Engineering, 30, 619-625.

Nadeem, S., & Hussain, S. T. H. (2016). Analysis of MHD Williamson Nano Fluid Flow over a

Heated Surface. Journal of Applied Fluid Mechanics, 9(2), 729-739. doi:10.18869/acadpub.jafm.68.225.21487

Nadeem, S., S. T. Hussain, & Lee, C. (2013c). Flow Of A Williamson Fluid Over A Stretching Sheet. Brazilian Journal of Chemical Engineering, 30(3), 619 - 625. doi:10.1590/s0104-66322013000300019

Nadeem, S., Ullah, N., Khan, A. U., & Akbar, T. (2017). Effect of Homogeneous-Heterogeneous Reactions on Ferrofluid in the Presence of Magnetic Dipole Along a Stretching Cylinder. Results in Physics, 7, 3574-3582. doi:10.1016/j.rinp.2017.09.006

Nandy, S. K., & Mahapatra, T. R. (2013). Effects Of Slip And Heat Generation/Absorption On MHD Stagnation Flow Of Nanofluid Past A Stretching/Shrinking Surface With Convective Boundary Conditions. International Journal of Heat and Mass Transfer, 64, 1091-1100. doi:10.1016/j.ijheatmasstransfer.2013.05.040

Naramgari, S., & Sulochana, C. (2016). MHD Flow Over A Permeable Stretching/Shrinking Sheet Of A Nanofluid With Suction/Injection. Alexandria Engineering Journal, 55(2), 819-827. doi:10.1016/j.aej.2016.02.001

Nazar, R., Amin, N., Filip, D., & Pop, I. (2004). Stagnation Point Flow Of A Micropolar Fluid Towards A Stretching Sheet. International Journal of Non-Linear Mechanics, 39(7), 1227-1235. doi:10.1016/j.ijnonlinmec.2003.08.007

Nazar, R. M. (2003). *Mathematical Models For Free And Mixed Convection Boundary Layer Flows Of Micropolar Fluids* University Teknologi Malaysia,

Nihoul, J. C. J. (1967). Magnetodynamic Turbulence At Low Magnetic Reynolds Number. Tellus A: Dynamic Meteorology and Oceanography, 19(4). doi:10.3402/tellusa.v19i4.9828

Oyama, S. T. (2011). Chapter 1 - Correlations. In S. T. Oyama & S. M. Stagg-Williams (Eds.), Membrane Science and Technology (Vol. 14, pp. 1-24): Elsevier.

Ozisik, M. N. (1985). Heat Transfer (Vol. 1): McGraw-Hill New York.

Papell, S. S. (1965). USA Patent No. United States Patent Office.

Rajendar, P., & Babu, L. A. (2018). MHD Stagnation Point Flow Of Williamson Nanofluid Over An Exponentially Inclined Stretching Surface With Thermal Radiation And Viscous Dissipation. Journal of Nanofluids, 7(4), 683-693. doi:10.1166/jon.2018.1493

Raju, S. S. K. (2022). Dynamics Of Magneto-Electric Hybrid Nanoparticles With Chemically Reacting And Radiated Moving Plate: Entropy Analysis. International Communications in Heat and Mass Transfer, 138. doi:10.1016/j.icheatmasstransfer.2022.106325

Ramli, N., & Ahmad, S. (2019). Stability Analysis of MHD mixed Convection Flow Over a Moving Flat Plate in Ferrofluids with Thermal Radiation, Suction and Second-order Slip Effects: Heat Flux Case. Paper presented at the Proceeding of the International Conference on Mathematical Sciences and Technology 2018 (MATHTECH2018): Innovative Technologies for Mathematics & Mathematics for Technological Innovation.

Ramli, N., Ahmad, S., & Pop, I. (2017). Slip Effects On MHD Flow And Heat Transfer Of Ferrofluids Over A Moving Flat Plate.

Rapp, B. E. (2017). Chapter 9 - Fluids. In B. E. Rapp (Ed.), Microfluidics: Modelling, Mechanics and Mathematics (pp. 243-263). Oxford: Elsevier.

Rashad, A. M. (2017). Impact of Anisotropic Slip On Transient Three Dimensional MHD Flow of Ferrofluid Over an Inclined Radiate Stretching Surface. Journal of the Egyptian Mathematical Society, 25(2), 230-237. doi:10.1016/j.joems.2016.12.001

Rashid, M., Ansar, K., & Nadeem, S. (2020). Effects Of Induced Magnetic Field For Peristaltic Flow Of Williamson Fluid In A Curved Channel. Physica A: Statistical Mechanics and its Applications, 553. doi:10.1016/j.physa.2019.123979

Rehman, K. U., Khan, A. U., Rehman, F., & Shatanawi, W. (2022). Thermal Case Study On Linearly Twisting Cylinder: A Radial Stagnation Point Flow Of Nanofluid. Case Studies in Thermal Engineering, 31. doi:10.1016/j.csite.2022.101861

Roy, U., & Roy, P. K. (2020). Chapter 7 - Advances in Heat Intensification Techniques in Shell and Tube Heat Exchanger. In L. Pekař (Ed.), Advanced Analytic and Control Techniques for Thermal Systems with Heat Exchangers (pp. 197-207): Academic Press.

Saeed, A., Alsubie, A., Kumam, P., Nasir, S., Gul, T., & Kumam, W. (2021a). Blood Based Hybrid Nanofluid Flow Together With Electromagnetic Field And Couple Stresses. Sci Rep, 11(1), 12865. doi:10.1038/s41598-021-92186-z

Saeed, M., Ahmad, B., & ul Hassan, Q. M. (2021b). Variable thermal effects of viscosity and radiation of ferrofluid submerged in porous medium. Ain Shams Engineering Journal. doi:10.1016/j.asej.2021.101653

Sahoo, R., Ussa-Aldana, P., Lancon, D., Rondelez, F., Morillas, J. R., Hidalgo-Alvarez, R., & de Vicente, J. (2022). Design Of Smart Lubricants Using The Inverse Ferrofluid Approach. Tribology International, 166. doi:10.1016/j.triboint.2021.107346

Sahoo, S. (2022). Stagnation Point Flow Of A Viscous Incompressible Fluid. Materials Today: Proceedings, 67, 1069-1072. doi:10.1016/j.matpr.2022.07.012

Sakiadis, B. C. (1961). Boundary ‐ Layer Behavior On Continuous Solid Surfaces: I. Boundary ‐ Layer Equations For Two ‐ Dimensional And Axisymmetric Flow. AIChE Journal, 7(1), 26-28.

Salleh, M. Z. (2011). *Mathematical Modelling For Convection Boundary Layer Flows With Newtonian Heating.* (Ph.D). Universiti Kebangsaan Malaysia, Malaysia,

Salleh, M. Z., Nazar, R., & Pop, I. (2009). Forced Convection Boundary Layer Flow at a Forward Stagnation Point with Newtonian Heating. Chemical Engineering Communications, 196(9), 987-996. doi:10.1080/00986440902797840

Salleh, M. Z., Nazar, R., & Pop, I. (2010). Boundary Layer Flow And Heat Transfer Over A Stretching Sheet With Newtonian Heating. Journal of the Taiwan Institute of Chemical Engineers, 41(6), 651-655. doi:10.1016/j.jtice.2010.01.013

Sandhya Rani, K., & Venkata Ramana Reddy, G. (2022). Cattaneo-Christov Heat and Mass Transfer Flux Across Electro-Hydrodynamics Blood-Based Hybrid NanoFluid Subject to Lorentz Force. CFD Letters, 14(7), 124-134. doi:10.37934/cfdl.14.7.124134

Sano, T. (1981). Unsteady Stagnation Point Heat Transfer with Blowing or Suction. Journal of Heat Transfer, 103(3), 448-452. doi:10.1115/1.3244484

Sarif, N. M., Salleh, M. Z., & Nazar, R. (2013). Numerical Solution of Flow and Heat Transfer over a Stretching Sheet with Newtonian Heating using the Keller Box Method. Procedia Engineering, 53, 542-554. doi:10.1016/j.proeng.2013.02.070

Shah, R. K., & London, A. L. (1978). Chapter III - Dimensionless Groups and Generalized Solutions. In R. K. Shah & A. L. London (Eds.), Laminar Flow Forced Convection in Ducts (pp. 37-60): Academic Press.

Sinha, S., & Sarma, M. K. (2020). Effect Of Stretching Parameter In A Non-Linear MHD Flow Close To Stagnation Point. J. Math. Comput. Sci., 10(6), 2249-2260.

Sokolova, I. (2019). Temperature Regulation☆. In B. Fath (Ed.), Encyclopedia of Ecology (Second Edition) (pp. 633-639). Oxford: Elsevier.

Sravanthi, C. S., Mabood, F., Nabi, S. G., & Shehzad, S. A. (2022). Heterogeneous And Homogeneous Reactive Flow Of Magnetite-Water Nanofluid Over A Magnetized Moving Plate. Propulsion and Power Research, 11(2), 265-275. doi:10.1016/j.jppr.2022.02.006

Srinivasulu, T., & Goud, B. S. (2021). Effect Of Inclined Magnetic Field On Flow, Heat And Mass Transfer Of Williamson Nanofluid Over A Stretching Sheet. Case Studies in Thermal Engineering, 23. doi:10.1016/j.csite.2020.100819

Subbarayudu, K., Suneetha, S., & Bala Anki Reddy, P. (2020). The Assessment Of Time Dependent Flow Of Williamson Fluid With Radiative Blood Flow Against A Wedge. Propulsion and Power Research, 9(1), 87-99. doi:10.1016/j.jppr.2019.07.001

Sundén, B. (2019). Chapter 2 - Electrochemistry and Thermodynamics. In B. Sundén (Ed.), Hydrogen, Batteries and Fuel Cells (pp. 15-36): Academic Press.

Swalmeh, M. Z., Alkasasbeh, H. T., Hussanan, A., & Mamat, M. (2018). Heat Transfer Flow Of Cu-Water And Al2O3-Water Micropolar Nanofluids About A Solid Sphere In The Presence Of Natural Convection Using Keller-Box Method. Results in Physics, 9, 717-724. doi:10.1016/j.rinp.2018.03.033

Swalmeh, M. Z., Alkasasbeh, H. T., Hussanan, A., Nguyen Thoi, T., & Mamat, M. (2019). Microstructure and Inertial Effects on Natural Convection Micropolar Nanofluid Flow About a Solid Sphere. International Journal of Ambient Energy, 43(1), 666-677. doi:10.1080/01430750.2019.1665582

Tani, I. (2003). History of Boundary Layer Theory. Annual Review of Fluid Mechanics, 9, 87-111. doi:10.1146/annurev.fl.09.010177.000511

Ullah Awan, A., Shah, S. A. A., & Ali, B. (2022). Bio-Convection Effects On Williamson Nanofluid Flow With Exponential Heat Source And Motile Microorganism Over A Stretching Sheet. Chinese Journal of Physics, 77, 2795-2810.

doi:10.1016/j.cjph.2022.04.002

Usafzai, W. K., & Aly, E. H. (2022). Exact Multiple Solutions Of 2-D Bidirectional Moving Plate Micropolar Hybrid Nanofluid Flow With Heat Transfer. Chinese Journal of Physics, 80, 414-426. doi:10.1016/j.cjph.2022.10.009

Vajravelu, K., & Prasad, K. V. (2014). Berlin, Boston: De Gruyter.

Vittal, C., Reddy, M. C. K., & Vijayalaxmi, T. (2017a). MHD Stagnation Point Flow and Heat Transfer of Williamson Fluid over Exponential Stretching Sheet Embedded in a Thermally Stratified Medium. Global Journal of Pure and Applied Mathematics, 13(6).

Vittal, C., Reddy, M. C. K., & Vijayalaxmi, T. (2017b). MHD Stagnation Point Flow And Heat Transfer Of Williamson Fluid Over Exponential Stretching Sheet Embedded In A Thermally Stratified Medium. Global Journal of Pure and Applied Mathematics, 13(6), 2033-2056.

Wang, C. Y. (2008). Stagnation flow towards a shrinking sheet. International Journal of Non-Linear Mechanics, 43(5), 377-382. doi:10.1016/j.ijnonlinmec.2007.12.021

Waqas, H., Ali Khan, S., & Muhammad, T. (2022). Thermal Analysis Of Magnetized Flow Of AA7072-AA7075/Blood-Based Hybrid Nanofluids In A Rotating Channel. Alexandria Engineering Journal, 61(4), 3059-3068. doi:10.1016/j.aej.2021.08.033

Waqas, H., Khan, S. A., Muhammad, T., & Raza Shah Naqvi, S. M. (2021). Heat Transfer Enhancement In Stagnation Point Flow Of Ferro-Copper Oxide/Water Hybrid Nanofluid: A Special Case Study. Case Studies in Thermal Engineering, 28. doi:10.1016/j.csite.2021.101615

Williamson, R. V. (1929). The Flow of Pseudoplastic Materials. Industrial & Engineering Chemistry, 21(11), 1108-1111. doi:10.1021/ie50239a035

Yacob, N. A., & Ishak, A. (2012). Stagnation Point Flow Towards A Stretching/Shrinking Sheet In A Micropolar Fluid With A Convective Surface Boundary Condition. The Canadian Journal of Chemical Engineering, 90(3), 621-626. doi:https://doi.org/10.1002/cjce.20517

Yacob, N. A., Ishak, A., & Pop, I. (2011). Falkner–Skan Problem For A Static Or Moving Wedge In Nanofluids. International Journal of Thermal Sciences, 50(2), 133-139. doi:10.1016/j.ijthermalsci.2010.10.008

Yahaya, R., Arin, N. M., & Isa, S. S. P. M. (2018). Dual solutions in MHD boundary layer flow of Carreau fluid over a shrinking sheet with convective boundary condition. ASM Science Journal, 12, 117-125.

Yahya, A. U., Salamat, N., Huang, W.-H., Siddique, I., Abdal, S., & Hussain, S. (2021). Thermal Charactristics For The Flow Of Williamson Hybrid Nanofluid (Mos2 + Zno) Based With Engine Oil Over A Streched Sheet. Case Studies in Thermal Engineering, 26. doi:10.1016/j.csite.2021.101196

Yap, B. K., Rahimah, J., Salleh, M. Z., Mohd, H. A., & Nooraini, Z. (2023). Magnetohydrodynamics Flow Of Ag-Tio2 Hybrid Nanofluid Over A Permeable Wedge With Thermal Radiation And Viscous Dissipation. Journal of Magnetism and Magnetic

Materials, 565. doi:10.1016/j.jmmm.2022.170284

Yaseen, M., Kumar, M., & Rawat, S. K. (2021). Assisting And Opposing Flow Of A MHD Hybrid Nanofluid Flow Past A Permeable Moving Surface With Heat Source/Sink And Thermal Radiation. Partial Differential Equations in Applied Mathematics, 4. doi:10.1016/j.padiff.2021.100168

Yasin, S. H. M., Mohamed, M. K. A., Ismail, Z., & Salleh, M. Z. (2020). Mathematical Solution on MHD Stagnation Point Flow of Ferrofluid. Defect and Diffusion Forum, 399, 38-54. doi:10.4028/www.scientific.net/DDF.399.38

Yasin, S. H. M., Mohamed, M. K. A., Ismail, Z., & Salleh, M. Z. (2021a). Magnetohydrodynamic Effects in Mixed Convection of Ferrofluid Flow at Lower Stagnation Point on Horizontal Circular Cylinder. Journal of Advanced Research in Fluid Mechanics and Thermal Sciences, 86(1), 52-63. doi:10.37934/arfmts.86.1.5263

Yasin, S. H. M., Mohamed, M. K. A., Ismail, Z., Widodo, B., & Salleh, M. Z. (2021b). Numerical Method Approach for Magnetohydrodynamic Radiative Ferrofluid Flows Over a Solid Sphere Surface. Thermal Science, 25(Spec. issue 2), 379-385. doi:10.2298/tsci21s2379m

Yasin, S. H. M., Mohamed, M. K. A., Ismail@Mustofa, Z., Widodo, B., & Salleh, M. Z. (2018a). Numerical Solution on MHD Stagnation Point Flow in Ferrofluid with Newtonian Heating and Thermal Radiation Effect. CFD Letters, 11(2), 21-31. Retrieved from https://www.akademiabaru.com/submit/index.php/arfmts/article/view/2523.

Yasin, S. H. M. Y., Mohamed, M. K. A., Ismail, Z., & Salleh, M. Z. (2022). Magnetite Water Based Ferrofluid Flow And Convection Heat Transfer On A Vertical Flat Plate: Mathematical And Statistical Modelling. Case Studies in Thermal Engineering, 40. doi:10.1016/j.csite.2022.102516

Yasin, S. H. M. Y., Mohamed, M. K. A., Ismail, Z., Widodo, B., & Salleh, M. Z. (2018b). Numerical Solution On MHD Stagnation Point Flow In Ferrofluid With Newtonian Heating And Thermal Radiation Effect. Journal of Advanced Research in Fluid Mechanics and Thermal Sciences, 57(1), 12-22.

Zainal, N. A., Nazar, R., Naganthran, K., & Pop, I. (2021). Unsteady MHD Stagnation Point Flow Induced By Exponentially Permeable Stretching/Shrinking Sheet Of Hybrid Nanofluid. Engineering Science and Technology, an International Journal, 24(5), 1201-1210. doi:10.1016/j.jestch.2021.01.018

Zeeshan, A., Majeed, A., & Ellahi, R. (2016). Effect Of Magnetic Dipole On Viscous Ferro-Fluid Past A Stretching Surface With Thermal Radiation. Journal of Molecular Liquids, 215, 549-554. doi:10.1016/j.molliq.2015.12.110

Zheng, L., Zhang, C., Zhang, X., & Zhang, J. (2013). Flow And Radiation Heat Transfer Of A Nanofluid Over A Stretching Sheet With Velocity Slip And Temperature Jump In Porous Medium. Journal of the Franklin Institute, 350(5), 990-1007. doi:10.1016/j.jfranklin.2013.01.022

APPENDICES

Appendix A: List of Symbol in Matlab

MATLAB	**Keller-box**
np	J
eta, etainf, deleta	$\eta,\ \eta_\infty,\ \Delta\eta$
f, u, v, s, t	$f, f', f'',\ \theta,\ \theta'$
cfb, cub, cvb, csb, ctb	$f_{j-1/2}^{n-1},\ u_{j-1/2}^{n-1},\ v_{j-1/2}^{n-1},\ s_{j-1/2}^{n-1},\ t_{j-1/2}^{n-1},$
cuub, cfvb, cftb, cusb	$\left(u_{j-1/2}^{n-1}\right)^2,\ f_{j-1/2}^{n-1}\ v_{j-1/2}^{n-1},\ f_{j-1/2}^{n-1}t_{j-1/2}^{n-1},\ u_{j-1/2}^{n-1}s_{j-1/2}^{n-1},$
cdervb, cdertb	$\left(v_j^{n-1}-v_{j-1}^{n-1}\right)h_j^{-1},\ \left(t_j^{n-1}-t_{j-1}^{n-1}\right)h_j^{-1}$
fb, ub, vb, sb, tb	$f_{j-1/2},\ u_{j-1/2},\ v_{j-1/2},\ s_{j-1/2},\ t_{j-1/2},$
uub, fvb, ftb, usb	$\left(u_{j-1/2}\right)^2,\ f_{j-1/2}v_{j-1/2},\ f_{j-1/2}t_{j-1/2},\ u_{j-1/2}s_{j-1/2},$
dervb, dertb	$\left(v_j-v_{j-1}\right)h_j^{-1},\ \left(t_j-t_{j-1}\right)h_j^{-1}$
a1 to a6	$(a1)_j$ **to** $(a6)_j$
b1 to b4	$(b1)_j$ **to** $(b4)_j$
r1 to r5	$(r1)_j$ **to** $(r5)_j$
R1, R2	$(R_1)_{j-1/2}^{n-1}$ **to** $(R_2)_{j-1/2}^{n-1}$
a, b, c	$[A_j], [B_j], [C_j]$
alfa, gamma	$[\alpha_j],\ [\Gamma_j]$
ww, rr,dell	$[W_j],\ [r_j],\ [\delta_j]$
delf, delu, delv, dels, delt	$\delta f,\ \delta u,\ \delta v,\ \delta s,\ \delta t$

Appendix B: MATLAB Program for Stagnation Point Flow of Williamson Hybrid Ferrofluid Over a Stretching Sheet

```
%%%%%%%%%%%%%%%%%%%%%%%%%%%%%%%%%%%%%%%%%%%%%%%%%%%%%%
% Stagnation Point Flow of Williamson Hybrid          %
% Ferrofluid Over a Stretching Sheet                  %
%                                                     %
% 1/aa*(f'''+Lf''f''')+ff'+1-f'^2-M(f'-1)=0           %
% knkf/ab*g''+Prfg'=0                                 %
% f(0)=0  f'(0)=ee  g(0)=1                            %
% f'(inf)=1  g(inf)=0                                 %
%%%%%%%%%%%%%%%%%%%%%%%%%%%%%%%%%%%%%%%%%%%%%%%%%%%%%%
key in the fluid :
clear all;clc;
blt =input('Input the thickness of boundary layer =
');
deleta = input('Input the step size of blt = ');
np = (blt / deleta) + 1;
pr = input ('Input the prandtl number = ');
input ('Input the stretching  parameter = ');
L =input ('Input the Lambda value = ');
M = input ('Input the M value = ');
aa = input ('Input the aa value = ');
ab= input ('Input the ab value = ');
knkf= input ('Input the knkf value = ');

%calculation for H1 and H2 value
H1= 1/aa
H2= knkf/ab

% Previous station
bil =5
    prandtl(1)=0;
    prandtl(2)=1;
    prandtl(3)=2;
    prandtl(4)=5;
    prandtl(5)=10;

for NumData = 1: bil
    M = prandtl(NumData)
stop = 1.0; k = 1;
while stop > 0.00001
eta(1,1) = 0.0;
for j = 2:np
```

```
        eta(j,1) = eta(j-1,1) + deleta;
end
  etanpq = eta(np,1) / 4;
  etau15 = 1 / eta(np,1);
  etanp = eta(np,1);
    for j = 1:np
        deta(j,k) = deleta;
        etab = eta(j,1) / eta(np,1);        etab1 =
etab^2;
        etab3 = ((3/2) - (1/2)* etab1);
        etau = eta(j,1);  etau3 =  (eta(j,1)) / 3;
       f(j,1) = (3/4)*eta(j,1)*etab -
(1/8)*eta(j,1)*etab1*etab + ee*(eta(j,1)-etau3*etab1);
       u(j,1) = etab * etab3  + ee * (1  - etab1);
        v(j,1) = (3/2) * etau15 * (1 - etab1)  + ee  *
(-2  * etau15  * etab);
        s(j,1) = (1-etab)^2;
        t(j,1) = 2* etau15*etab;
    end
    % Present station
    for j = 2:np
      fb(j,k) = 0.5 * ( f(j,k) + f(j-1,k) );
      ub(j,k) = 0.5 * ( u(j,k) + u(j-1,k) );
      vb(j,k) = 0.5 * ( v(j,k) + v(j-1,k) );
      sb(j,k) = 0.5 * ( s(j,k) + s(j-1,k) );
      tb(j,k) = 0.5 * ( t(j,k) + t(j-1,k) );
      fvb(j,k) = fb(j,k) * vb(j,k);
      uub(j,k) = ub(j,k) * ub(j,k);
      ftb(j,k) = fb(j,k) * tb(j,k);
      vv(j,k) = v(j,k) * v(j,k);
      vv(j-1,k) = v(j-1,k) * v(j-1,k);


    a1(j,k) = H1*(1.0+L*v(j,k)) + (0.5 * deta(j,k) *
fb(j,k));
    a2(j,k) = -H1*(1.0+L*v(j-1,k)) + (0.5 * deta(j,k)
* fb(j,k));
    a3(j,k) = 0.5 * deta(j,k) * vb(j,k);
    a4(j,k) = a3(j,k);
    a5(j,k) = -deta(j,k)*(ub(j,k) + 0.5*M);
    a6(j,k) = a5(j,k);

    b1(j,k) = H2 + 0.5* pr * deta(j,k)*fb(j,k);
    b2(j,k) = b1(j,k) - 2.0*H2;
    b3(j,k) = 0.5* pr * deta(j,k) * tb(j,k);
```

```
    b4(j,k) = b3(j,k);

        r1(j,k) = (f(j-1,k) - f(j,k)) + (deta(j,k) *
ub(j,k));
        r2(j,k) = (u(j-1,k) - u(j,k)) + (deta(j,k) *
vb(j,k));
        r3(j,k) = (s(j-1,k) - s(j,k)) + (deta(j,k) *
tb(j,k));
        r4(j,k) = H1*(v(j-1,k) - v(j,k)) -
H1*0.5*L*(vv(j,k) - vv(j-1,k)) - deta(j,k)*fvb(j,k) +
deta(j,k)*uub(j,k) +  M*deta(j,k)*ub(j,k)  -
M*deta(j,k) - deta(j,k);
        r5(j,k) = H2*(t(j-1,k) - t(j,k)) - pr*deta(j,k)*
ftb(j,k);
   end


    a{2,k} = [ 0 0 1 0 0; ...
              -0.5*deta(2,k) 0 0 -0.5*deta(2,k) 0; ...
               0 -0.5*deta(2,k) 0 0 -0.5*deta(2,k) ;
...

               a2(2,k) 0 a3(2,k) a1(2,k) 0;.....
               0 b2(2,k) b3(2,k) 0 b1(2,k)];

    for j = 3:np
      a{j,k} = [ -0.5*deta(j,k) 0 1 0 0; ...
                 -1 0 0 -0.5*deta(j,k) 0 ; ...
                  0 -1 0 0 -0.5*deta(j,k); ...
                  a6(j,k) 0 a3(j,k) a1(j,k) 0; ...
                  0 0 b3(j,k) 0 b1(j,k) ];

      b{j,k} = [ 0 0 -1 0 0;  ...
                 0 0 0 -0.5*deta(j,k) 0; ...
                 0 0 0 0 -0.5*deta(j,k); ...
                 0 0 a4(j,k) a2(j,k) 0; ...
                 0 0 b4(j,k) 0 b2(j,k)];
    end


    for j = 2:np-1
    c{j,k} = [ -0.5*deta(j,k) 0 0 0 0; ...
                1 0 0 0 0; ...
                0 1 0 0 0; ...
                a5(j,k) 0 0 0 0 ; ...
                0 0 0 0 0];
```

```
    end

    alfa{2,k} = a{2,k};
    gamma{2,k} = inv(alfa{2,k}) * c{2,k};

    for j = 3:np

     gamma{j,k} = b{j,k} * inv(alfa{j-1,k});
     alfa{j,k} = a{j,k} - gamma{j,k} * c{j-1,k};

    end

    for j = 2:np
        rr{j,k} = [ r1(j,k); r2(j,k); r3(j,k);
r4(j,k); r5(j,k)];
    end

    ww{2,k} = rr{2,k};

    for j = 3:np

    ww{j,k} = rr{j,k} - gamma{j,k} * ww{j-1,k};
    end


    delf(1,k) = 0;
    delu(1,k) = 0;
    dels(1,k) = 0;
    delu(np,k) = 0;
    dels(np,k) = 0;
    %check here
    %    dell{np,k} = ww{np,k};
  dell{np,k} = inv(alfa{np,k}) * ww{np,k};

    for j = np-1:-1:2
       dell{j,k} = inv(alfa{j,k}) * (ww{j,k} - (c{j,k}
* dell{j+1,k}));
    end


      delv(1,k) = dell{2,k}(1,1);
      delt(1,k) = dell{2,k}(2,1);
      delf(2,k) = dell{2,k}(3,1);
      delv(2,k) = dell{2,k}(4,1);
      delt(2,k) = dell{2,k}(5,1);
```

```
    for j = np:-1:3
      delu(j-1,k) = dell{j,k}(1,1);
      dels(j-1,k) = dell{j,k}(2,1);
      delf(j,k)   = dell{j,k}(3,1);
      delv(j,k)   = dell{j,k}(4,1);
      delt(j,k)   = dell{j,k}(5,1);
    end

    for j = 1:np
    f(j,k+1) = f(j,k) + delf(j,k);
    u(j,k+1) = u(j,k) + delu(j,k);
    v(j,k+1) = v(j,k) + delv(j,k);
    s(j,k+1) = s(j,k) + dels(j,k);
    t(j,k+1) = t(j,k) + delt(j,k);
    end

stop = abs(delv(1,k));
kmax = k;
k = k+1;

end
kmax
f_0=f(1,kmax)
u_0=u(1,kmax)
u_inf=u(np,kmax)
v_0=v(1,kmax)
s_0=s(1,kmax)
t_0=-t(1,kmax)
f_inf=f(np,kmax)
s_inf=s(np,kmax)
    xlabel('\eta')
     ylabel('\theta(\eta)')
plot (eta,s(:,kmax));hold on
plot (eta,u(:,kmax));hold on
end
```

Appendix C: List of Publications

1. Journal Published

- W. Rosli, W., Mohamed, M., Sarif, N., Mohammad, N. and Soid, S. 2022. Blood Conveying Ferroparticle Flow On A Stagnation Point Over A Stretching Sheet: Non-Newtonian Williamson Hybrid Ferrofluid. Journal of Advanced Research in Fluid Mechanics and Thermal Sciences. 97(2): 175-185.

- W. Rosli, W., Mohamed, M., Sarif, N., Mohammad, N. and Soid, S. 2023. Boundary Layer Flow Of Williamson Hybrid Ferrofluid Over A Permeable Stretching Sheet With Thermal Radiation Effects. CFD Letters. 15(3): 112-122

- W. Rosli, W., Mohamed, M., Sarif, N., & Ong, H. (2024). Convective Boundary Layer Flow of Williamson Hybrid Ferrofluid over a Moving Flat Plate with Viscous Dissipation. Journal of Advanced Research in Fluid Mechanics and Thermal Sciences, 112(1), 176-188.

- Mohamed, M., Ishak, A., W. Rosli, W., Soid, S., & Alkasasbeh, H.(2023). MHD Natural Convection Flow of Casson Ferrofluid over a Vertical Truncated Cone. Journal of Advanced Research in Fluid Mechanics and Thermal Sciences, 112(1), 94–105.

2. Presented

- W. Rosli, W., Mohamed, M., Sarif, N., Mohammad, N. and Soid, S. 2023. Boundary Layer Flow Of Williamson Hybrid Ferrofluid Over A Permeable Stretching Sheet With Thermal Radiation Effects. CFD Letters. 15(3): 112-122, 3rd International Conference on Applied & Industrial Mathematics and Statistics 2023, 24-26 August 2022, Pahang, Malaysia.

- W. Rosli, W., Mohamed, M., Sarif, N., Ong, H. 2023. Convective Boundary Layer Flow of Williamson Hybrid Ferrofluid over a Moving Flat Plate with Viscous Dissipation. 4th International Conference on Applied & Industrial Mathematics and Statistics 2023, 22-24 August 2023, Pahang, Malaysia.